PARTICLE ENHANCED FOAM FLOW IN POROUS MEDIA NEAR THE CRITICAL MICELLE CONCENTRATION

PARTICLE ENHANCED FOAM FLOW IN POROUS MEDIA NEAR THE CRITICAL MICELLE CONCENTRATION

Proefschrift

ter verkrijging van de graad van doctor
aan de Technische Universiteit Delft,
op gezag van de Rector Magnificus prof. ir. K.C.A.M. Luyben,
voorzitter van het College voor Promoties,
in het openbaar te verdedigen op donderdag 31 maart 2016 om 10:00 uur

door

Rahul THORAT

Master of Technology in Mechanical Engineering,
Dr. Babasaheb Ambedkar Technological University

geboren te Varud, India.

Dit proefschrift is goedgekeurd door de

promotor: Prof. dr. J. Bruining

Samenstelling promotiecommissie:

Rector Magnificus,	voorzitter
Prof. dr. J. Bruining,	Technische Universiteit Delft, promotor
Onafhankelijke leden:	
Prof. dr. P. L. J. Zitha,	Technische Universiteit Delft
Prof. dr. T. J. Heimovaara,	Technische Universiteit Delft
Prof. dr. R. Krastev,	Naturwissenschaftliches und Medizinisches Institut Tübingen
Prof. dr. R. Schotting,	Utrecht Universiteit Utrecht
dr. S.Y.F. Vincent-Bonnieu,	Shell Rijswijk
dr. A. Andrianov,	Eni Italy
Prof. dr. ir. J. D. Jansen,	Technische Universiteit Delft, reservelid

Keywords: Foam, Bubble population model, Symbolic regression, Critical Micelle Concentration, Colloid chemistry, Ash particles

Printed by:

Front : Bottom : Flow scheme of the setup used for the foam experiments, adopted from the original sketch by Henk van Asten (Laboratory Technician).

Back: Top : About the thesis, Bottom : An artistic interpretation of the particle enhanced foam flow in the porous media.

ISBN 000-00-0000-000-0

An electronic version of this dissertation is available at
http://repository.tudelft.nl/.

Science is a wonderful thing
if one does not have to earn one's living at it.

Albert Einstein

CONTENTS

NOMENCLATURE

Table 1: Abbreviations and Subscripts

Abbreviations	Description	Subscripts	Description
		a	Adsorption
AOS	Alpha Olefin Sulfonate	app	Apparent (viscosity)
av	Average (bubble density)	cap	Capillary (diffusion)
BP	Back pressure	d	Desorption
CMC	Critical micelle concentration	e	Effective
DD	Doubly Distilled (water)	eqd	Equilibrium adsorption density
Edl	Electric double layer	f	Foam
IEP	Isoelectric point	g	Gas
ini	Initial (bubble density)	gr	Irreducible (gas saturation)
inj	Injection (bubble density)	ism	Injected surfactant molecular (weight)
KI	Potassium Iodide	L	Left hand side (or Lamella)
PEI	PolyethyleneImine (polymer)	R	Right hand side
PV	Pore volumes	rg	Relative (permeability) to gas
St	Steric (force)	rw	Relative (permeability) to water
TOC	Total Organic Carbon	s	Surface (or surfactant)
UV	Ultra violet (light)	sap	Specific surface area of pores
VdW	Van der Waals (force)	ss	Steady state
		st	Start
		wc	Connate water
		we	Effective water (saturation)

Table 2: Constants

Symbol	Description	Value	Unit
A	Hamakar constant	6.31×10^{-19}	[J]
e	Electric charge	1.60×10^{-19}	[Coulomb]
F	Faraday's constant	96508.65	[C/mol]
g	Acceleration due to gravity	9.81	[m/s^2]
k_B	Boltzmann constant	1.3806×10^{-23}	[J/K]
N_A	Avogadro's constant	6.0221×10^{23}	[/mol]
R	Gas constant	8.314	[J/mole/K]
T	Temperature	293	[K]
A_0	Data driven parameter (Chapter 4)	6073	[N/((mol/l)(m/s)$^{mol/l}$)]
K_a	Adsorption rate (Chapter 3)	5	[10^{-5} mg/gs]
K_d	Desorption rate (Chapter 3)	90	[10^{-5} /s]
Q_s	Maximum adsorption capacity (Chapter 3)	14.28	[10^{-5} mmol/m^2]

Table 3: Symbols

Symbol	Description	Unit
A	Surface/interstitial area	[m^2]
C	(Molar) Concentration	[mol/l]
c	Compressibility	
D	Diffusion coefficient	[m^2/s]
d	Diameter (Appendix A)	[m]
H	Interparticle distance	[m]
h	Total head	[m]
I	Ionic strength	[mol/l]
k	Permeability	[m^2]
K	Hydraulic conductivity	[m/s]
L	Length	[m]
m	Mass of the ash particle	[g]
M	Molecular weight	[mg/mmol]
n	Bubble density	[/m]
Nc	Salinity	[mol/l]
Q	Flow rate	[m^3/s]
q	Volumetric flow rate	[m^3/s]
R	(Capillary) Radius	[m]
r	Ramp function (Chapter 3)	
r	Radius of the particle (Chapter 5 and 6)	[m]
S	Saturation	
t	Time	[s]
u	Superficial velocity	[m/s]
V	Energy	[J /s]
v	Darcy Velocity	[m/s]
X	Fraction (of flowing foam)	
z	Charge number	
Greek Symbol	**Description**	**Unit**
α	Viscosity coefficient	[$Ns^{2/3}/m^{4/3}$]
χ	Flory-Huggins parameter (Chapter 5)	
δ	Polymer layer thickness on the particles (Chapter 5)	[nm]
ΔP	Pressure drop	[N/m]
ϵ	Dielectric costant	
ϵ_0	Permittivity of free space	[F/m]
η	Foam quality	
Γ	Adsorbed amount (of polymer/surfactant)	[mol/m^2] or [mg/m^2]
γ	Skewness (Appendix)	
κ^{-1}	Debye Length	[m]
λ	Pore size distriubtion index	
λ	London-Van der Waals constant	[J m^6]
μ	Viscosity	[Ns/m^2]
Ω	Volume of the particles (Chapter 5)	
ω_p	specific partial volume of the polymer (Chapter 5)	
ω_s	molar volume of the solvent	[m^3 per mole]
ρ	Density	[g/cc]
σ	Surface tension	mN/m
θ	Contact angle	[radian]
φ	Porosity	[%]

1

INTRODUCTION AND OVERVIEW

The first principle is that you must not fool yourself
and you are the easiest person to fool.

Dr. Richard Feynman

This chapter gives the introduction and the overview of the thesis. We introduce the topic of the thesis with the background and knowledge gap about foam. We make a statement of the problems and the motivation to solve it. The significance of the study and the primary questions are described. The hypotheses and the ensuing experimental design and theoretical framework are mentioned. We specify the assumptions used in the discussion and approximations used in the conclusions. The limitations in the research design, limitations of the measuring instruments and possible biases are mentioned. The scope of the study with the possible future work is stated. We finish the introduction and overview with a brief outline of the subsequent chapters.

1.1. INTRODUCTION

Foam (a mixture of gas and surfactant with water) can be used to increase the oil recovery [1–4], for hazardous waste control [5], for acid diversion [6] and for aquifer remediation [7–9]. In addition, foam can promote deeper penetration of particles (e.g. hematite [10]), delaying particle cake formation. As observed in bulk foam, gravity drainage and gas diffusion can destruct foam in porous media [11]. The trapping of particles in the Plateau borders as well as in the lamellae retards liquid drainage and bubble coalescence [12, 13], thereby increasing the stability of the foam films for above mentioned applications. The increased stability of foam films due to particles can be observed as a pressure drop increase across the porous media during foam flow [14–16]. Most literature studies focus on the use of manufactured particles, mainly silica. Ash particles (a waste product from the coal industry) have properties similar to silica, and contain considerable alumina. Therefore, this study focuses on using ash particles to enhance the stability of foam. An important part of the study is to establish a reference, viz. the behavior of foam in the absence of ash particles in porous media by combining selected experimental results with an extensive literature study (given in chapter 3 and 4). The efficiency of ash particles in foam flow through porous media depends critically on its colloidal stability. A prerequisite for their application is that the bulk particle dispersions are stable against sedimentation and coagulation (given in chapter 5). A direct evidence of the effect of ash particles is achieved by additional foam flow experiments in porous media with particles and their comparison to experiments without particles (given in chapter 6).

This introductory chapter is organized in sections. We begin with section 1.2 about the major findings in the field of foam flow modeling, effect of fluid and porous media properties on foam, coagulation/sedimentation of particle dispersions and particle enhanced foam flow through porous media. We focus on aspects that constitute a gap in the knowledge, in particular foam behavior near the critical micelle concentration found in the current literature. The background leads to the next section 1.3, which contains the general need for the study and the specific problems that will be addressed. The next section 1.4 identifies the research approach, which is experimental, statistical, or a combination of both and uses colloid chemical interpretation. The physical properties of interest for the studies such as pressure drop and settling rate are identified. Section 1.5 explains why it is important to identify some aspects of the gap in the knowledge. Our contribution to the knowledge framework is described. We further summarize stakeholders who will be able to use the knowledge to make better technical decisions or for other applications of the new information. The significance of our study is that it can be used to fill a gap in the knowledge framework. In section 1.6, we define the basis for data collection arising from the purpose of the study, i.e. the effect of fluid and porous media properties variables such as the permeability on the pressure drop and effect of pH on the settling rate of particles. Our contribution to the knowledge gap will be to answer some of these questions. In section 1.7, we state the hypotheses, ensuing from the research questions upon which they are based. The hypotheses are tested by experiments and modeling. In section 1.8, we give a summary of the methodology and a brief outline of: (a) the materials used, (b) the instrumentation used to collect data, and (c) the procedure that will be followed. In section 1.9, we give the theories that formed the foundation of the thesis. In section 1.10, we give the arguments that we consider essential to develop

our ideas. Section 1.11 gives limitations of the instruments, possible biases and limitations imposed on the research design by us. We discuss the universality of the study in section 1.12, i.e. the extent to which the data are applicable for cases/conditions outside the area for which the study is intended. We end with a small description of each chapter in the last section 1.13.

1.2. BACKGROUND

Predicting foam behavior in porous media relies on proper modeling of the mobility reduction validated by experiments. Most modeling attempts in the literature are for experiments with surfactant concentrations well above the critical micelle concentration (CMC) to avoid adsorption losses of surfactant [17]. Researchers have reported only a few experimental data with injected concentrations around the CMC that are characterized by an observed delay in the build up of the steady pressure drop. To explain such a delay one needs models that incorporate the transient development of foam in porous media. Such models (e.g. Flowing bubbles in a capillary tube [18]) often consider foam as bubbles surrounded by thin liquid films in contact with the pore wall. The models contain a bubble density equation with a bubble generation-coalescence function [19] expressed as a source term, which is in essence a difference between generation and coalescence rates of bubbles. In most cases, the source term is assumes foam generation-coalescence mechanisms, e.g. lamellae creation by capillary snap-off, bubble division and bubble coalescence by mass transfer between bubbles. Several researchers [20–22] have proposed a saturation based foam generation-coalescence function. However, if the initial (water) saturation and flowing fraction of foam is unknown, an exact bubble generation-coalescence function cannot be directly obtained from the experiments.

Foam behavior in porous media depends on many variables, e.g. the permeability of the porous medium, the surfactant type, the surfactant concentration, flow rates etc.. To simplify the complex system of multiple variables, most research studies focus on a base case after which they modify one or two variable(s) at a time to study their effect on the steady state pressure drop, for example, the flow rate and concentration [23] or gas velocity and surfactant solution velocity [24, 25]. In addition, such studies use a physical concept to construct a model for explaining the steady state, i.e. a mechanistic approach [26, 27]. The modeling approaches mentioned above pose practical difficulties for reasons of the required large number of experiments and the large number of fitting parameters. Such models require physical understanding and are difficult to derive for such a complex system as foam flow. In addition, there is a lack of experimental data that use orthogonal or even box design [28] for variables such as permeability, surfactant concentration, foam quality and salinity affecting the pressure drop. It is difficult to generalize conclusions from the literature as those studies are (deliberately) unique and for restricted variable spaces.

To determine whether the particles are suitable for the applications mentioned in the introduction, it is important to study their stability in a bulk dispersion. To calculate the fraction of particle collisions that lead to coagulation, it is necessary to sum the interparticle forces such as the double layer forces [29] and the Van der Waals forces [30]. The forces are named DLVO forces after Derjaguin, Landau, Verwey and Overbeek [31]. However, the interaction between two particles in a medium is not independent of the

surrounding medium interactions [32], e.g. structural forces [33, 34] and steric repulsion forces [35]. These forces determine the activation barrier [36] that particles have to cross before coagulation can occur. The forces are subjected to solution properties such as pH, ionic strength and surfactant content. Therefore, it is necessary to determine the effect of pH, ionic strength and surfactant on the stability of the particles in a dispersion.
Researchers use the bulk tests for foamability to screen the surfactant [37] before their further use in foam flow experiments. In addition, most studies use a high concentration of surfactant, e.g. Wang [12] and Singh [13] used 0.4 wt % and 0.5 wt % of surfactant respectively. The studies discuss particle added foam flow without accounting for the stability of the particles in a dispersion. In addition they did not extensively discuss the effect of particle flow along with the surfactant solution on the permeability of porous media. The pressure drop during foam flow due to particles in a surfactant solution with a concentration near the critical micelles concentration (CMC) is not studied in the literature. The experimental pressure drop can be further used to calculate the apparent foam viscosity [23, 38, 39] and to validate foam flow models [40–43].

1.3. STATEMENT OF THE PROBLEMS

From the background information, we observe following gaps in the knowledge of foam flow in porous media near the Critical Micelle Concentration: (a) an exact bubble generation coalescence function directly derived from the experiments, (b) experiments where the effect of more than three variables on the foam pressure drop is studied, (c) the optimal condition for the colloidal stability of ash particle dispersions and (d) the foam pressure drop due to the particle enhanced foam flow at those optimal conditions. Based on the gaps we define following problems: (a) modeling foam as bubbles through porous media using the experimental pressure drop, (b) finding the hierarchy of the variables affecting the pressure drop, (c) finding the colloidal stability of particles in the injected dispersions for properties such as pH, ionic strength and surfactant content, and finally (d) quantify the effect of particle addition on the pressure drop during foam flow through porous media.

1.4. PURPOSE OF THE STUDY

In order to solve the above problems, we identify the experimental, theoretical and statistical research design (approach). To determine whether we can use the observed pressure drop for modeling foam flow in a porous medium, we estimate the bubble generation function from the observed pressure drop. We identify the pressure drop across two measuring points during foam flow through porous media as a dependent research variable for a statistical study. The dependence of the pressure drop on multiple variables (permeability, gas velocity, water velocity, etc.) given in the background information could be elucidated with data driven (for example, genetic algorithm based) models constructed by applying regression to experimental results. However, conventional regression involves a presumed interrelationship between the variables, which might miss the importance of one variable over another affecting the pressure drop. Therefore, we are motivated to find the hierarchy of the variables with a maximally feasible set of experiments using a non conventional regression analysis called symbolic regression [44, 45].

Further, we aim to establish an experimental procedure with which the coagulation and sedimentation rates of ash particle dispersions can be quantified for various pH with and without surfactant. Finally, we would like to prove or disprove the effect of particles on the increase of the pressure drop for foam flow in porous media. However permeability change due to surfactant adsorption [46] on or particle retention in the porous medium [47] can cause a larger pressure drop. Therefore we also study the adsorption of the surfactant used in the study.

1.5. SIGNIFICANCE OF THE STUDY

The specific results of the study can be applied to the cases mentioned in the introduction of this chapter: oil recovery, hazardous waste control, acid diversion and aquifer remediation. Our contribution to the body of knowledge can be used to make better decisions or improve policies for above applications. The study gives the individual contribution of accumulation and transport terms to the source term in the bubble population equation. The study shows the missing data necessary to find the interdependence of the variables affecting the pressure drop. In addition to criteria for a model selection, the study shows that accurate model verification / validation is also important to assess the merit of the selected model. Fly ash particles are a waste product from coal-fired power plants. By using such ash particles into a porous medium for foam flow applications, we can cheaply increase foam efficiency. The study gives conditions (e.g. pH and surfactant) for which optimum colloidal stability can be achieved.

1.6. PRIMARY RESEARCH QUESTIONS

The primary research questions that we pose are as follows: (i) can the bubble population approach adequately model foam flow through porous media?, (ii) is it possible to obtain an exact bubble generation-coalescence function from the experimental pressure drop history?, (iii) can our limited experimental data represent the whole population of foam experiments from the literature?, (iv) is there a way to use the previous experimental results to generalize the effect of various variables on the steady state pressure drop?, (v) can we rank the effect of variables on the pressure drop? (vi) is the foam film stability in the bulk related to foam stability in the porous media?, (vii) is a pressure drop between two measuring points across the porous medium representative of the foam stability in the porous medium, and (viii) is there a link between the stability of the colloidal dispersion of ash particles and its effect to enhance the foam stability and particle adsorption in the porous medium?

1.7. HYPOTHESES

We hypothesize that the source term in the bubble population equation is a derivative of the bubble density and can be obtained from history matching of the experimental pressure drop. The rate of change of the bubble density during the transient state can be equated to the bubble density generation-coalescence function plus the terms that account for bubble transport by convection and diffusion divided by porosity and saturation. We hypothesize that the model obtained from symbolic regression can explain

the general behavior and hierarchy of the variables affecting the steady state pressure drop. Our hypothesis is that ash particles stabilize foam in porous media by slowing the drainage of liquid from lamellae. Such an enhanced stabilization can reduce the relative gas permeability observed as an increased pressure gradient in foam flow tests. The surfactant adsorption and particle retention in the porous medium can also change the permeability of the medium. We hypothesize that such a change in the permeability can be detected by permeability measurements before and after the foam flow experiment.

1.8. EXPERIMENTAL DESIGN

We measured pressure drop histories before and after injection of an Alpha Olefin Sulfonate solution (AOS) with nitrogen gas (N_2) between two measuring points in unconsolidated sandpacks (1860 and 130 Darcy) and a Bentheimer sand stone core (3 Darcy) for various surfactant concentrations (0.0375, 0.075 and 0.15 w/w %), for various gas and surfactant solution velocities (0.27-3.97 m/day), for two salinities (0 and 0.5M NaCl) and for two pH values (6.5 and 3.0). We studied the effect of particle addition on the stability of foam flow through porous media with combinations of a particle dispersion and an AOS solution. Permeability tests are conducted on sandpacks and a Bentheimer core between foam flow experiments. The ash particles are treated with a polymer, polyethelyenemine (PEI). We used short cores, i.e. 15 cm of sandpack and 17 cm of Bentheimer core to conduct the experiments faster than long cores, thereby able to conduct more experiments. As we use surfactant at the critical micelle concentration, we conducted a surfactant adsorption test to quantify surfactant losses. We developed a data driven model to understand an interactive effect of variables affecting the pressure drop thereby foam stability. To study the colloidal stability we prepared ash particle dispersions with and without surfactant for pH values 3 to 11. We measured the zeta potential, the particle size and the particle size distribution of ash particles in the dispersions with the Malvern "Zeta sizer". In addition, we use a ultra-violet visible light spectrometer and an inhouse built laser scattering set up to estimate the sedimentation rate of the particles. In order to attach a particle to the bubble, the surfactant needs to lower the contact angle between solid and gas but not overload it to prevent aggregation. Therefore we selected a concentration for flow experiments, which is close to the critical micelle concentration. In addition, we conducted auxiliary experiments measuring surface tension and “foamability” of the dispersions in a test tube.

1.9. THEORETICAL FRAMEWORK

Contrary to earlier studies, we infer the bubble generation-coalescence function, i.e. the source term from the experimental pressure drop without a priori knowledge of foamed gas saturation and flowing fraction of foam. In our procedure, a first estimate of the bubble density is obtained by relating the viscosity coefficient (α, given by Kovscek [19]) to the surface tension of the injected surfactant concentration derived from the work of Hirasaki [18]. In addition, we calculate the water saturation with the estimated bubble density for a constant foam quality. With the saturation and the flowing fraction of foam known, the source term when fully implemented in a flow model gives a simulated pressure drop history that corresponds to the experimental pressure drop history. With the

values of the pressure drop comparable to each other, we propose a realistic contribution of the derivative of the bubble density to the source term. We include the gravity term in the model equations and further in the numerical simulation.
We used the experimental results from the literature along with our own results to search for the model form that best describes the data behavior using a minimal number of fitting parameters. To overcome the difficulty of statistical inference with only 14 (our) data points, we add 112 data points from Martinez [24, 25], 21 data points from Jante and Osterloh [48] and 12 data points from Persoff [39]. We used Eureqa® [49], a software package based on symbolic regression to determine the relation between the independent variables and the dependent variable, i.e. the observed pressure drop. The software searches the fitting parameters and the form of the equations simultaneously [44]. The software produced a small set of possible analytical expressions given in Appendix B. To select a model from the candidate expressions, we use Akaike's information criterion (AIC) [50], which is a balance between accuracy and complexity of the model. For the purpose of determining the accuracy of the model parameter, we use a bootstrap method [51, 52] to generate 50 simulated data sets different from the original data set.
We use Smoluchowski's theory of rapid and slow coagulation [36] to determine the settling velocity of the particles in the bulk aqueous phase. We use the radius of the particles to calculate the number of particles per size, i.e. by dividing mass of particles of a particular size with number average "molecular weight" [36]. We use the number of particles per cubic micron and the particle size to estimate attenuation constant (per mm) by Mie scattering [53]. We calculate the energy of interaction between polymer coated spherical particles (V) of identical radius R in an aqueous medium as a function of inter particle distance H as the addition of the Van der Waals energy (V_{VdW}), the electric double layer energy (V_{Edl}) and the energy due to steric forces (V_s) [54, 55]. We determine the variation of the surface (zeta) potential with pH on the particle surface using Gouy-Chapman-Stern model [56]. Finally we relate the colloidal stability of the particles to their effect to enhance the pressure drop during foam flow through porous media.

1.10. ASSUMPTIONS AND APPROXIMATIONS

We have made the following assumptions for the modeling of foam flow through porous media. The foam flows in a porous medium as a two-phase fluid according to Darcy's law, i.e. foamed gas and water [3, 57]. Therefore, the total superficial velocity u_t is the sum of the superficial velocities of the water and foam phase. To estimate the varying viscosity of foam in the two-phase concept, the smallest pores are filled with the surfactant solution and other pores with gas bubbles separated by lamellae [18]. The radius of curvature of the lamella is equal to the capillary radius. The resistance per lamella in the capillary tube is the viscosity coefficient α. At low concentration (around CMC), α varies when the surfactant concentration in the porous medium varies. As the saturation and flowing fraction of foam is unknown, we assume initially that foaming gas is the only phase in the porous medium and all the foamed gas is flowing. Therefore, the foam relative permeability is equivalent to the gas permeability. In the next step of estimation of the source term, the number of trapped bubbles is equal to the number of flowing bubbles as in the work by Kovscek [19]. In order to derive the pressure equation we assume that the water density ρ_w is pressure dependent. We assume that the surfactant

concentration in the lamellae and in the injected water are the same. The number of lamellae is equal to the number of bubbles. The gas saturation remains below the critical gas saturation; therefore foam does not collapse [58]. As the water saturation is very low, the local interstitial velocity is equal to the global (total) interstitial velocity. The initial value of pore size distribution index λ is 5 for Bentheimer core with complex mineral composition being slightly larger for the medium with a narrow range of pore sizes [59]. To find the significant variable affecting the pressure drop during foam flow experiments, we assume that the examples from literature uses injecting solutions of pH 5.0. All data contain same surfactant (AOS, mol/l) and the same salinity formulation (NaCl, mol/l). As the error in the observed pressure drop was not known, we assume that all measurements have the same standard deviation. For validation, the data points are independently and identically distributed. We assume that the particles are spherical to calculate their volume and their mass in a dispersion. As the concentration density of the particles is fixed, i.e. 0.4 kg/m^3, we assume that the relationship between particle size and the number of particles is inversely proportional, i.e. the smaller the particle size, the higher the number of particles in a dispersion. We use the Debye–Hückel linear approximation to calculate the Debye length. The unit of permeability, one Darcy, is approximated to 1×10^{-12} m^2.

1.11. LIMITATIONS

We give here the issues that could be addressed in future work. As ample information is available in the literature about the foamability tests for Alpha Olefin Sulfonate (AOS) surfactant, we conducted a limited number of foamability tests. We were limited by the manometer ranges (0-3 bar) and accuracy (30 mbar) for the measurement of the pressure drop during foam flow experiments. As we conducted the experiments during day and night, a temperature fluctuation of 3-5°C was noted. We used short cores (15 cm of sandpack and 17 cm of Bentheimer core) for flow experiments, which can lead to mainly capillary end effect that consequently affects foam mobility measurements [60]. In case of the bubble population model, we observed that the mean absolute error between theoretical and experimental pressure drop is 1.06×10^5 Pa/m, i.e. within 10 % of the experimental pressure drop. Possible reasons for the imperfect match between simulation based on the proposed theoretical procedure and the experimental results are lack of fitting profiles in case of the uncertainty to estimate (a) the bubble density from the experimental pressure drop, (b) the change in the bubble density w.r.t. time from the bubble density and (c) the adsorption parameters from the adsorption experiment. In addition, we selected the adsorption parameters from the single phase experiment where the available surface area for adsorption is less than the surface area for multiphase foam flow. The role of bubble diffusion in the bubble population model is not very well understood.
Our data set and the data set of Jante and Osterloh [48] show significant deviation from the chosen symbolic regression model. Possible reasons are included in the chapter 4. The Debye–Hückel equation cannot be used to calculate the surface charge on the particles in the solutions of surfactant, when the micelles are present.

1.12. SCOPE OF THE THESIS

As our primary goal of modeling was to relate the bubble generation function to the experimental pressure drop, we consider a detailed convergence analysis of the simulation for such a non-linear problem outside the scope of current work. To use the procedure of bubble population estimation by the experimental pressure drop in the field, a further upscaling step is required, for instance using homogenization [61]. Due to the adsorption of the surfactant during foam flow experiments, there are reactions on the surface of the particles, which determine the charge and therefore, the surface potential. The surface charge calculation on the polymer coated particles in the presence of surfactant solution by the surface complexation models demand considerable attention. Therefore, we consider surface complexation models outside the scope of the present work. The modeling of particle enhanced foam flow in porous media is considered beyond the scope of the work and could be addressed in future work.

1.13. STRUCTURE OF THE THESIS

We have organized the thesis in chapters. Chapter 2 describes the experimental set-up, sample preparation and measurement techniques. In addition, the chapter describes the instruments used to characterize the colloidal stability of the particles in a dispersion.
In chapter 3, we present an estimation of the bubble generation function from a laboratory experiment that co-inject nitrogen and Sodium C_{14-16} Alpha Olefin Sulfonate (AOS) with a concentration near the critical micelle concentration in a Bentheimer sandstone of 3 Darcy. We explain the experimental pressure drop by a model that leads to four equations, viz. a pressure equation, a water saturation equation, a bubble density equation and a surfactant transport-adsorption equation.
Chapter 4 investigates the steady state pressure drop by combining six variables, viz. permeability, surfactant concentration, pH, salinity, surfactant solution velocity and gas velocity. We register total 14 pressure drop histories for an Alpha Olefin Sulfonate solution before and after the injection of nitrogen gas across the unconsolidated sandpacks of two mean grain sizes and across a Bentheimer consolidated core. We combine our data set with data sets from the literature leading to 157 data points. We apply symbolic regression to the entire data set to produce a number of analytical expressions describing the interactive effect of the fluid and porous media properties without prior knowledge of an underlying physical process. We select a simple model with only one fitting parameter to compare with the experimental data. We determine the precision of the model parameter by a bootstrap method.
Chapter 5 investigates the stability of aqueous dispersions of the ash particles for foam flow. The study comprises the measurement of the zeta potential and particle size distributions, UV-visible absorption and turbidimetry. The relative settling rate is considered as the main criterion for stability optimization. Moreover we quantify the dependence of the colloidal stability of 0.04 w/w% ash dispersion on the pH and surfactant (Alpha Olefin Sulfonate).
Chapter 6 builds on the studies conducted so far by describing information about foam flow experiments with AOS-particles suspension. It summarizes experimental work to

establish the effect of particles on foam stability in fine sand of 130 Darcy and a Bentheimer consolidated core of 3 Darcy. Foam flow experiments with and without particles are compared.
Chapter 7 gives general remarks and conclusions about the preceding work.
Appendix A gives the permeabilities for single phase flow through sandpacks (Fine and Coarse sand) determined by flow experiments, gravity measurements and by the Kozeny-Carman relation inclusive the grain-size heterogeneity factor [62]. Appendix A further gives the calibration of pressure manometers and general calibration of a pH meter.
In Appendix B we give our experimental data with the data from Martinez [24, 25], Jante and Osterloh [48] and Persoff [39] in Table B.1. Section B.2 shows a small set of possible analytical expressions to determine the relation between the independent variables and the dependent variable (the observed pressure drop) produced by Eureqa® [49], a software package based on symbolic regression.
Appendix C gives the information about the relation between the sedimentation rate and particle size, the treatment of ash particles with a polymer (PEI), surface energy change due to particle at the gas/water interface, the particle size and zeta potential of the particles at a pH of 6.0.
The thesis ends with a short summary.

2

Common Methodology, Research Instruments

door meten tot weten
By measurement to knowledge

Heike Kamerlingh Onnes

This chapter gives information about the porous media, the solutions used, the foam flow experimental set up and the supplementary bulk tests. We describe the procedure for the flow experiments, working of instruments such as zeta sizer, inhouse built laser set up and the spectrophotometer. We illustrate a surfactant adsorption test to quantify surfactant losses. The information about the specific solutions and dispersion used during the experiments is given in the relevant chapters.

Table 2.1: Porous media used in the experiments

Porous media	**Length** mm	**Mean grain size** mm	**Porosity** %	**Permeability** Darcy
Coarse sandpack	150	1.00±0.12	38	1860±100
Fine sandpack	150	0.30±0.08	30	130±30
Bentheimer	170	-	21±1	3.0±0.5

2.1. MATERIALS

2.1.1. POROUS MEDIA

We used three types of porous media for the foam flow experiments, viz. coarse sand, fine sand and Bentheimer cores. Table 2.1 shows the grain size, porosity, permeability and length of the porous media. The advantage of the short core is that we could finish experiments faster than the experiments with the long cores, thereby able to conduct more experiments. The disadvantages of the short cores for foam experiments are mainly due to the capillary end effect [63]. Indeed it is technically difficult to separately produce two phases (Oleic phase and aqueous phase) and hence difficult to regulate the capillary pressure at the end, which is usually close to zero. The capillary end effect affects foam mobility measurements [60]. We measured the surface area of 259 grains each for fine and coarse sand under the optical microscope. As the diameter of the particle perpendicular to the flat surface is smallest and therefore not visible, only the largest diameters are visible and this tends to overestimate the average particle diameter, but the errors are usually small [64]. Figure 2.1 and 2.2 shows the pore size distribution for the unconsolidated sands. We calculated the particle size by $\sqrt{4\,A}/\pi$, where A is surface area. We selected mean size of the sample. We used a potassium-dichromate-sulfuric acid solution to treat the sand before its use to make it completely water-wet. The sand was kept in the acid for one day and rinsed with tap water to remove the acid according to the procedure mentioned by Furniss [65]. Subsequently we dried the sand and poured in an acrylic tube using the procedure of the seven sieves [66]. Here onwards we refer the acrylic tube with the sand as the sandpack. In case of Bentheimer, we cut the core from larger samples and did not pretreat before its usage. Figure 2.4 and Figure 2.5 show photographs of the unconsolidated sandpack and the Bentheimer core respectively with the positions to measure the pressure difference. We assumed the porosity of the unconsolidated coarse and fine sandpack [62]. We measured the porosity of the Bentheimer core by comparing its weight with and without water. We measured the permeability of the sandpack and core by a single phase water permeability test before foam flow experiments. Appendix A shows a gravity setup for coarse and fine sand to calculate their respective permeabilities.

2.1.2. SURFACTANT

We used Bio-TERGE® AS-40, an Alpha Olefin Sulfonate (AOS) solution, with 39.1 w/w % active content in doubly distilled water. AOS is an anionic surfactant, which dissociates in water in an amphiphilic anion $R-CH=CH-SO_3^-$ and in a cation Na^+ [67]. It is a salt of sulfonic acid with formula $C_nH_{2n-1}SO_3Na$ where $n = 14-16$ and consists mainly

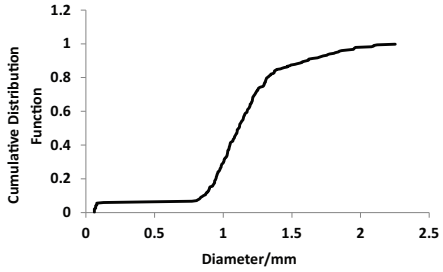

Figure 2.1: Particle size distribution for the unconsolidated coarse sand. 15 % of the sample particles are below 1 mm, 10% are above 1.5 mm. Majority of the sample particles are between 1 mm and 1.5 mm.

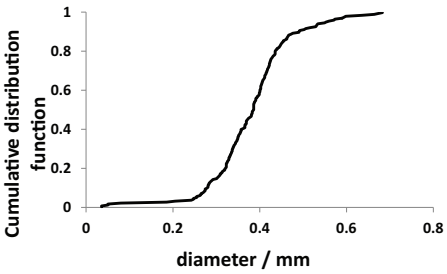

Figure 2.2: Particle size distribution for the unconsolidated fine sand. 5 % of the sample particles are below 0.2 mm, 5% are above 0.5 mm. Majority of the sample particles are between 0.2 mm and 0.5 mm.

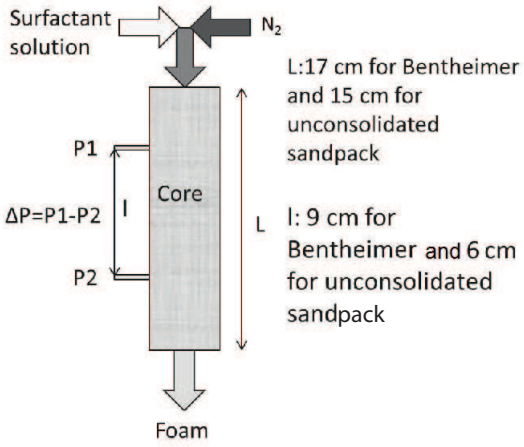

Figure 2.3: Schematic drawing of the Sandpacks and Bentheimer core. The foam flow was bottom-to-top for the unconsolidated sandpacks and top-to-bottom for the Bentheimer core.

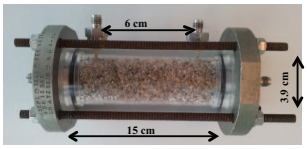

Figure 2.4: Sandpack with the coarse grains of size ≈ 1 mm. Later experiments were conducted with the fine grains of size ≈ 0.3 mm.

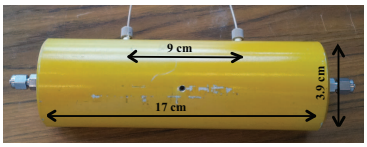

Figure 2.5: Bentheimer core fitted in the yellow core holder.

39.1 w/w % AOS ml	DD water ml	Final solution ml
2.57	97.43 (0.3 w/w % Brine)	100(0.3 w/w %AOS in Brine)
7.67	992.33 (DD water)	1000 (0.3 w/w % AOS)

Table 2.2: Preparation of the AOS solutions for foam flow experiments.

of sodium alkene sulfonates and sodium hydroxyalkane sulfonates. A pH of 6.34 is measured for 0.0375 w/w % AOS in doubly distilled water exposed to atmosphere. Table 2.2 shows two types of initial solutions, prepared from 39.1 w/w % Bio-TERGE® AS-40. The solutions were further diluted or added with HCl/NaOH to change the pH as described in following chapters.

2.1.3. PARTICLES

We received ash particles (pH=3, 0.05 g/ml, 250 ml) from a power plant Kraftwerk Altbach/Deizisau near Stuttgart in Germany. The particles mostly contain oxides of Silicon, Aluminum and mixed aluminum silicates. The elemental composition in w/w % is given as O (53 %), C (22 %), Si (13 %) Al (7 %) and Fe (1 %). Also found but only as traces are the elements: Na, Mg, K, Ca, Cu, Ti, P and S. Ash particles were surface treated with PolyethyleneImine (PEI) and characterized with bulk tests at the Naturwissenschaftliches und Medizinisches Institut (NMI) Tübingen, Germany, described in Appendix C.

2.2. FLOW EXPERIMENTAL SET UP

Figure 2.6 shows the set up for the foam flow experiments. The set-up consisted of an injection module, the core holder containing the sample (24), a production module and measurement equipments. The injection module used a Pharmacia pump P-900 (12) of the reciprocating type (two cylinders, one for injection and one for refill) with a pumping rate 15 - 450 ml/hour. The injection module further had a storage glass vessel (13) containing the surfactant solution and a nitrogen gas supply system (1). We connected the storage vessel to the pump by a polymer (nylon) tubing with an inside diameter of 2 mm and an approximate length of 1 m. Nylon tubing with the same diameter connected the pump to a T-junction via valves 3 and 4. Valve 3 could open nitrogen gas at a pressure 7.0 ± 0.1 barA (absolute pressure) in the stream of solution. The core holder contained either an unconsolidated sandpack or a Bentheimer sandstone core. We conducted experiments with the sandpack of coarse sand with the flow from bottom to top. However, it was easier to do experiments with our set up with the flow direction from top to bottom. Therefore we switched the direction for the subsequent experiments. The production module consisted of a fluid collection vessel (14) to collect the sample and a back pressure valve (17) to control back pressure. Figure 2.7 shows the photograph of right side of the set up and Figure 2.8 shows the photograph of left side of the set up. Initially we had visual cell installed in the experimental set up. However, the pressure drop was very high across the visual cell, which jeopardized an accurate measurement of the pressure drop across the measuring points. For this reason we disconnected the

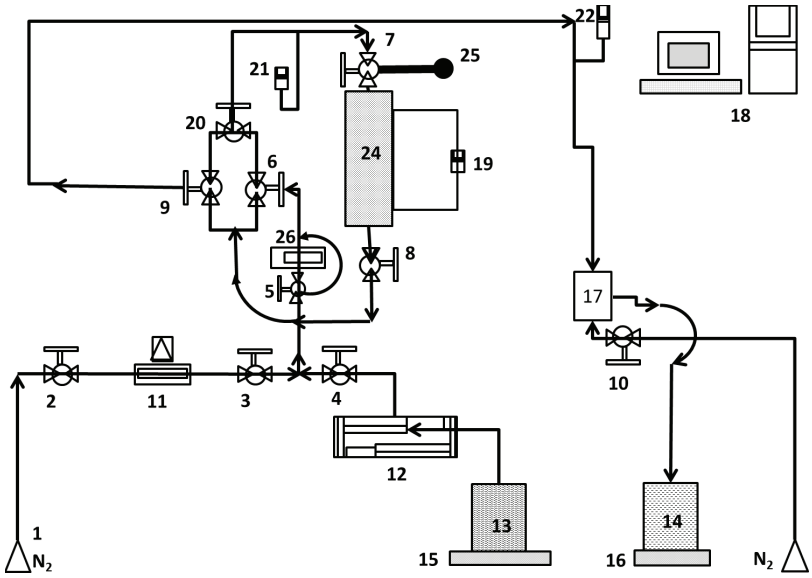

Figure 2.6: Flow scheme of the setup used for the foam experiments, adopted from the original sketch by Henk van Asten (Laboratory Technician). The directional signs show the path of the fluids (for example top to the bottom of the porous medium). The surfactant solution (13) is mixed with N_2 gas by opening valves (3) and (4) upstream of the unconsolidated sand pack or a Bentheimer core (24). The valves (2 to 10 and 20) control the flow while manometers (19, 21 and 22) measure the pressures recorded by the computer system (18).

visual cell from the set up. Moreover, the bubble sizes measured in external visual cells may not be representative. Ettinger [68], Ransohoff [69] and Friedmann [40] describe an overview of the problems when a visual cell is used. We regulated the back pressure valve (17) by high pressure nitrogen from a cylinder, not shown in the photographs. We used the outlet of the sandpack/coreholder to connect to nylon tubing with the same internal diameter as the injection tubing, but has a length of 50 cm. There is a flow distributor at the bottom and the top between the injection tube and sandpack to avoid spurious entrance and production effects. The bottom of the sandpack contained a steel and nylon filter of mesh size 10/cm and a thickness of 0.12 mm to avoid sand spillage. By switching valves (6),(9) and (20) it was possible to change the direction of the flow in the core. The flow rate of the injected mass was of the range 5.5 to 175.0 $\times$ 10^{-9} kg/sec and kept constant during the foam experiment. We collected the foam in the production vessel after it passed through the porous medium.

MEASUREMENT OF PRESSURE, MASS FLOW AND TEMPERATURE

Table 2.3 gives measured property, brand/model, range and accuracy of the instruments used in the set up. We connected the manometers (19, 21 and 22) and mass balances (15 and 16) to a data acquisition system and a computer (18) to record the pressures and mass flow versus time. The mass balances (15) and (16) measured the mass flow in (13) and out (14) of the core respectively by weighing the storage vessels. Figure 2.3 shows the measurement points of the pressure difference across the Bentheimer core and the

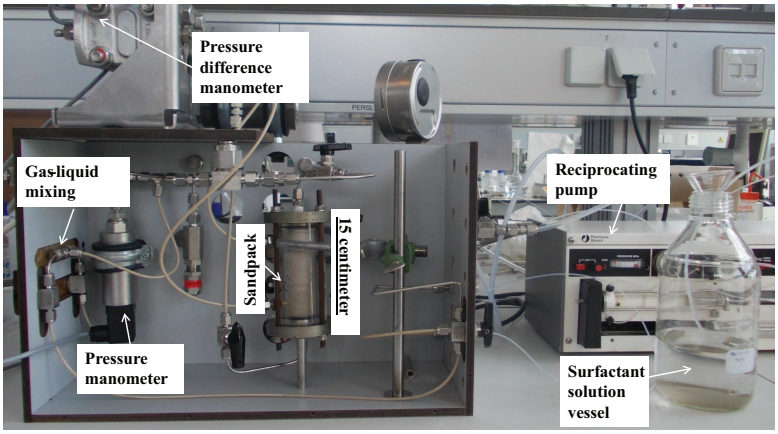

Figure 2.7: Photograph of the right side of the set up (injection module). The surfactant solution is injected from the vessel by the reciprocating pump to mix with the nitrogen gas at the mixing junction. The foam proceeds further through the inlet pressure manometer, foam generator and finally into the porous medium.

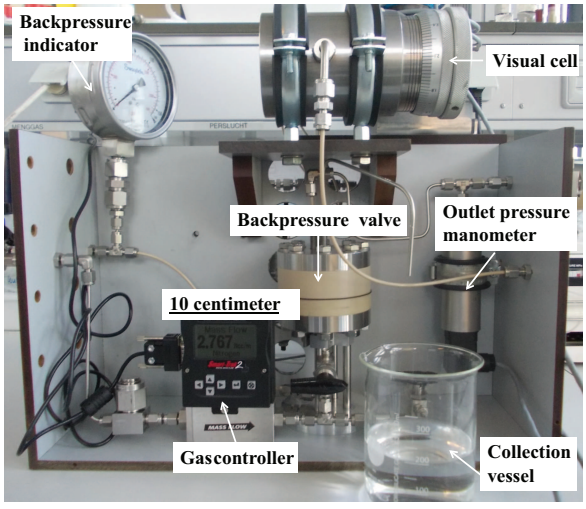

Figure 2.8: Photograph of the left side of the set up (production module). After the porous medium, the foam proceeds through the visual cell, the pressure manometer and the back pressure valve. Finally, it is collected in the fluid collection vessel. The gas controller seen here is a part of the injection module to let the nitrogen gas in the mixing zone on the right side of the set up (Figure 2.7).

Table 2.3: Technical specification of the instruments used in the experiments

Instrument	Measurement	Unit	Brand/model	Range	Accuracy±
Reciprocating pump	Surfactant solution mass	ml/hour	Pharmacia P-900	0 to 500	1.5–2
Manometer	Pressure	bar	Endress+Houser	0 to 65	0.1
Manometer	Pressure difference	bar	Endress+Houser	0 to 3	0.03
Flow controller	Gas mass	slpm[a]	Sierra instruments[b]	0-1000	10

[a]standard liter per minute, [b]Smart Trak® 2 100.

unconsolidated sandpack. There were four pressure measurement points, viz, at the outlet, inlet, and two (for a pressure difference meter) in the middle at 0.06 m apart for the sandpack and 0.09 m apart for the Bentheimer core. The pressure difference manometer ranged between 0-3 barA (19) with the precision ± 30 mbarA. The injection (21) and production side (22) manometers measured absolute pressures in the range 0-65 barA and were ± 100 mbarA precise. We calibrated the pressure manometers with a pressure calibrator 2095PC (range 1 to 10 bar and 3 to 100 bar). We did not measure the temperature in the sandpack experiments. In case of the Bentheimer core experiments, we used a Platinum/Rhodium alloy thermocouple (25) of type R to measure the temperature at the inlet of the core and was 10.0 μV/°C sensitive.

2.3. BULK TESTS

2.3.1. SURFACE TENSION

We used KSV sigma 700/701 tensiometer with a Platinum-Iridium Du Nouy ring with a radius R = 9.545 mm and a radius of the wire (r) = 0.185 mm to note surface tension of the surfactant solutions. The tensiometer measured surface tension 18-20 times to get average values with standard deviation value. The temperature fluctuated between 25 and 28°C during the measurements.

2.3.2. ZETA POTENTIAL AND PARTICLE SIZE

We used the zeta sizer "ZS" from Malvern [70] to measure zeta potential, size and size distribution of the dispersions. The instrument uses Non-Invasive Back Scatter technology (NIBS) to give the highest sensitivity simultaneously with the highest dynamic size and concentration range [70]. The particle size obtained by the technique is a hydrodynamic diameter. The zeta sizer "measures" diffusion coefficients of particles moving under Brownian motion and converts this to a size distribution [71]. For the zeta potential, the instrument applies an electric field across the dispersion. Particles migrate towards the electrode of opposite charge with a velocity measured as a frequency shift or phase shift of an incident laser beam. The instrument converts this velocity to the zeta potential by applying Smoluchowski or Hückel theories (see Lesson 2, Theory of Electrophoresis [36] and Chapter 3.3, Electrophoresis [56]). The temperature was kept 25°C during tests.

2.3.3. SEDIMENTATION

Laser set up Figure 2.9 shows the setup used to study the sedimentation behavior of the dispersions with a red laser of 3 mW power and 632 nm wavelength. We used a cu-

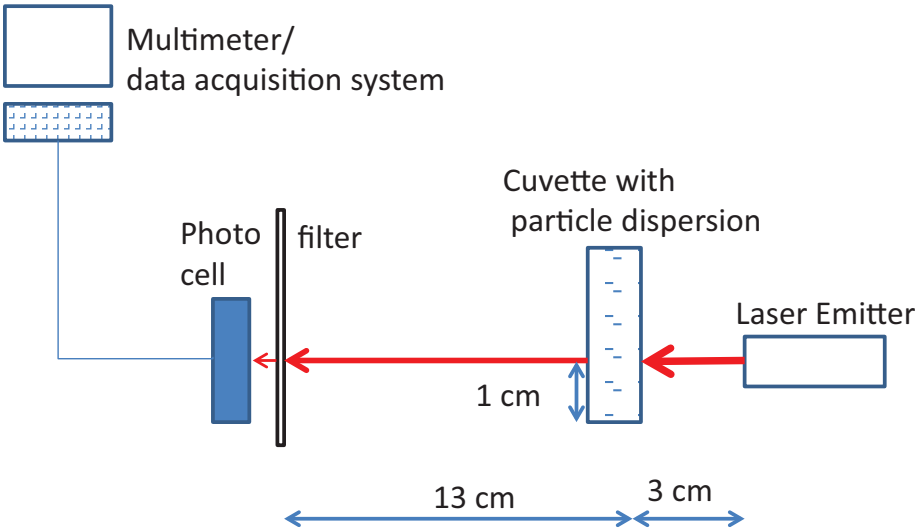

Figure 2.9: Inhouse built Laser set up

vette of Helma® made of Polystyrene with outer dimensions 10 × 10 × 45 mm. The inner dimensions of the cuvette were 5 × 5 × 40 mm. We used a black container to avoid day light. The laser transmits its beam from the right side (Figure 2.9) through cuvette filled with the dispersion. We used a photo diode to collect the transmitted light and a voltage amplifier to transfer the signal to the data acquisition system. We used a A4 size paper as a filter on photo diode to get the reading on a multimeter. The multimeter measured a value of 10.62 V when photo cell detected the full signal and a value of 6.00 V on shutting off the laser source. We considered these reading as upper and lower level for subsequent tests. The change in voltage for an hour show sedimentation in the dispersions.

UV-vis Spectrophotometer The light absorption of the bulk dispersions is studied by ultra violet visible (UV-vis) light 1800 Shimadzo Spectrophotometer. The light of wavelength between 1000 nm to 200 nm falls on the cuvette filled with a dispersion and a reference cuvette filled with deionized water. A computer program records the corresponding absorption spectrum at 0, 20 and 40 minutes.

2.4. ADSORPTION TEST

For the adsorption test, we maintained conditions identical to the Bentheimer foam experiment, i.e. 0.0375 w/w % AOS in DD water with pH 3 and the same liquid velocity (3.11 m/d). Before the adsorption test, we determined the permeability of Bentheimer to doubly distilled water for the flow rates 50-250 ml/hr. We used Potassium Iodide (KI), 7 gm as a tracer. From the start of surfactant injection, we collected effluents at the outlet in plastic tubes by fraction collector at various intervals. We analyzed the effluents for Total Organic Carbon (TOC), using a Dhormann 80 apparatus. The potassium Iodide tracer

was analyzed by an ultraviolet-visible Spectrophotometer UV Mini 1240 (Shimadzu). Figure 2.10 shows the surface tension (N/m) corresponding to the various values of the surfactant concentration (mmol/l). Figure 2.11 shows the ratio of produced concentration to injected concentration vs the injected pore volume in the Bentheimer core during the adsorption test. The profile with plus sign shows the KI transport. The surfactant transport in the Bentheimer for given conditions (0.0375 w/w% AOS in doubly distilled water with pH 3) shows time dependent adsorption. Similarly, Kuhlman [72] notes that AOS does not show a Langmuir isotherm and the solution with lowest concentration and highest concentration move relatively fast. However the intermediate concentrations (slightly lower than CMC) are considerably delayed.

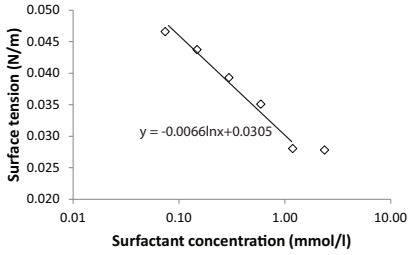

Figure 2.10: Surface tension-surfactant concentration relation:The CMC for AOS in case of DD water was found at 1.2 mmol/l.

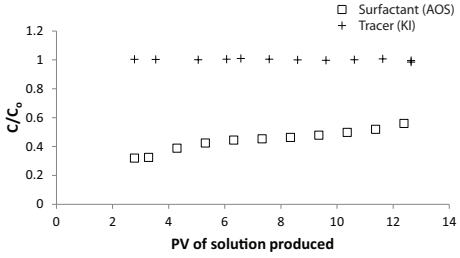

Figure 2.11: Adsorption curve: The porous medium is not saturated with the surfactant, even after 14 PV of injection of 0.0375 w/w % AOS.

3

ESTIMATION OF THE BUBBLE GENERATION-COALESCENCE FUNCTION FROM A FOAM FLOW EXPERIMENT

Since all models are wrong the scientist must be alert to what is importantly wrong. It is inappropriate to be concerned about mice when there are tigers abroad.

G.P. Box [74]

We present here estimation of bubble generation function from a laboratory experiment of co-injecting nitrogen and Sodium C_{14-16} Alpha Olefin Sulfonate (AOS) with a concentration near the critical micelles concentration (CMC) in a Bentheimer sandstone of 3 Darcy. We obtained the steady state pressure drop after injection of 12-15 pore volume of AOS solution. We use a model to explain the experimental pressure drop that leads to four equations, viz. a pressure equation, a water saturation equation, a bubble density equation and a surfactant transport-adsorption equation. We assert that a first estimate of the average bubble density can be obtained from the experimental pressure drop across the measurement points. To test this hypothesis, we used the experimental pressure drop to derive the bubble density as a function of time as if the water saturation were zero. Then we corrected the bubble density generation function for non zero water saturation by considering injected foam quality. Thus obtained bubble generation function is implemented in the COMSOL. To validate this procedure, we compare the simulated pressure drop with the experimental pressure drop. When we consider the flowing fraction of foam, the rate of change of the bubble density during transient state equates to the bubble density

Parts of this chapter have been published in Transport in Porous Media [73].

generation-coalescence function plus the terms accounted for bubble transport by convection and diffusion divided by porosity and saturation.

3.1. INTRODUCTION

Foam can improve a water flood or a gas drive by decreasing the mobility (phase permeability/apparent viscosity) of the displacing fluids in the reservoir [1–3]. Predicting foam behavior in porous media relies on proper modeling of the mobility reduction validated by experiments. In case of co-injection of gas and surfactant solution, i.e. pre-generation of foam, we can use the saturation profiles, surfactant concentration profiles, the effluent water cut and the experimental pressure drop to validate models [23, 38–43, 75]. Ma [76] gives a detailed summary of the literature on foam models. Most modeling attempts are for experiments with surfactant concentrations well above the critical micelles concentration (CMC) where the build up of pressure profiles occurs before one pore volume. There are only a few experimental data reported in the literature with injected concentrations around the CMC, for example by Apaydin [77]. The effluent concentration profile of 0.02 w/w % Suntech IV (an alkyl toluene sulfonate) in case of Berea sand stone indicates a retardation factor of about 12 [78]. Chou [79] have observed the steady pressure drop profile after injecting 3-6 pore volumes (PV) of Chaser CD1040 (an Alpha Olefin Sulfonate) with concentrations near the CMC in case of Berea sandstones. To interpret such an observed delay in the pressure drop one needs models that incorporate the transient development of foam. Therefore our interest is in bubble population models [19, 20, 22, 37, 68] that can explain the transient pressure drop at low concentrations, i.e. around CMC.

The bubble population models, mentioned above, combine bubble density balance inside the multi-phase flow equations. These multiphase flow equations consist of a water equation, an equation for foam that behaves as a gas with an enhanced viscosity μ_f, a bubble density equation and occasionally a surfactant transport equation. We can solve the equations by using the IMPES method (IMplicit Pressure Explicit Saturation) described by Aziz [80]. We follow approach from Friedmann [40], considering local equilibrium between flowing and trapped bubbles. Kovscek [19] argue that some of the trapped bubbles coarsen and remobilize to be replaced by subsequent trapping of flowing bubbles. Therefore, he assumes that the flowing bubble density is equal to the nonflowing (trapped) bubble density. We consider the foam flow in the porous media due to co-injection of gas and surfactant water as a flow of two phases, given by the standard Darcy's law, i.e.

$$u_f = -\frac{k k_{rf}}{\mu_f}(\Delta p_f - \rho_f g), \tag{3.1}$$

where, for foam, u_f is the superficial velocity, k is the absolute permeability, k_{rf} is the relative permeability to foam, ρ_f is the foam density and Δp_f is the observed pressure drop. However, during a transient state of foam flow, μ_f is not constant. To estimate the varying viscosity of foam in the two-phase concept, researchers assume the smallest pores filled with a surfactant solution and other pores with gas bubbles separated by lamellae. A pore level model of foam in porous media consists of bubbles moving in a straight capillary tube [18]. The main resistance of the bubble is due to the lamellae that

separate the bubble from the pore wall [81]. In addition, the surface tension gradient across the moving bubble contributes significantly to the resistance to bubble flow [18]. One can use the added resistance of all bubbles inside the tube to obtain expressions for the apparent foam viscosity. Consequently the bubble density is an important parameter to estimate the foam viscosity with a fitting parameter α [$Ns^{2/3}/m^{4/3}$] as given by Kovscek [19];

$$\mu_f = \mu_g + \frac{\alpha\, n_f}{v_f^{1/3}}, \tag{3.2}$$

where, n_f is the bubble density (number of bubbles per unit distance of the capillary), μ_g is the viscosity of unfoamed gas and v_f is the local interstitial velocity depending on the foamed gas saturation and the fraction of flowing foamed gas.
The bubble density equation, with the apparent viscosity of foam as given above, contains a bubble generation-coalescence function expressed by a source term, R, which is in essence a difference between generation and coalescence rates of bubbles. In most literature, this source term is based on the assumed foam generation-coalescence mechanisms, e.g. lamellae creation by capillary snap-off, bubble division and bubble coalescence by mass transfer between bubbles [20, 21]. For example, Kovscek [19] expresses the generation rate with the gas and liquid velocities and the coalescence rate as a function of the bubble density. Similarly, Zitha [22] proposes a foam generation-coalescence function with an exponential growth of the bubble density for transient foam flow. However, if saturation and flowing fraction of the foam is unknown, an exact bubble generation-coalescence function cannot be directly obtained from the experiments. Therefore, in comparison with previous studies, we propose to determine the bubble generation-coalescence function, i.e. the source term approximately from the experimental pressure drop without a priori knowledge of foamed gas saturation and flowing fraction of foam. In our procedure, a first estimate of the bubble density n_f is obtained from history matching of the experimental pressure drop. Combining Eq. 3.1 and Eq. 3.2, we obtain disregarding μ_g that

$$n_f = \frac{k k_{rf}(\Delta p_f - \rho_f g)}{\alpha\, u_f}(v_f)^{1/3}. \tag{3.3}$$

As gas saturation and flowing fraction of foam is unknown, we assume that foamed gas is the only phase in the porous medium and all foamed gas (foam) is flowing. Therefore, the foam relative permeability, k_{rf} is equal to the permeability, k and the local interstitial velocity v_f is approximately $\frac{u_f}{\varphi}$, using that the water saturation is very low. We hypothesize that in such a case, the source term is the derivative of the bubble density, estimated from the experimental pressure drop with respect to time, $R(n_f) \approx dn_f/dt$. For a low concentration (around CMC), we assume that the viscosity coefficient α varies when the surfactant concentration in the porous medium varies. For such cases, we calculate α from the surface tension of the injected surfactant concentration derived from the work of Hirasaki [18]. The procedure to estimate $R(n_f)$ is only a first estimate. Once we estimate the bubble density from the experimental pressure drop, we can estimate the flowing fraction of foam (bubbles) by the approximation used by Tang [82] elaborated in subsection 3.3.3. In addition, we calculate the water saturation with the estimated

bubble density for a constant foam quality. We assume that the gas saturation remains below the critical gas saturation; therefore foam does not collapse [58]. With the saturation and the flowing fraction of foam is known, the flow model gives a simulated pressure drop history that corresponds to the experimental pressure drop history. With the values of the pressure drop from experiment and simulation comparable to each other, we propose a realistic contribution of the derivative of the bubble density to the source term.
To validate our procedure, we used a foam flow experiment that used co-injection of N_2 gas and AOS solution at critical micelle concentration, i.e. at 0.0375 w/w % in acidic water (pH 3) in case of a Bentheimer core of 3 Darcy. In chapter 6 we use the experiment for a comparison with experiments where particles were co-injected. The ideal stability of these particles is found at the acidic pH, i.e. pH 3 as shown in chapter 5. Therefore we selected the AOS solution of pH 3. Subsection 2.2 from chapter 2 describes the experimental set-up, sample preparation and measurement techniques. Section 3.3 from this chapter is about modeling where subsection 3.3.1 describes the 1-D model considering downward vertical flow. We describe the equations for water-foamed gas and for bubble density with a bubble generation-coalescence function in subsection 3.3.2. In addition, the pressure equation is used to simulate the pressure drop. In the same subsection 3.3.2, we include two model equations for the surfactant adsorption and transport. We explain the procedure to estimate the source term $R(n_f)$ from the measured pressure drop in terms of the bubble density in subsection 3.3.3. Subsection 3.3.4 gives the procedure to estimate α, a fitting parameter in the viscosity Eq. 3.2 from the surfactant concentration. We describe boundary conditions in subsection 3.3.5. We use experimental conditions for the numerical simulation. The model equations from subsection 3.3.2 are converted into weak form [83] in subsection 3.3.6 to facilitate implementation in COMSOL, a commercial finite element software package. Subsequently, we describe the simulation results (subsection 3.3.7) in terms of the water saturation and flowing fraction of foam. In addition, we describe the relation between the bubble density and surfactant concentration for the given simulation. Further, instead of splitting the source term $R(n_f)$ like in most studies, we investigate terms on the other side of the bubble density equation, i.e. accumulation, convection and dispersion (diffusion). We determine the relative importance of the bubble accumulation and convection-diffusion terms in subsection 3.3.8 with the flowing fraction of foam and the water saturation. In subsection 3.4 we compare the experimental pressure drop and the simulated pressure drop for the case of Bentheimer. We end with some conclusions about the procedure used, about the foam generation-coalescence function and about the estimate of the experimental pressure drop.

3.2. FLOW EXPERIMENTS

For flow experiments in Bentheimer, we used a 0.0375 w/w % AOS in acidic water (pH 3, CMC). Chapter 2, Section 2.1.2 gives the preparation of the surfactant solution. As the goal of chapter 3 is to show the procedure of extracting parameters for the bubble generation-coalescence function, we selected only one experiment for reasons of concise presentation. The foam flow was from top to bottom. We maintained 4 barA back pressure throughout the experiment. Before the foam experiment, we conducted permeability test as described in Appendix A. We started the measurements for the foam

Table 3.1: Summary of the foam flow experiment for Bentheimer

Porous media	**Solvent**	**AOS** w/w **%**	**BP** **barA**	u_{inj}^{atm} **m/d**	u_f **m/d**	u_w **m/d**	ΔP $\times 10^5$ **Pa/m**
Bentheimer	Acidic (pH 3)	0.0375	4	6.8	1.70	3.11	23.0±0.2

BP = Back pressure, Atm. = atmospheric pressure, u_{inj}^{atm} = gas velocity at the injection for an atmospheric pressure, u_f = foam velocity.

flow experiment at t=0 seconds by flushing a surfactant solution of 0.0375 w/w % concentration (≈ CMC) at a rate of 3.11 m/d[1]. We waited to achieve a steady liquid pressure drop of 15300 Pa/m between measuring points. At t=3610 seconds (after 94 ml of AOS solution passed into the core), we injected N_2 gas in the already flowing AOS solution at a flow velocity of 6.8 m/d. The inlet and outlet pressure at the time of gas injection were 4.22 and 4.18 barA respectively. After injection of approximately 600 ml of AOS solution with a corresponding amount of gas, we stopped the measurements by closing the gas and liquid flow. The measured temperature fluctuated between 16 and 17°C. Table 3.1 summarizes the experiments mentioned above.

3.3. MODELING

3.3.1. PHYSICAL MODEL

We consider isothermal foam as flow of two phases as proposed by Buckley [57], i.e. a water AOS solution and a high viscosity gaseous phase (foam). We assume that the flow of the foam phase and water phase obeys Darcy's law for multiphase flow. The total superficial velocity u_t, i.e. the sum of the superficial velocities of water and foam phase and the corresponding experimental values of the pressure drop, ΔP_w and ΔP_f are expressed as

$$u_t = u_w + u_f, \tag{3.4}$$

$$u_t = -\frac{kk_{rw}(\Delta P_w - \rho_w\, g)}{\mu_w} - \frac{kk_{rf}(\Delta P_f - \rho_f\, g)}{\mu_f}. \tag{3.5}$$

We drop the subindexes w and f in the pressure drop ΔP (the pressure difference divided by the distance between the measurement points), thus ignoring capillary pressure. The foam phase consists of the bubbles bounded by AOS soap films. The resistance to bubble flow in a cylindrical tube can be considered as an apparent viscosity of the foam phase, often expressed as an extrapolation of the Bretherton equation [81] by Hirasaki [18] and Kovscek [19], i.e.

$$\mu_f = \mu_g + \alpha \frac{n_f}{v_f^c}, \tag{3.6}$$

where μ_g is the gas viscosity, n_f is the bubble density and α is a fitting parameter for the surfactant effect. Bretherton [81] used $c = 1/3$ for the exponent. The local interstitial

[1] 1 m/day= 1.15×10^{-05} m/s

foam velocity v_f is equal to $u_f/(\varphi X_f S_g)$, where X_f is the flowing foam fraction and S_g is the total saturation of foam. The flowing foam saturation S_f is related to the total foam saturation by $S_f = X_f S_g$. The superficial foam velocity depends on the pressure inside the core, i.e. $u_f = u_{inj}^{atm} p_{atm}/p_{inj}$, where u_{inj}^{atm} is a foamed gas velocity at the injection point for atmospheric pressure, p_{atm}. We denote the injection pressure at the inlet of the porous medium by p_{inj}. Brooks and Corey [59] give the relative permeabilities for water (k_{rw}) and unfoamed gas (k_{rg}) by

$$k_{rw} = k'_{rw} S_{we}^{\frac{2+3\lambda}{\lambda}}, k_{rg} = k'_{rg}(1-S_{we})^2(1-S_{we}^{\frac{2+\lambda}{\lambda}}), \tag{3.7}$$

where λ is pore size distribution index, k'_{rw} (=1) is the permeability to water at the irreducible saturation of gas (S_{gr}), which we take equal to zero. The permeability to gas at an irreducible water saturation S_{wc} is k'_{rg} (=1). Moreover, $S_{we} = (S_w - S_{wc})/(1-S_{wc})$ is the effective water saturation, where S_w is the water saturation. We assume a slightly different relationship than proposed by Kovscek [19], where the foam relative permeability is a fraction of gas relative permeability connected by the flowing fraction of foam, i.e. $k_{rf} = X_f k_{rg}$.

3.3.2. MODEL EQUATIONS

We describe foam flow through porous media with four equations: a mass balance equation for the water-foamed gas solution, a pressure equation, a bubble concentration equation and a surfactant transport-adsorption equation. Lake [84] describes the flow of water with dissolved AOS in the vertical direction as a function of its saturation, viz.

$$\varphi\partial_t(\rho_w\, S_w) - \partial_x\left(\rho_w\, \frac{k k_{rw}}{\mu_w}(\partial_x p - \rho_w\, g)\right) = \partial_x\left(D_{cap}\rho_w \partial_x S_w\right), \tag{3.8}$$

where ρ_w is the water density, k_w is the water permeability, μ_w is the water viscosity, D_{cap} is the capillary diffusion coefficient and p is the pressure. We disregard the saturation dependence of the capillary diffusion coefficient. In order to derive the pressure equation we assume that the water density ρ_w is pressure dependent. Dividing the equation by ρ_w and rearranging the terms we obtain

$$\begin{aligned}&\varphi\partial_t\, S_w + \varphi S_w \partial_t \ln\rho_w - \partial_x\left(\frac{k k_{rw}}{\mu_w}(\partial_x p - \rho_w\, g)\right)\\ &-\left(\partial_x \ln\rho_w\right)\left(\frac{k k_{rw}}{\mu_w}(\partial_x p - \rho_w\, g)\right) = \partial_x\left(D_{cap}\partial_x S_w\right),\end{aligned} \tag{3.9}$$

where we disregard the term involving differentiation towards ρ_w in the diffusion term, i.e. $\left(\partial_x \rho_w\right)\left(D_{cap}\partial_x S_w\right)$. For the mass balance of foam we take into account trapped gas. We consider that foam flow through porous media consists of three flow regimes, as described by Ettinger [68], i.e. 1. moving liquid 2. foam as a bubble train and 3. trapped bubble train. Therefore, for the given physical model, the trapped foam corresponds to the trapped bubbles and the flowing foam corresponds to the flowing bubbles. We assume the number of trapped bubbles equal to the number of flowing bubbles as by Kovscek [19]; i.e. $S_f n_f + S_t n_t$ becomes $S_g n_f$, where S_t is trapped gas saturation, n_f and

n_t are the number of flowing and trapped bubbles per distance of the porous medium. The relative permeability of the trapped gas is zero. Therefore, the overall mass balance equation for the foamed gas (foam) reads

$$\varphi\partial_t(\rho_f(p)S_g) - \partial_x(\rho_f(p)\frac{kk_{rf}}{\mu_f}(\partial_x p - \rho_f(p)\ g)) = \partial_x\left(\rho_f(p)D_{cap}\partial_x S_g\right), \tag{3.10}$$

where $\rho_f(p)$ is a foamed gas density, which depends on the pressure at which the foam is flowing through the porous medium. After expanding the differentiation and dividing by $\rho_f(p)$ we obtain

$$\begin{aligned}\varphi\partial_t\ S_g + \varphi S_g\partial_t \ln\rho_f(p) - \partial_x\left(\frac{kk_f}{\mu_f}(\partial_x p - \rho_f(p)\ g)\right)\\ -\partial_x\left(\ln\rho_f(p)\right)\left(\frac{kk_{rf}}{\mu_f}(\partial_x p - \rho_f(p)\ g)\right) = \partial_x\left(D_{cap}\partial_x S_g\right),\end{aligned} \tag{3.11}$$

where we disregard the term, $\left(\partial_x\rho_f\right)\left(D_{cap}\partial_x S_g\right)$ involving differentiation towards ρ_f in the diffusion term. We introduce c_w and c_f as the compressibilities for water and foamed gas respectively. Thus the term $\partial_t \ln\rho_f(p) = c_f\partial_t p$ and the term $\partial_x \ln\rho_f(p) = c_f\partial_x p$. Addition of Eqs. (3.9) and (3.11) leads to the pressure equation, i.e.

$$\begin{aligned}\varphi\ (S_w c_w + S_g c_f)\partial_t p - \partial_x\left((\frac{kk_{rw}}{\mu_w} + \frac{kk_{rf}}{\mu_f})\partial_x p\right) + \partial_x\left(\frac{kk_{rf}}{\mu_f}\rho_f(p)\ g + \frac{kk_{rw}}{\mu_w}\rho_w(p)\ g\right)\\ -c_w\partial_x\left(p\right)\left(\frac{kk_{rw}}{\mu_w}(\partial_x p - \rho_w\ g)\right) - c_f\partial_x(p)\left(\frac{kk_{rf}}{\mu_f}(\partial_x p - \rho_f(p)\ g)\right) = 0,\end{aligned} \tag{3.12}$$

where the capillary diffusion terms cancel. The flowing bubble density equation considers accumulation of bubbles in the foam phase convected with the flow. It consists of an accumulation term, a convection term, a kinetic bubble generation-coalescence function estimated from the experiment and diffusion terms. The bubble density equation is given by

$$\begin{aligned}\varphi\partial_t(S_g n_f) - \partial_x\left(n_f\ \frac{kk_{rf}}{\mu_f}(\partial_x p - \rho_f(p)\ g)\right) - \varphi\ S_g R(n_f) =\\ X_f(n)[\partial_x\left(\varphi S_g D_{n_f}\partial_x n_f\right) + \partial_x\left(D_{cap}n_f\partial_x S_g\right)],\end{aligned} \tag{3.13}$$

where $R(n_f)$ is a source term estimated by a procedure that uses the Hirasaki-Lawson equation. D_{n_f} and D_{cap} are the bubble diffusion and capillary diffusion terms to consider diffusion of flowing fraction of foam bubbles. The model equations for the convection, adsorption and diffusion (CDA) of the surfactant transport are taken from Trogus [17] as

$$\partial_t C + \frac{u_w}{\varphi}\partial_x C + \frac{A_s}{\varphi}\partial_t C_s = D_s\frac{\partial^2 C}{\partial x^2} \tag{3.14}$$

$$\partial_t C_s = K_a(Q_s - C_s)C - K_d C_s, \tag{3.15}$$

where, C is the surfactant concentration in the water, C_s is the adsorbed surface concentration, A_s is the rock interstitial area per unit volume (total volume), Q_s is the total adsorption capacity of the adsorbent, K_a is the rate of adsorption, K_d is the rate of desorption and D_s is the surfactant diffusion coefficient. We assume that the surfactant concentration in the lamellae and the injected water are the same.

3.3.3. ROUGH ESTIMATION OF BUBBLE DENSITY AND THE SOURCE TERM

To estimate the bubble density, we follow the bubble population approach adopted from Kovscek [19] for multiphase flow. Darcy's law for the foam velocity during multiphase flow reads

$$u_f = -\left(\frac{k k_{rf}}{\mu_f}(\partial_x p - \rho_f(p)\, g)\right) = -\left(\frac{k k_{rf}\, v_f^{1/3}}{\alpha\, n_f}(\partial_x p - \rho_f(p)\, g)\right), \tag{3.16}$$

where we substitute the foam viscosity from Eq. 3.6. Hence we obtain

$$\partial_x p = -\frac{\alpha\, n_f}{v_f^{1/3}}\frac{u_f}{k k_{rf}}, \tag{3.17}$$

where we disregard the gravity effect; $\rho_f(p)\, g$. Integration of Eq. (3.17) between the measurement points, x_L and x_R leads to an expression for the pressure drop, i.e.

$$\int_{x_L}^{x_R} \partial_x p\, dx = -\int_{x_L}^{x_R} \frac{\alpha\, n_f\, u_f}{v_f^{1/3}\, k k_{rf}} dx. \tag{3.18}$$

Here x_L, x_R denote the left and right position of the pressure difference measurement points. Initially we consider only single phase flow. As the saturation and flowing fraction of foam is unknown, we assume that foaming gas is the only phase in the porous medium and all the foamed gas is flowing. Therefore, we assume that the foam relative permeability equal to the permeability at water saturation close to zero, $k_{rf} = k_g$. For water wet media the nonwetting phase permeabilities is close to the single phase permeabilities at small water saturation [59]. As we assume very low water saturation, the local interstitial velocity is equal to the interstitial velocity, i.e. $v_f = \frac{u_f}{\varphi\, S_g} \approx \frac{u_f}{\varphi}$. We assume that the quantities on the right side of the Eq. 3.18 can be approximated by their average value between the two measurement points, i.e.

$$\frac{p(x_R) - p(x_L)}{x_R - x_L} = -\frac{\alpha\, n_{f,av}\, u_{f,av}}{v_{f,av}^{1/3}\, k_{av}}.$$

We get the bubble density (ignoring the negative sign for flow) in terms of experimental pressure drop as

$$n_{f,av}(t) = \frac{k_{av}\, v_{f,av}^{1/3}}{\alpha\, u_{f,av}}\frac{p(x_L) - p(x_R)}{x_R - x_L}. \tag{3.19}$$

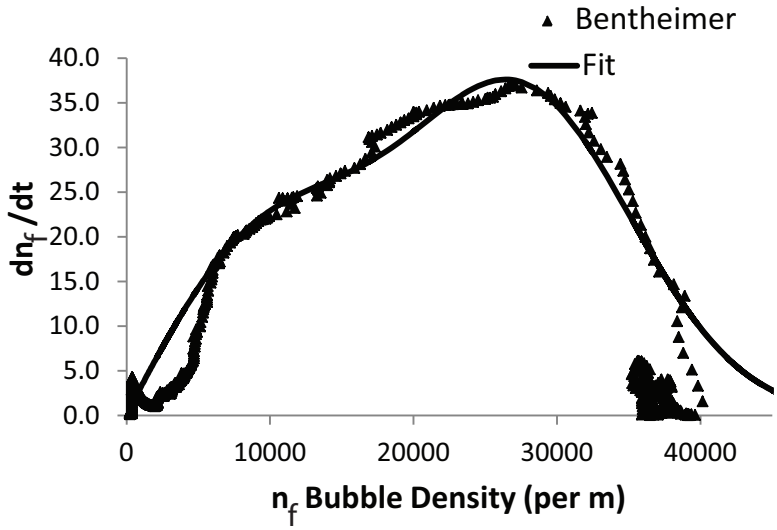

Figure 3.1: The bubble density ($n_{f,av}$) versus the derivative of bubble density over time ($dn_{f,av}/dt$) in case of Bentheimer. We used the experimental pressure drop to derive the bubble density (Eq. 3.3) as a function of time as if the water saturation were zero. Then we corrected ($dn_{f,av}/dt$) for non zero water saturation by considering injected foam quality. Thus obtained bubble generation function is implemented in COMSOL. For the relation between the source term $R(n_f)$ and $dn_{f,av}/dt$), please refer to subsection 3.3.3.

As the saturation and flowing fraction of foam are unknown, we determine part of the bubble generation-coalescence function, i.e. the source term $R(n_f)$ in Eq. 3.13 from the experimental pressure drop in terms of the estimated bubble density as

$$R(n_{f,av}) \approx \frac{dn_{f,av}}{dt}. \tag{3.20}$$

Figure 3.1 shows bubble density ($n_{f,av}$) versus the derivative of bubble density over time ($dn_{f,av}/dt$) in case of Bentheimer. We calculated the derivative $dn_{f,av}/dt$ as the slope of the line that joins fifty $n_{f,av}(t)$ values to the corresponding $t = 50$ seconds with the LINEST[2] function from Microsoft Excel. We considered the interval of 50 seconds optimal in avoiding spurious scattering (for short times) and loosing details (for long times). We used a fitted exponential form of $dn_{f,av}/dt$ versus n_f for Bentheimer experiment. We show the fitted curve in the figure as a line.

[2]The "least squares" method calculates a straight line that best fits your data, and then returns an array that describes the line.

3.3.4. ESTIMATION OF VISCOSITY COEFFICIENT α FROM SURFACTANT CONCENTRATION

The apparent foam viscosity due to the shape of the bubble in a cylindrical tube is given by Hirasaki [18] as

$$\mu_{app}^{shape} = 0.85 \frac{(\mu_w n_L R)}{(\frac{r_c}{R})} (\frac{3\mu_w U}{\sigma})^{-1/3} [(\frac{r_c}{R})^2 + 1], \tag{3.21}$$

where, μ_w is the water viscosity, R is the capillary radius, r_c is the radius of curvature of lamella and σ is the surface tension between surfactant water and gas. This equation can be considered similar to Eq. 3.6 of viscosity as

$$\mu_{app}^{shape} = \frac{\alpha_{shape}\, n_f}{v_f^{1/3}}, \tag{3.22}$$

where, $n_L = n_f$, i.e. the lamellae density is equal to the bubble density and $U = v_f$, i.e. the gas velocity in the capillary tube from Eq. 3.21 is equal to the local interstitial foam velocity in Eq. 3.6. The resistance to flow due to the shape of the bubble can be accounted for by the parameter α_{shape} as

$$\alpha_{shape} = 0.85 \frac{\mu_w R}{(\frac{r_c}{R})} (\frac{3\mu_w}{\sigma})^{-1/3} [(\frac{r_c}{R})^2 + 1]. \tag{3.23}$$

We assume that the radius of curvature of the lamella is equal to the capillary radius, i.e. $r_c = R$. Therefore Eq. 3.23 simplifies as,

$$\alpha_{shape} = 1.18 R\, \mu_w^{2/3}\, \sigma^{1/3}. \tag{3.24}$$

Hirasaki [18] gives the resistance of surface tension gradient to bubble flow in the capillary tube 10 times higher than the resistance due to the shape of the bubble. Therefore the total resistance can be considered as a sum given by,

$$\alpha = \alpha_{shape} + 10\alpha_{shape}. \tag{3.25}$$

Therefore α varies when the surfactant concentration in the porous medium varies at low concentration (below CMC). We can assume the viscosity coefficient α constant for the case where the adsorption condition is satisfied, i.e. the porous medium is saturated with surfactant, which happens at high concentration.

3.3.5. BOUNDARY CONDITIONS

Here we define boundary conditions based on experiments to be used in the simulations.

Bubble density: The boundary condition for the bubble density at the injection point $x = 0$, is given by

$$n_f(x = 0, t) = n_{init} + (n_{inj} - n_{init})\, r(t), \tag{3.26}$$

where n_{init} is the initial bubble density, n_{inj} is the bubble density at the point where the bubble-water mixture enters in the core. We estimated the bubble density from the Eq. 3.3 by replacing $\Delta p_f - \rho_f g$ with $\Delta p_w - \rho_w g$ assuming that the initial pressure drop observed for two-phase flow is equal to the pressure drop obtained for single phase water flow. The ramp function $r(t)$, used to avoid discontinuous initial conditions is zero for $t \leq 0$ and one for $t \geq 1$. It increases linearly with time in the transition region. For simplicity, we considered $n_{init} = n_{inj}$ in all the cases of our simulations. At the production point $x = L$ the derivative of the bubble density is given by

$$\partial_x n_f(x = L, t) = 0. \tag{3.27}$$

Aqueous phase saturation: Researchers have considered the flowing fraction of foamed gas during transient flow constant, e.g. by Falls [20], Zitha [22] or varying, e.g. by Apaydin [77] and Tang [82]. In order to estimate the aqueous phase saturation, we consider the flowing fraction of foam dependent on the bubble density with the relation $X_f = (\frac{n_f}{n_{inj}})^{-0.4}$, modified from the work by Tang [82] with the injection bubble density, n_{inj} to make the flowing fraction dimensionless. The bubble density at the injection side is given by n_f and is equal to $n_{f,avg}$ estimated in the previous subsection 3.3.3. At the injection side $x = 0$, we infer the water phase saturation from the foam quality η, i.e.

$$\eta = \frac{u_f}{u_w + u_f}. \tag{3.28}$$

We derive the water saturation boundary condition at the injection side by eliminating the pressure drop from Darcy's law

$$\begin{aligned} u_w &= -\frac{kk_{rw}}{\mu_w}\left(\nabla p \pm \rho_w g\right), \\ u_f &= \frac{-\frac{kk_{rf}}{\alpha\, n_f}\left(\nabla p \pm \rho_f g\right)}{\left(\frac{u_f}{\varphi S_g X_f}\right)^{1/3}}, \end{aligned} \tag{3.29}$$

where the minus sign in $\pm$ is for the flow from the top to the bottom and the plus sign is for the flow from the bottom to the top. The foam injection velocity is given by the mass injection velocity of nitrogen multiplied by the density and is equal to the injection velocity u_{inj}^{atm} at atmospheric pressure. Eliminating the pressure drop from the water equation in Eq. 3.29 with $\nabla p = \left(\mu_w u_w / kk_{rw}\right) \pm \rho_w g$, we obtain

$$u_{inj}^{atm}\frac{p_{atm}}{p_{inj}} = -\frac{kk_{rf}}{\alpha n_f}\left(\frac{\varphi S_g X_f}{u_{inj}^{atm}\frac{p_{atm}}{p_{inj}}}\right)^{1/3}\left(\frac{\mu_w u_w}{kk_{rw}} \pm \left(\rho_w - \rho_f\right) g\right), \tag{3.30}$$

where p_{inj} is the pressure at the injection point. This equation is solved to find the saturation at the injection point. Figure 3.2 shows the resultant water saturation S_{bound} as a function of bubble density for the experiment with the Bentheimer. The water saturation varies from the initial (S_{init}) to the final water saturation (S_{bound}) and has Dirichet boundary condition $S_{init} + (S_{bound} - S_{init})\, r(t)$, where the ramp function is again used to

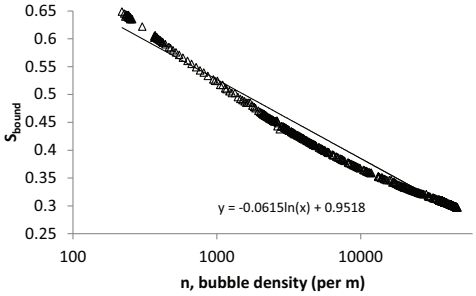

Figure 3.2: S_{bound} is estimated from the bubble density considering constant foam quality. The flowing fraction of foam is considered as a function of the estimated bubble density.

avoid a discontinuous saturation at the injection side. A non-zero water compressibility c_w is required to avoid incompressible flow at the initial condition because $S_w = 1$ and $S_g = 0$. At the production point ($x = L$), we specify the derivative of the saturation zero [85], i.e. $\partial_x S_w = 0$. Once the water saturation and flowing fraction of foam is known, we calculate the other saturations, i.e. $S_g = 1 - S_w$ and $S_f = X_f\, S_g$.

Surfactant concentration: We applied Dirichet boundary condition at the inlet with the prescribed value of surfactant concentration, C, as $C_{init} + (C_{bound} - C_{init})r(t)$ where, C_{init} is initial surfactant concentration and C_{bound} is produced surfactant concentration. $C = C_{init}$ at t=0 (at the time of gas injection) at all distances (x), $C = C_{init}$ at $x = 0$ for the whole duration t, $C = C_{bound}$ at $x = L$ for all duration t. During the foam experiment with Bentheimer, we injected 3 pore volumes of surfactant solution before gas co-injection. From the adsorption experiment, the adsorbed surface concentration, C_s after 3 pore volumes of surfactant is 3×10^{-6} mmol/m^2 at t=0 for all x.

3.3.6. NUMERICAL SCHEME

We consider here the Bentheimer experiment with a low concentration (≈ CMC) and with a varying foam viscosity. We calculated the viscosity coefficient α from Eq. 3.25 with varying surfactant concentration, calculated from the adsorption test. We used the four 1D equations from subsection 3.3.2 in their weak form [83] along coordinate x, i.e. the water saturation equation (Eq. 3.8), the pressure equation (Eq. 3.12), the bubble density equation (Eq. 3.13) and the surfactant transport-adsorption equation (Eq. 3.15). We implemented the model in the multiphysics module of the commercial finite element software; COMSOL version 5.0. A 1-D geometry consists of a single domain with a length of 0.17 m for the Bentheimer core. We used the quadratic Lagrangian elements with an element size of 0.00017 m for the Bentheimer core. A time dependent solver (generalized alpha) uses a linear predictor and an amplification for high frequency of 0.75 (dimensionless) [86]. In addition, we split the accumulation term of the bubble density and saturation product equation (Eq. 3.19) in COMSOL into a sum, containing a saturation derivative and a bubble density derivative. We based the termination technique on a prescribed tolerance, i.e. sum of absolute error (for each dependent variable)

and relative error with maximum iterations of 5. The convergence criterion for the solution was to arrive at a solution within the specified tolerance. The program accepted the step if the solver's estimate of the (local) absolute error in the solution committed during a time step is smaller than the sum of absolute and relative error.
We obtained the velocity, pressure, saturation and surfactant concentration at each node point. Further, the simulation of the foam propagation lasts for $t = 10000$ seconds with output after each 100 seconds. The gas compressibility c_f for ideal gas is $1/p$ and the water compressibility is considered to be 4.58×10^{-10} Pa^{-1}. Nitrogen has a density of 1.15 kg/m^3 at atmospheric pressure. The gravity term $(\rho_f(p)\ g)_{av}L$, where L is length between measurement points, is about 0.69 Pa, which is negligible with respect to the measured pressure difference. We assumed that the initial value of λ is 5 for Bentheimer core with complex mineral composition being slightly larger for the medium with a narrow range of pore sizes [59]. The capillary radius is given by capillary theory; $R = \sqrt{\frac{8k}{\varphi}}$ [87], k the permeability of the core and φ is the porosity of the core. We obtained the value of the viscosity coefficient, α_{shape} in Eq. 3.24 from the surface tension corresponding to the surfactant concentration. Maximum adsorption capacity, Q_s (mmol/m^2) is equal to $Q_{eqd}/(S_{sap}M_{ism})$, where, Q_{eqd} is equilibrium adsorption density (0.45 mg/g). The specific surface area of pores is denoted by S_{sap} (10 m^2/g). The injected surfactant molecular weight, M_{ism} is 315 mg/mmol. We assume that the weight of the core, W_c is 200 grams. We calculated rock interstitial area, A_s by $S_{sap}W_c/(PV)$ as $20\times\ 10^6$ m^2/m^3. The fitting parameters for the adsorption curve of the single phase flow simulation are adsorption parameters k_a and k_d. Table 3.2 shows the parameters the simulation uses.

3.3.7. NUMERICAL RESULTS

The main output of the foam flow simulation is the pressure drop, water saturation and bubble density. As our primary goal in this work was to relate the bubble generation function to the experimental pressure drop, we considered a detailed convergence analysis for such a non-linear problem outside the scope of current work. In case of the Bentheimer core for a low concentration, we compared the surfactant concentration and the surfactant adsorption from simulation with the experimental results.
We measured the effect of spatial grid and temporal density on the simulated pressure drop profile. The solution is "mesh convergent" as mesh refinement from 0.00017 m to 0.00005 m did not significantly change pressure drop profile. Similarly the change in prescribed tolerance, i.e. temporal density from 1×10^{-8} to 1×10^{-6} did not change the pressure drop profile. Numerical experiments study the effect of perturbation of parameters, i.e. capillary diffusion, D_{cap} and bubble diffusion, D_{nf} on the pressure drop profile. Initially we selected parameters capillary diffusion, D_{cap} , 1×10^{-8} m^2/s (here taken as constant) and bubble diffusion D_{nf} , 1×10^{-7} m^2/s. We followed an optimization routine in COMSOL for different values of bubble diffusion and capillary diffusion for a minimization of the difference between experimental and predicted pressure drop. Table 3.2 shows the optimum values, which simulate result closer to the experimental result. Figure 3.3 and Figure 3.4 give a sense of the impact of the possible uncertainties in the pressure profile for the given values of bubble diffusion and capillary diffusion respectively.

Table 3.2: Parameters used for implementation of the model in the commercial software

Notation	Units	Description	Value
		Fluid properties	
α	$[10^{-7}]$ $Ns^{2/3}/m^{4/3}$	Estimated viscosity coefficient	4.73-4.39
μ_w	$[10^{-5}]$ N s/m^2	Water viscosity	100
μ_g	$[10^{-5}]$ N s/m^2	Gas viscosity	8.5
C_{AOS}	[] mmol/l	Surfactant concentration	1.19
M_{AOS}	g/mmol	Molecular weight of AOS	0.315
C_{CMC}	[] mmol/l	Critical micelle concentration	1.19
pH	[-]	pH of the solution	3.30
u_{inj}^{atm}	$[10^{-5}]$m/s	Injected Gas velocity	7.88
u_f	$[10^{-5}]$m/s	Foam velocity	1.97
u_w	$[10^{-5}]$m/s	Injected liquid velocity	3.76
η	-	Foam quality $(u_f/(u_w+u_f))$	0.33
D_{cap}	$[10^{-7}]$ m^2/s	Capillary diffusion coefficient	9.30
D_{n_f}	$[10^{-5}]$ m^2/s	Bubble diffusion	2.20
n_{inj}	/m	Injection bubbles density	231.00
n_{init}	/m	Initial bubbles density	231.00
n_{inf}	/m	Maximum bubbles density	47180.00
D_s	$[10^{-7}]$ m^2/s	Surfactant diffusion	2.00
C_s	$[10^{-5}]$ mmol/m^2	Initial surfactant adsorbed	0.30
S_{init}		Initial water saturation	0.99
		Porous media properties	
φ	-	Porosity	0.21
λ	-	Pore size distribution index	5.00
k	$[10^{-12}]$ m^2	Permeability	3.00
L	m	Length of the core	0.17
R	$[10^{-5}]$ m	Capillary radius	1.10
A_s	$[10^{6}]$ m^2/m^3	Rock interstitial area	20.00
p_{exit}	barA	Pressure at the exit	4.10
Q_s	$[10^{-5}]$ mmol/m^2	Maximum adsorption capacity	14.28
k_a	$[10^{-5}]$ mg/gs	Surface adsorption parameter	5.00
k_d	$[10^{-5}]$ /s	Surface desorption parameter	90.00

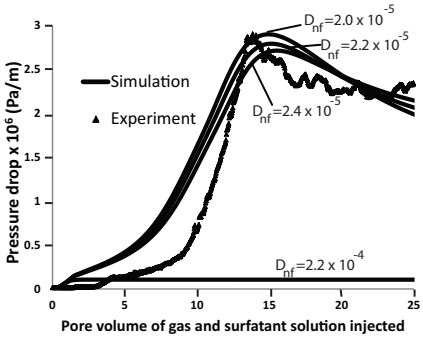

Figure 3.3: Variation in bubble diffusion, D_{nf}. Capillary diffusion is constant, e.g. D_{cap} =9.3 × 10^{-7} m^2/s.

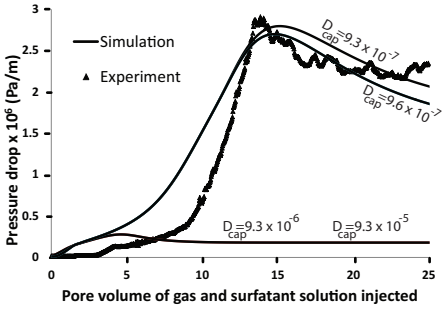

Figure 3.4: Variation in capillary diffusion, D_{cap}. Bubble diffusion is constant, e.g. D_{nf} =2.2 × 10^{-5} m^2/s

Saturation profile: Figure 3.5 shows the simulated saturation profile for the foam flow across the Bentheimer core. Change in the initial condition from a step function to a tanh has a minor but noticeable effect on the results. The curves show the saturation across the length of the core at the indicated times in seconds and in pore volumes (PV) in brackets. The 100 second curve shows that the saturation at the entrance of the Bentheimer is ≈ 0.62. As time passes, i.e. 200 seconds after co-injection of the surfactant solution and gas, the water saturation shows typical front as observed in the article by Buckley and Leverett [57]. After 5000 seconds, the saturation increases, leading to a decrease in the pressure drop. At the end of the simulation (10000 seconds), the water saturation is still a decreasing function of the distance from the injection point. Figure 3.6 shows the flowing fraction of foam. As the time passes the flowing fraction decreases. The flowing fraction of foam is varying during the transient state and constant at steady state. At the steady state the flowing fraction is ≈ 0.12, which is similar to the values mentioned by Tang [82].

Bubble density profile: Figure 3.7 shows the simulated bubble density profile along with the corresponding surfactant concentration profile for Bentheimer. As time passes, i.e. 100 seconds to 1000 seconds, the bubble density increases from 231 $/m$ at the inlet to a maximum value of 47810 $/m$ at the exit of the Bentheimer core. The bubble density continues to increase even though water saturation increases after 5000 seconds as shown in Figure 3.5. The variation in surfactant concentration affects the bubble density via varying viscosity coefficient α in Eq. 3.2. The bubble density increase is directly proportional to the surfactant concentration increase in the core. The surfactant concentration (dotted curve) propagates as a moving front (100 seconds, 200 seconds-1000 seconds). At the end of the simulation, the concentration is almost equal everywhere, i.e. $C_{produced}/C_{injected}$ = 0.95, where $C_{produced}$ is the surfactant concentration in the produced solution, while $C_{injected}$ is the injected surfactant concentration. Corresponding bubble density is not equal everywhere affecting the calculation of the source term from

the experimental pressure drop between the measurement points.

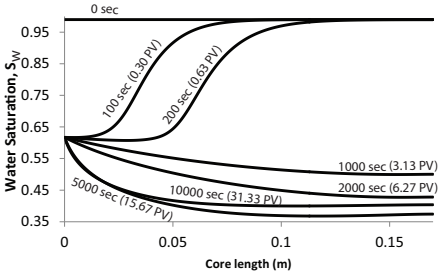

Figure 3.5: Numerical saturation profile in the direction of x for Bentheimer case.

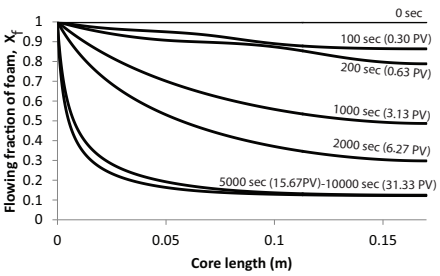

Figure 3.6: Flowing fraction of foam in the direction x for Bentheimer case.

3.3.8. TERMS CONTRIBUTING TO THE PRESSURE DROP

Here we determine the relative importance of the terms in the bubble density equation. The bubble density equation Eq. 3.13 has been modified, replacing the potential gradient terms by the Darcy velocity of the foam, i.e.

$$\begin{aligned} \varphi n_f \partial_t S_g + \varphi S_g \partial_t n_f - \partial_x \left(n_f\ u_f\right) - \\ X_f [\partial_x \left(\varphi S_g D_{n_f} \partial_x n_f\right) + \partial_x \left(D_{cap} n_f \partial_x S_g\right)] = \\ \varphi\ S_g R(n_f). \end{aligned} \tag{3.31}$$

Figure 3.8 shows the terms from Eq. 3.31 in case of Bentheimer averaged over the domain between the measurement points. The gas saturation change over time ($\varphi\ n_f\ \partial_t S_g$) hardly contributes to the generation-coalescence function throughout the simulation. During transient flow (from 0 till 4200 seconds ≈12 PV), the bubble density change w.r.t. time and the convection-diffusion of bubbles balance the source term, $R(n_f)$. We based initial estimate, $R(n_f) \approx \partial_t n_f$ (Figure 3.1) on the assumption that gas is the only phase in the porous medium $S_g = 1$ and all gas is flowing as a foam, $X_f = 1$. However, in the simulation we consider two-phase flow (Figure 3.5) and there is a varying foamed gas flowing fraction (Figure 3.6). Therefore, in addition to bubble density variation over time affected by surfactant concentration (Figure 3.7), convection-diffusion terms contributed the source term. After transient flow, when the foam is in apparent steady state, $\partial_t n$ is zero, the number of bubbles is constant. During this steady state, the convection and the diffusion mechanisms are dominant.

3.4. COMPARISON BETWEEN EXPERIMENTAL AND SIMULATION RESULTS

The simulated pressure drop profile in case of the Bentheimer experiment in Figure 3.9 mimics features observed in the experimental result: the delayed foam generation and

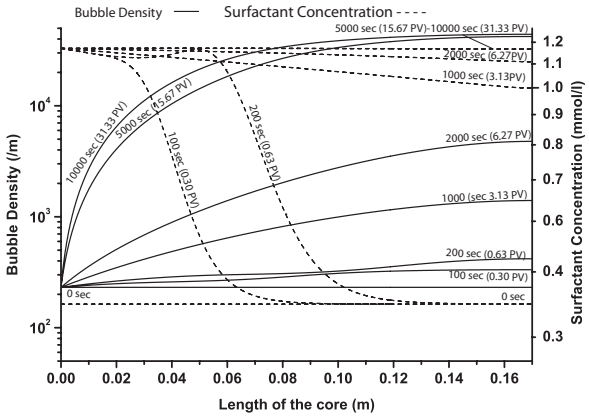

Figure 3.7: Numerical bubble density and surfactant concentration plot in the x-direction for Bentheimer. The dashed curve is the surfactant concentration and the drawn curve is the bubble density. There is a non zero gradient of the bubble density in the domain between the measurement points (4.5 cm and 13.5 cm), even after long times. This shows the need to use an average bubble density ($n_{f,av}$) in Eq. 3.19.

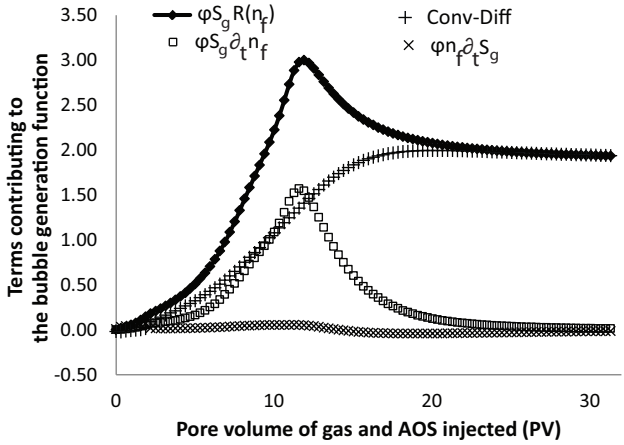

Figure 3.8: Terms contributing to the bubble generation-coalescence function (line with pyramid) in flow simulation for the Bentheimer due to (1) accumulation terms: gas saturation change over time ($\varphi n_f \partial_t S_g$,crosses) and bubble density change over time ($\varphi S_g \partial_t n_f$, small squares), (2) convection-diffusion terms (plus sign) from Eq. 3.31. Unlike the first estimate of $R(n_f)$ in Figure 3.1, here we consider two-phase flow (Figure 3.5) and the flowing foam fraction (Figure 3.6).

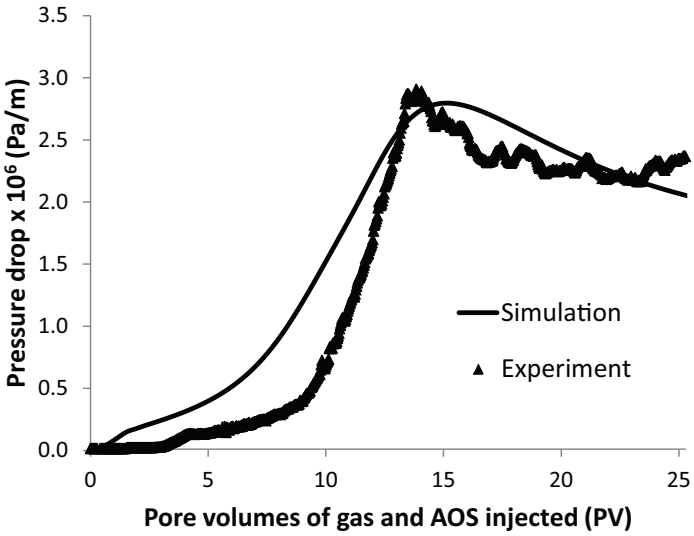

Figure 3.9: Comparison between experiment and simulation pressure drop profiles.

decrease in the pressure drop before it reaches steady value of 2.3×10^6 Pa/m. The simulation shows that the water saturation increases after foam achieved the maximum pressure drop. The increase in water saturation causes a decrease in the pressure drop across the measurement points. However, the bubble density continues to increase in this part of the simulation. After 15 PV of AOS and gas injection, the simulated water saturation achieved a constant value of 0.62, corresponding to the steady value of the pressure drop 2.3×10^6 Pa/m. The mean absolute error between theoretical and experimental pressure drop is 1.06×10^5 Pa/m, i.e. within 10 % of the experimental pressure drop. Possible reasons for the imperfect match between simulation based on the proposed theoretical procedure and the experimental results are lack of fitting profiles in case of the uncertainty to estimate (a) the bubble density n_f from the experimental pressure drop, (b) the change in the bubble density w.r.t. time, dn_f/dt from the bubble density, n_f and c) the adsorption parameters k_a and k_d from the adsorption experiment. In addition, we took the adsorption parameters from the single phase experiment where the available surface area for adsorption is less than the surface area for multiphase foam flow. The role of bubble diffusion is not very well understood. These issues could be addressed in future work. In addition, to use the above procedure in the field, a further upscaling step is required, for instance using homogenization [61].

3.5. CHAPTER SUMMARY

- We can measure the pressure drop for a Bentheimer sandstone of permeability 3 Darcy for a low concentration of AOS surfactant (of the order of the critical micelle concentration (CMC)). The experiment achieved the steady state pressure drop af-

ter injection of 12 - 15 pore volume due to adsorption behavior. The experimental pressure drop shows a strong maximum in the pressure drop profile.

- A model that leads to four equations, viz. a pressure equation, a water saturation equation, a bubble density equation and a surfactant transport-adsorption equation can describe the pressure drop during the foam flow experiments. We estimated the viscosity coefficient α in the Hirasaki-Lawson equation from the surfactant concentration to relate the foam viscosity to the estimated bubble density. Bubble density can take into account the trapped gas fraction and the water saturation.

- The simulations indicate that the maximum in the pressure drop corresponds to a minimum in the water saturation. With the assumption that all gas is foamed and foam is the only phase in the porous medium, we assert that the dependence between the source term and bubble density is approximate. The difference between simulated and experimental pressure drop is within 10 %, which suggests that the first estimate of the bubble generation coalescence function is of the right order of magnitude.

- The numerical study separates the overall bubble generation-coalescence function, $R(n_f)$ into contributions of accumulation, convection and dispersion (diffusion) of bubbles. As we approximated the viscosity coefficient α as a resistance per lamella in the capillary tube, the generation-coalescence function can only be obtained within a factor. If we consider water saturation (two-phase flow) and the flowing fraction of foam, the rate of change of bubble density during transient state is equal to the bubble density generation function plus the terms that account for bubble transport by convection and diffusion divided by porosity and saturation.

4

DETERMINATION OF THE MOST SIGNIFICANT VARIABLES AFFECTING THE STEADY STATE PRESSURE DROP

With four parameters I can fit an elephant,
and with five I can make him wiggle his trunk:

Attributed to von Neumann by Enrico Fermi, as quoted by Freeman Dyson [89].

In laboratory experiments, researchers express the foam mobility in terms of the pressure drop across the porous medium to relate many physical processes. There is lack of data that relate the pressure drop to three or more variables simultaneously. This chapter investigates the steady state pressure drop for six variables, viz. permeability, surfactant concentration, pH, salinity, surfactant solution velocity and gas velocity. We measured fourteen pressure drop histories for an Alpha Olefin Sulfonate solution before and after nitrogen gas injection across the unconsolidated sandpacks of two mean grain sizes and across a Bentheimer consolidated core. We combined our data set with data sets from the literature leading to 157 data points. Symbolic regression produces a number of analytical expressions describing the interactive effect of the variables without prior knowledge of an underlying physical process. We selected a simple model with only one fitting parameter to compare with the experimental data. The slope between the observed pressure drop and the predicted pressure drop is 0.85 ± 0.03. A sensitivity analysis of the chosen model shows that the variables affecting the predicted pressure drop, in order of importance, are permeability, salinity and surfactant solution velocity. A bootstrap method (a statistical method determines the precision of the model parameter, explained more in the text. The pressure drop from our data set and one specific data set from the literature show significant deviation with respect to the pressure drop obtained from the regression equation.

Parts of this chapter have been published in Journal of Petroleum Science and Engineering [88].

The purpose of the data driven model applied to experimental data is only to improve the models based on physical processes, i.e. mechanistic models. In addition the data driven model can indicate the variable spaces for which we need more experiments.

4.1. INTRODUCTION

In the laboratory, foam is generated by (1) co-injection of gas and surfactant solution in a porous medium pre-saturated with surfactant [40, 79] or (2) by injection of alternate slugs of gas and surfactant solution through the core [90, 91]. The surfactant lowers the surface tension of the solution and thereby, with the gas, creates and sustains lamellae in the porous medium. The gas trapped by the lamellae [18, 38] and the immobile fraction of gas [82, 92–94] result into a pressure drop increase across the porous medium. Foam propagation occurs in two states: an initial unsteady state, characterized by an increase in pressure drop and later, a steady state, where the pressure drop becomes constant. During the steady state, the two-phase Darcy's law can describe foam propagation through porous media [3]. In other words, researchers assume that gas travels through the porous medium as a separate phase and the relative permeabilities determine the flow rate [57]. In such a steady state, a ratio of the effective permeability and the apparent viscosity, i.e. k_e/μ_{app} can express the gas mobility. Furthermore, the gas mobility is related to the flow rate of foam and the pressure drop observed across the core [48]. A boundary condition affects the gas mobility where no water exits the core until $S_w = 1 - S_{gr}$ (S_{gr} is irreducible gas saturation and S_w water saturation) is the so-called capillary end effect condition [95]. Such condition leads to an enhanced saturation at the end of the core [96] and may cause a non-representative value of the pressure drop in the measurement during experimentation [97]. The errors due to the capillary end effect can be eliminated by (1) measuring the saturation far enough away from the outflow face (Penn State Method) and (2) using high flow rates to make the error in the measured saturation negligible (Gas flow method) [97]. The observed steady state pressure drop can be further used to calculate the foam resistance factor [98] or mobility reduction factor [99].

The steady state pressure drop is affected by several variables, i.e. permeability of the porous medium, surfactant formulation/concentration, injection rates, presence of oil, gas fraction, temperature, etc.. [37, 40, 78, 90, 100–104]. Therefore, the steady state pressure drop during foam flow through porous media depends on a complex system of multiple variables. To simplify the complex system of multiple variables, most research studies focus on a base case after which they modify one or two variable(s) at a time to study their effect on the steady state pressure drop, for example, flow rate and concentration [23] or gas velocity and surfactant solution velocity [24, 25]. In addition, such studies use a physical base to construct a model for explaining the steady state, i.e. a mechanistic approach [26, 27]. In this respect, Khatib [75] explains flow experiments with a model based on the capillary pressure (pressure difference between gas and surfactant solution phase), which itself depends on the surfactant formulation, the permeability and the gas velocity. However, some other researchers [39, 105] observe that the steady state pressure drop is a function of the permeability and surfactant velocity, dominated by bubble trapping and mobilization. To explain both contrasting results, Jante and Osterloh [48] and further Rossen [106, 107] propose two regions in the pressure drop contour plot

vs. gas and surfactant solution velocity for a given surfactant formulation and permeability. The region in the pressure drop contour plot, where the pressure drop is nearly independent of the gas velocity, is called the high quality region; the term "quality" is defined as the ratio of gas volume and total, i.e. gas plus surfactant solution volume. The region in the pressure drop contour plot, where the pressure drop is nearly independent of surfactant solution velocity, is called the low quality region. Martinez [24, 25] introduces the concept of critical foam quality to distinguish between the two regions. In addition, there are other models based on the concepts of local equilibrium (foam texture is an algebraic function of local conditions [27, 108–111]) and foam bubble population [20, 22, 26, 68, 112, 113]. The difference between local steady state and bubble population models is well described in Ma [114]. In combination with the mechanistic approaches discussed above, Zhao [115] studied the effect of salinity and surfactant formulation on the steady state pressure drop by orthogonal experiments [116] to increase the oil displacement efficiency. Similarly, Wang [117] studied the quantitative effect of surfactant concentration, foam quality, temperature and oil saturation on the steady state pressure drop by Design and Analysis of Experiment (DAoE) methodology [116]. The ensuing polynomial expression consists of the product of the individual effects of interacting variables, e.g. foam quality and surfactant concentration, along with a fitting parameter for each combination of the variables to accommodate the interactive effect. Among the variables, the effect of pH on the liquid film for the applications in porous media has been well considered [118, 119], however, not in combination with other variables.

The modeling approaches mentioned above pose practical difficulties for reasons of the required large number of experiments and the large number of fitting parameters. For example, the high and low quality regions for constant permeability and constant surfactant concentration are found by doing experiments for a range of combination of gas and surfactant solution velocities [120, 121]. Such models require physical understanding and are difficult to derive for such a complex system as foam flow. In addition, there is a lack of experimental data that combine orthogonal or even box design [28] for variables such as permeability, surfactant concentration, foam quality and salinity affecting the pressure drop. It is difficult to generalize conclusions from the literature as those studies are (deliberately) unique and are for restricted variable spaces. One might ask: (i) can limited experimental data with DAOE methodology represent whole population of foam experiments from the literature?, (ii) is there a way to use the previous experimental results to generalize the effect of various variables on the steady state pressure drop? and finally, (iii) can we rank the effect of variables on the pressure drop? The path towards resolving these questions could be elucidated with data driven models constructed by applying regression to experimental results. However, conventional regression involves a presumed interrelationship between the variables, which might miss the importance of one variable over another affecting the pressure drop. Therefore, we are motivated to find the hierarchy between the variables with a maximally feasible set of experiments using a non-conventional regression analysis called symbolic regression [44, 45]. Symbolic regression, with its ability to search for the model that best describes the data behavior without imposing a priori assumptions, would offer the advantage over conventional multiple regression. Based on a literature survey, we attempt the ran-

dom variation of six experimental variables, viz. permeability (1860 Darcy, 130 Darcy and 3 Darcy), the concentration of surfactant (0.0375 w/w %, 0.075 w/w % and 0.15 w/w %), gas and surfactant solution velocity (0.27-3.97 m/day), salinity (zero, 0.5M NaCl) and the pH (6.5, 3.0) as representative conditions in a reservoir. Complimentary to studies conducted in the literature [99], we conducted experiments with Bentheimer with a low AOS concentration (0.0375 w/w %) and at a low gas fraction for two injection rates. Such random variation would avoid the practical difficulty of conducting an infeasible number of experiments (orthogonal or box design) to rank the variables with respect to their relative importance to affect the pressure drop. We designed our experiments to add data points that are at conditions less studied in the literature. To overcome the difficulty of statistical inference with only 14 (our) data points, we add 112 data points from Martinez [24, 25], 21 data points from Jante and Osterloh [48] and 12 data points from Persoff [39]. The selected data points were similar in some experimental conditions (surfactant-nitrogen co-injection) and surfactant solutions (AOS), but also had slight variations, viz. single experiment with various steady state pressure drop values corresponding to various gas and surfactant solution velocities: Martinez [24, 25] and mixing of two surfactants: Jante and Osterloh [48]. We used the experimental results from the literature along with our own results to search for the model form that best describes the data behavior using a minimal number of fitting parameters. We used a freely downloadable software Eureqa® [49] with the aforementioned data set to create a host of model expressions. To select a model from the candidate expressions, Akaike's information criterion (AIC) [50] measures the goodness of fit of the statistical models by incorporating both the likelihood of the model and a penalty for extra parameters.

In addition to criteria for model choice, right model verification / validation is also important to assess the merit of the selected model. The symbolic regression software characterizes the sensitivity of the predicted pressure drop to the variable in the model. Further, we compared the observed pressure drop and the predicted pressure drop by plotting them on Y and X axis respectively. The traditional approach of using the same data, both to build the model and to estimate its predictive performance, tends to bias the estimate of the model-prediction error. The fitted parameters are connected with the original data set and therefore cannot necessarily be used for different data sets [122]. The approach of cutting the data in half (one half for modeling and another half for validation) has a drawback of not utilizing precious data points for model building. Therefore, for the purpose of validating the model, we used a bootstrap method [51, 52] to generate 50 simulated data sets different from the original data set. A given bootstrap sample data set consists of some original data points repeated in the set while some appear only once and some not at all [123]. We used the standard deviation obtained from the 50 data sets to determine the precision of the fitting parameter of the model.
For the purpose of describing our data set, we explain the experimental procedure in section 4.2 for co-injection of nitrogen and water with dissolved surfactant in different porous media, namely (1) an unconsolidated sandpack of 1860 Darcy, (2) an unconsolidated sandpack of 130 Darcy and (3) a consolidated Bentheimer core of 3 Darcy. We described the porous media, solutions and the set up in chapter 2. Subsection 4.2.1 describes 14 experiments with the random variation of six experimental variables, viz. permeability, salinity (NaCl), surfactant concentration, pH (hydrogen ion concentration),

surfactant solution velocity and gas velocity. In section 4.3, we report the steady state pressure drop measured across the porous medium to show the effect of the used variables on foam flow. In the subsection 4.3.1, we explain application of symbolic regression on 157 experimental data points. A procedure is given for an ideal choice of the selected rational expression with fitting parameter A_0. Furthermore, we use the simplest bootstrap method to get 50 simulated data sets. The model from symbolic regression with the fitting parameter A_0 is applied to 50 data sets. A parameter for each simulated data set ($A_1^S - - A_{50}^S$) has been found by variance minimization between predicted and observed pressure drop. The deviation of those simulated parameters with respect to the predicted parameter estimates the error in the predicted parameter. The experimental results in subsection 4.4.1 are compared for the relationship between the variables and their interactive effect on the pressure drop. The analysis shows the parameter subspaces where there are insufficient data, necessary to find the interdependence of the variables affecting the pressure drop. In the subsection 4.4.2, we discuss the merit and drawback of symbolic regression and the bootstrap method. We end with some conclusions in section 4.5 about the experimental procedure, about the symbolic regression and about the estimate of the observed pressure drop.

4.2. EXPERIMENTAL SECTION

Table 2.1 in chapter 2 shows three types of porous media used for the foam flow experiments, viz. coarse sand, fine sand and Bentheimer cores . Figure 2.4 and Figure 2.5 in chapter 2 show photographs of the unconsolidated sandpack and the Bentheimer core respectively with the positions to measure the pressure difference. We described the experimental set up for the foam experiments in chapter 2 in section 2.2. We used a 39.1 w/w % Bio-TERGE® AS-40, Sodium C_{14}-C_{16} Alpha Olefin Sulfonate (AOS) to prepare 0.3 w/w % AOS solution in both: a 3 w/w % brine (0.5M ± 0.01 NaCl) and doubly distilled water with dissolved HCl (pH = 3.0 ± 0.3). Both solutions were further diluted to prepare a 0.075 w/w % AOS solution in 0.3 w/w % brine for the unconsolidated coarse sandpack and a 0.0375 w/w % AOS in acidic water for Bentheimer. For the fine sandpack we used an AOS solution in doubly distilled water (pH = 6.5 ± 0.2) with varying concentration (0.0375, 0.075, 0.15 w/w %) for various experiments.

4.2.1. FOAM FLOW EXPERIMENTS

We report here fourteen experiments, i.e. five with coarse sandpack, seven with fine sandpack and two with a Bentheimer sandstone core. We carried out all experiments at room temperature. As we carried the experiments during day time only, we assume a temperature fluctuation of 3-5°C. Table 4.1 shows porous media, test name, time, date, back pressure, surfactant concentration, medium, flow direction, injected surfactant velocity and the pore volume injected (PV) before the start of gas injection for each experiment. We calculated the pore volume of the injected surfactant solution by $(u_w\ t)/(\varphi\ L)$ where u_w is the surfactant solution velocity (m/s), t is the time (seconds), φ is the porosity of the porous media and L is the distance (m) across measurement points. Table 4.1 further shows the pressure at the inlet manometer (P_{in}), pressure at the outlet manometer (P_{out}) and the pressure difference across the measurement points (ΔP), before the

start of the experiments and during the steady flow of single phase surfactant solution. Table 4.2 focuses on the steady state foam flow after the surfactant solution and gas mixing. The gas velocity at the inlet of the porous medium during steady state (u_g^{ss}) depends on the pressure at the inlet (P_{in}). Therefore, we calculated the gas velocity during steady state by dividing the injected gas velocity by the pressure ratio at the inlet manometer. The total superficial velocity u_t is the addition of the corrected gas steady state velocity u_g^{ss} and the surfactant solution velocity u_w. Other parameters mentioned in Table 4.2 are back pressure (BP, barA), foam quality ($\eta_{ss} = u_g^{ss}/u_t^{ss}$) and the foam pressure drop ΔP_f at steady state.

Coarse sandpack All experiments in the unconsolidated sandpack of 1860 Darcy used a surfactant solution of 0.075 w/w % AOS concentration in 0.5M Brine (NaCl). The flow was from the bottom to the top of the sandpack. The first foam experiment "A" started on the 14^{th} February 2011 by flushing a surfactant solution at a rate 1.44 m/d using a back pressure of 7 barA. At t = 300 seconds, the back pressure is released by opening the back pressure valve. At t = 811 seconds from the start of the experiment, i.e. 500 seconds after the release of the back pressure valve, we injected nitrogen gas at a rate 3.17 m/d in the already flowing AOS solution 30 cm upstream of the inlet of the sandpack. We used the same unconsolidated sandpack next day for the next foam experiment "B" with AOS flow rate of 1.44 m/d and a back pressure of 21 barA. At t = 3193 seconds, i.e. after flushing 2.5 PV of AOS, we opened the back pressure valve and waited 167 seconds to open the gas valve. The third foam experiment "C" is conducted on the 17^{th} February 2011 by flushing the surfactant solution at 1.09 m/d. The back pressure is released at t = 3309 seconds from the start of the experiment and at t=3346 seconds, we injected nitrogen gas with an initial gas velocity of 1.62 m/d. We started the next foam experiment "D" on the 19^{th} Feb 2011 with the same unconsolidated sandpack. The measurement started after mixing an unknown pore volume of 0.075 w/w % AOS with gas at the total superficial velocity of 3.30 m/d. Experiment "D" is repeated on the 21^{st} February 2011, designated as "E".

Fine sandpack We conducted seven foam experiments with the fine sandpack of 130 Darcy with various AOS solutions (0.0375, 0.075 and 0.15 w/w % in the doubly distilled water of 6.5 pH) with atmospheric back pressure. The flow direction was from the top to the bottom. The tap water, as a single phase was used to conduct the permeability tests between the foam experiments. The first foam experiment "F" was with 0.075 w/w % AOS. The next experiment "G" was on the 9^{th} August 2011 with a low concentration of 0.0375 w/w % AOS. For experiment "H" on the 19^{th} August 2011, we saturated the fine sandpack during the previous evening. After experiment "H", a permeability experiment is conducted for three hours with tap water at a varying rate of 0.1 to 1.0 m/d. Experiment "I" was on the same day by injecting 0.0375 w/w % AOS at 15:38 at a rate of 1.73 m/d. We started the foam experiment "X" on the 21^{st} August 2011 by injecting 0.15 w/w% AOS solution at 1.73 m/d with an atmospheric back pressure. After four hours (i.e. 70.0 pore volumes injected),the experiment was stopped because of lack of solvent. We injected 2.0 pore volumes of surfactant solution on the next day before opening the gas valve for Experiment "J". Experiment "J" was, therefore, considered as a continuation

of the previous experiment. Next day on the 23^{rd} August 2011,we repeated experiment "I" under the name "K". After 2158 seconds, keeping the back pressure atmospheric, we added nitrogen gas at a flow rate of 6.91 m/d to the already flowing 0.0375 w/w % AOS solution. We continued the experiment for four hours, i.e. 40.0 pore volumes. A day before the next foam experiment, we rinsed the sandpack with tap water. Five pore volumes of surfactant solution - gas was injected at an injection velocity 1.09 m/d to conduct the high concentration 0.15 w/w% AOS experiment "L" on the 29^{th} August 2011.

Bentheimer We carried out two experiments with the Bentheimer core of 3 Darcy for low AOS concentration of 0.0375 w/w % in acidic (pH=3.0) water. The back-pressure was kept at 4 barA throughout the experiment. We removed the filter (that generates the foam) and a visual cell (implemented to observe foam) to avoid large pressure gradient at the entrance. Before the experiment started, we flushed the Bentheimer core with CO_2 for five minutes. The CO_2 was followed by 100 ml of doubly distilled water with HCl (pH 3.0) at a rate 0.61 m/d for five minutes to remove any trapped gas. Foam experiment "M" is started on the 19^{th} April 2012 by flushing the surfactant solution at a velocity of 3.25 m/d. After 97 ml (4.5 pore volumes) of surfactant solution passed into the core, we injected nitrogen gas at a superficial velocity of 1.62 m/d in the already flowing solution. After injection of 700 ml (30 pore volumes) of surfactant solution, the gas and liquid flow is stopped. The measured temperature fluctuated between 15° and 16° C. For experiment "N" on the 26^{th} September 2012, we followed the initial steps of the previous experiment. The foam experiment is started by flushing the surfactant solution of 0.0375 w/w % concentration at a velocity of 0.81 m/d in the Bentheimer core. After 78 ml (3.5 pore volumes) of surfactant solution passed into the core, nitrogen gas was mixed at a rate of 0.41 m/d. After injecting 400 ml (50 pore volumes) of AOS solution we stopped the experiment. The measured temperature fluctuated between 13° C and 15° C.

4.3. RESULTS

The main result is the pressure drop across the measurement points during the steady state foam flow (ΔP_f). From here on, we refer to the pressure drop divided by the distance between the measurement points as the pressure drop, unit Pa/m. The plots contain the observed pressure divided by the distance between the measuring points versus the pore volume of surfactant solution and gas injected after opening of the gas valve. We measured the total superficial velocity by adding surfactant injection velocity and steady state gas velocity (gas velocity at steady state divided by the back pressure), and is given along with the quality (ratio of gas to total velocity) in the brackets. The chronological sequence of the experimental results for each porous medium is given below.

Coarse sandpack For all experiments with the coarse sandpack of 1860 ± 100 Darcy, we used 0.075 w/w % AOS solution in 0.50 M brine. The pressure profiles for the experiment "A" and "B" are shown in Figure 4.1. For experiment "A", after 2000 seconds of 2.1 pore volumes of gas and surfactant solution injection, the pressure drop increased rapidly. After 3268 seconds of 3.1 pore volumes of gas and surfactant solution injection, the pressure drop was 17.0×10^5 Pa/m. However, the manometer reached its limit to measure

Table 4.1: Experimental details before the gas injection

Porous media	**Test**	**Date**	**Time started**	**Medium**	**AOS concentration**	**Initial conditions before start**			**Entry solution**	**Steady state single phase AOS**				**AOS solution before gas injection**
		dd/mm/yy	hh:mm		w/w%	P_{in} barA	P_{out} barA	$\Delta P \times 10^4$ Pa/m		u_w m/d	P_{in} barA	P_{out} barA	$\Delta P \times 10^4$ Pa/m	PV
Coarse	A	14/02/11	16:33	0.5M Brine	0.075	7.33	7.22	8.00	bottom	1.44	1.67	1.18	3.67	0.6
	B	15/02/11	09:43	0.5M Brine	0.075	1.53	1.18	15.30	bottom	1.44	4.83	2.26	8.67	2.5
	C	17/02/11	10:53	0.5M Brine	0.075	1.87	1.73	22.16	bottom	1.09	8.36	7.51	3.55	1.0
	D	19/02/11	14:43	0.5M Brine	0.075	2.74	1.36	120.00	bottom	2.76				
	E	21/02/11	10:37	0.5M Brine	0.075	3.09	1.18		bottom	2.76			1597.26	
Fine	F	24/06/11	09:40	pH 6.5[a]	0.075	1.46	1.00	0.10	top	1.09	8.86	1.07	17.7	1.0
	G	09/08/11	13:47	pH 6.5	0.0375	0.99	1.03	0.87	top	1.09	1.26	1.09	9.00	3.8
	H	19/08/11	07:45	pH 6.5	0.0375	0.95	1.04	-2.54	top	1.09	1.19	1.04	1.40	0.4
	I	19/08/11	15:38	pH 6.5	0.0375	1.26	1.10	17.00	top	1.73	1.26	1.10	26.00	8.0
	X	21/08/11	09:37	pH 6.5	0.15	0.06	1.04	0.58	top	1.73	0.07	1.04	0.88	0.5
	J	22/08/11	15:11	pH 6.5	0.15	2.40	1.34	140.00	top	1.73	2.20	1.19	117.58	
	K	23/08/11	15:38	pH 6.5	0.0375	0.97	1.04	1.21	top	1.73	1.01	1.04	4.22	2.0
	L	29/08/11	10:02	pH 6.5	0.15	0.03	1.04	-1.97	top	1.09	2.01	1.05	4.80	3.0
Bentheimer	M	19/04/12	10:44	pH 3.0[b]	0.0375	3.36	3.35	0.01	top	3.25	4.18	4.12	1.36	4.5
	N	26/09/12	13:37	pH 3.0	0.0375	1.21	1.22	-0.13	top	0.81	4.74	4.72	1.14	3.5

$^{P_{in}}$Pressure at inlet manometer, $^{P_{out}}$Pressure at outlet manometer, ^{u_w}Surfactant solution velocity, ^{AOS}Alpha Olefin Sulfonate, $^{\Delta P}$Pressure drop across the measuring points, ^{PV}Pore volume of surfactant solution, [a]pH value fluctuated ± 0.2 in doubly distilled water, [b]pH value fluctuated ± 0.3 in doubly distilled water with HCl.

Table 4.2: Experimental details during the steady state foam flow after the gas injection

Porous media	Test	BP	u_g^{st}	P_1^{ss}	u_g^{ss}	u_w	u_t^{ss}	η^{ss}	AOS	ΔP_f $\times 10^5$
		barA	m/d	Pa	m/d	m/d	m/d	quality	w/w%	Pa/m
Coarse	A	Atm.	3.17	3.56	0.89	1.44	2.33	0.38	0.075	17.0[a]
	B	Atm.	2.17	2.93	0.74	1.44	2.18	0.34	0.075	26.5±0.20
	C	Atm.	1.09	3.30	0.33	1.09	1.41	0.23	0.075	21.0±0.07
	D	Atm.	4.15	3.91	1.06	2.76	3.82	0.28	0.075	26.6±0.03
	E	Atm.	4.15	3.91	1.06	2.76	3.82	0.28	0.075	26.8±0.20
Fine	F	Atm.	5.43	6.96	0.78	1.09	1.87	0.42	0.075	7.5±0.50
	G	Atm.	4.34	2.78	1.56	1.09	2.65	0.59	0.0375	1.5±0.10
	H	Atm.	4.34	1.24	3.50	1.09	4.59	0.76	0.0375	1.6±0.08
	I	Atm.	6.94	1.74	3.97	1.73	5.70	0.70	0.0375	3.7±0.80
	J	Atm.	6.94	2.78	2.49	1.73	4.22	0.59	0.15	15.0±0.10
	K	Atm.	6.94	1.74	3.97	1.73	5.70	0.70	0.0375	3.7±0.20
	L	Atm.	4.15	3.40	1.22	1.09	2.31	0.53	0.15	26.0±0.70
Bentheimer	M	4.1	1.62	1.82	0.89	3.25	4.14	0.22	0.0375	23.7±0.05
	N	4.1	0.41	1.51	0.27	0.81	1.08	0.25	0.0375	42.5±0.10

u_g^{st} Gas velocity at the start, u_w Surfactant solution velocity; ^{BP}Back pressure, ^{AOS}Alpha Olefin Sulfonate, $^{\Delta P_f}$ Foam pressure drop, Steady state: i. P_1^{ss} Pressure at the inlet, ii. u_g^{ss} Gas velocity iii. u_t^{ss} total velocity iv. η^{ss} quality, [a]Steady state pressure drop not recorded due to the limit of the manometer.

the pressure drop and therefore we could not measure the steady state pressure drop. In case of experiment "B", the pressure drop immediately increased to 10.0 × 10^5 Pa/m after injecting gas. During the next 2000 seconds, i.e, 2.0 pore volumes, the pressure drop did not increase. After t = 2560 seconds of 2.8 pore volumes of gas and surfactant solution injection, the pressure drop fluctuated around 26.5 ± 0.20 × 10^5 Pa/m, which we took as the steady state pressure drop. The steady pressure drop remained around this value during the rest of the experiment for next 2000 seconds of 2.0 pore volumes injection. Figure 4.2 shows two experiments "C" and "E" for the total superficial flow velocities 1.41 m/d and 3.82 m/d respectively. In case of experiment "C", we achieved a steady pressure drop of 21.0 ± 0.07 × 10^5 Pa/m after 1.3 pore volumes. We continued the experiment for 6.0 pore volumes of surfactant solution-gas mixture. Experiment "E" shows a steady pressure drop of 26.8 ± 0.2 × 10^5 Pa/m after injecting 5.0 pore volumes of solution-gas mixture for 3000 seconds. The pressure drop remained steady during the rest of the experiment, i.e. next 6000 seconds and 15.0 pore volumes.

Fine sandpack Figure 4.3 shows the foam pressure profile for 0.075 w/w % AOS for experiment "F" of 130 Darcy fine sandpack. After an initial fluctuation of 10 to 15 seconds due to the opening of the gas valve, we observed a steady pressure drop of 5.0 × 10^5 Pa/m. However, after 10.0 pore volumes the pressure drop increased and after 15.0 pore volumes the pressure drop was 7.5 ± 0.50 × 10^5 Pa/m, which we consider as the steady state pressure drop. Figure 4.4 shows the pressure drop for experiments "H" and "I" using 0.0375 w/w % AOS solution. We observed a sudden jump in the pressure drop upon nitrogen injection for both experiments. In experiment "H", the pressure drop decreased steadily to a steady value of 1.6 ± 0.08 × 10^5 Pa/m after an initial steep decrease for about 5.0 pore volumes. In experiment "I", which was later repeated as experiment "K", the pressure drop decreased to attain a steady value of 3.7 ± 0.80 × 10^5 Pa/m af-

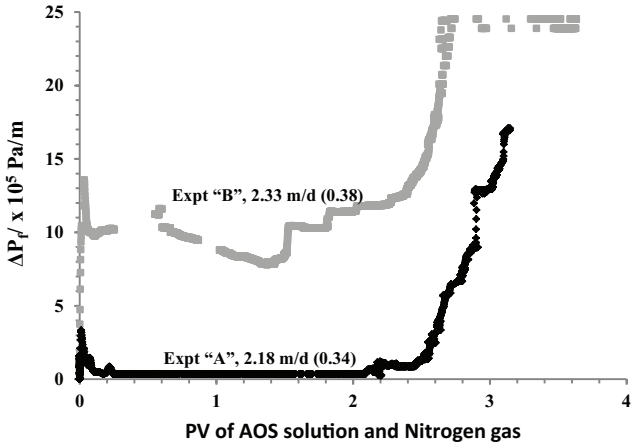

Figure 4.1: Effect of surfactant adsorption on the pressure drop for the unconsolidated sandpack of 1860 ± 100 Darcy with 0.075 w/w% AOS solution and nitrogen. The surfactant solutions injected before gas injection were 0.58 pore volume for experiment "A" and 2.5 pore volumes for experiment "B". Figures show the foam quality in the brackets here onwards.

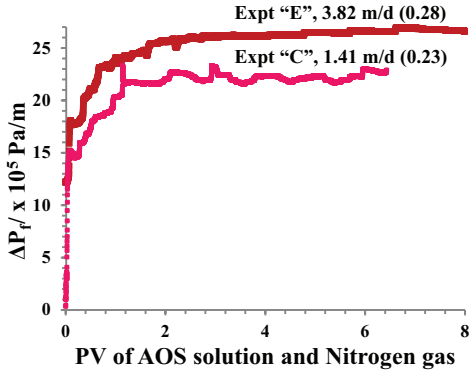

Figure 4.2: Effect of flow rate on the pressure drop for the unconsolidated sandpack of 1860 ± 100 Darcy with 0.075 w/w% AOS solution and nitrogen. As the total superficial velocity increased, the pressure drop increased.

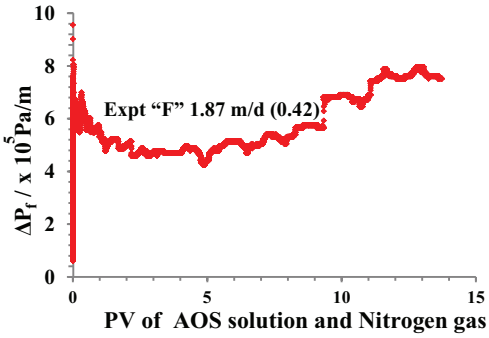

Figure 4.3: Foam pressure profile for unconsolidated sandpack (130 Darcy) with 0.075 w/w % AOS solution and nitrogen. We assume that the steady state pressure drop is 7.5 × 10^5 Pa/m.

ter about 2 hours (20.0 pore volumes). Figure 4.5 shows the pressure drop values for a high AOS concentration (0.15 w/w %) experiments "J" and "L". The steady state values achieved are: 15.0 ± 0.10 × 10^5 Pa/m for the high total superficial velocity (4.22 m/d) and 26.0 ± 0.70 × 10^5 Pa/m for the low total superficial velocity (2.31 m/d). For Experiment "J", the pressure drop attained a steady state value of 15.0 ± 0.10 × 10^5 Pa/m after 1.0 pore volumes of surfactant and gas injection. For experiment "L", the pressure drop climbed from a value of 0.48 ×10^5 Pa/m to a steady pressure drop of 26.0 ± 0.70 × 10^5 Pa/m after 1.5 pore volumes of surfactant solution and gas injection.

Bentheimer Figure 4.6 shows two experiments with the Bentheimer core for 0.0375 w/w % AOS solution and a pH of 3.0. The pressure drop for experiment "M" was 2.0 × 10^4 Pa/m during initial 2.0 pore volumes of AOS-gas injection at a total superficial velocity of 4.14 m/d. The pressure drop achieved a steady value of 23.7 ± 0.05× 10^5 Pa/m after injecting 10.0 pore volumes. The initial pressure drop for experiment "N" due to gas injection was 9.6 × 10^4 Pa/m at total superficial velocity 1.08 m/d. After 3.7 pore volumes, the pressure began to increase and around 25.0 pore volumes of gas and AOS injection the pressure drop attained a steady value 42.5 ± 0.10× 10^5 Pa/m.

4.3.1. STATISTICAL MODELING

Figure 4.8 shows the complete procedure of the statistical approach, i.e. data processing, modeling and verification/validation. Based on a literature survey and the experimental results in Table 4.2 we selected permeability, salinity (NaCl), pH, surfactant concentration, surfactant solution velocity and gas velocity as the independent variables affecting the pressure drop. We coupled our experimental data with the data from Martinez [24, 25], Jante and Osterloh [48] and Persoff [39] to get 157 data points. Flow conditions for the data points used from above literature is given in Appendix B. For our experiment "A", where the pressure crossed the limit of the manometer, we consider maximum observed pressure drop as the steady state pressure drop. We quantified the effect of pH in terms of hydrogen ion concentration, i.e. pH 5.0 = 1 × 10^{-5} mol/l. We assumed the

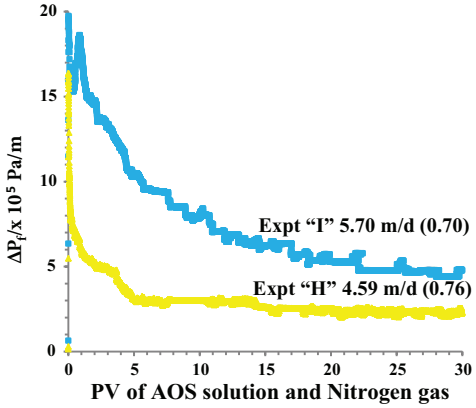

Figure 4.4: 0.0375 w/w % AOS for fine sandpack (130 Darcy): As the total superficial velocity increased, the pressure drop increased.

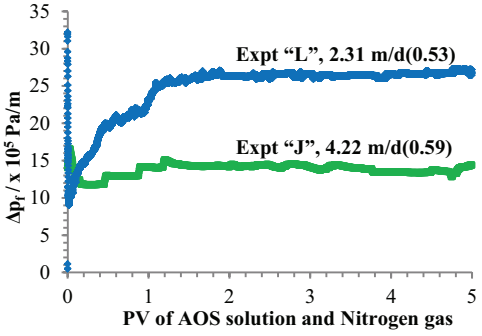

Figure 4.5: 0.15 w/w % AOS for fine sandpack (130 Darcy): As the total superficial velocity increased, the pressure drop decreased.

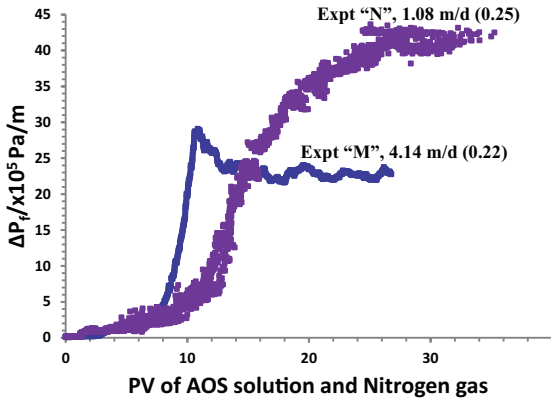

Figure 4.6: Foam pressure profile for the Bentheimer core (3 Darcy) with 0.0375 w/w % AOS and nitrogen. The pressure drop increased with the decrease in the total superficial velocity.

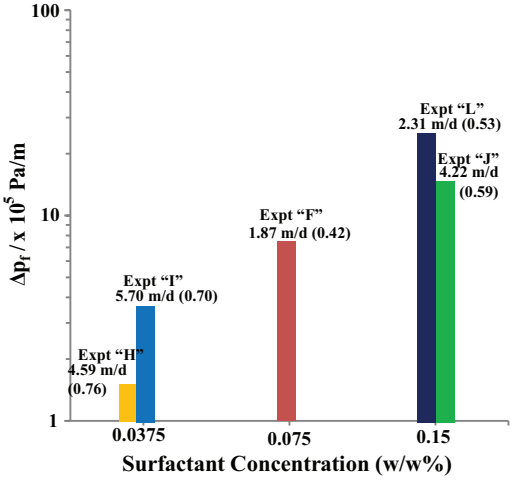

Figure 4.7: Summary of experiments with the fine sandpack. Compared to high concentration, the pressure drop in case of low concentration responded opposite to the increase in the total velocity.

cases from the literature with pH 5.0. All data assumed to have same surfactant (AOS, mol/l) and same salinity formulation (NaCl, mol/l), given in Appendix B, Table B.1. For the modeling part, Eureqa® [49], a software package based on symbolic regression finds the relation between the independent variables and the dependent variable, i.e. the observed pressure drop. The software searches the fitting parameters and the form of the equations simultaneously [44]. From these symbolic functions, the program derives partial derivatives for the same pairs of variables for each candidate function. The program repeats the steps of deriving numerical and symbolic partial derivatives to get the best solutions. The background article [44] and an article on genetic programming [124] gives details. The supporting information (Appendix B, Section B.2) gives a small set of possible analytical expressions. We follow the criticism of Von Neumann [89] and avoid models with too many fitting parameters. Indeed, we made a trade-off between error and complexity to select a model from the expressions, which is of the form:

$$\Delta P = \frac{A_0 Nc\ u_w^{Nc}}{\sqrt{k}} \tag{4.1}$$

where k, Nc, and u_w are the permeability (m^2), the salinity, i.e. NaCl (mol/l) and the surfactant solution velocity (m/s). A_0 is the only fitting parameter. ΔP is the predicted (modeled) pressure drop. The calculation of how a variable (for example permeability: k) influenced the predicted pressure drop ΔP at all input data points is as follows. Eureqa uses $|\overline{\partial \Delta P_k}|\ \sigma(k)/\sigma(\Delta P)$ to calculate the influence of the permeability on the pressure drop, where $|\overline{\partial \Delta P_k}|$ is the absolute average value of the partial derivative of ΔP with respect to k. $\sigma(k)$ is the standard deviation of k in the input data and $\sigma(\Delta P)$ is the standard deviation of ΔP. If the sensitivity value is 0.5, when the variable k is changed by one standard deviation, the output variable ΔP would change by 0.5 of its standard deviation [125]. The percentage of data points for which $\partial \Delta P_k > 0$, is denoted as % positive, i.e. the data points for which an increase in the variable k would lead to an increase in the pressure drop, ΔP. The percentage of data points where $\partial \Delta P_k < 0$, is denoted as % negative, i.e. the data points for which an increase in the variable k would lead to a decrease in the pressure drop, ΔP. We calculated the magnitude of the positive and negative increase by $|\overline{\partial \Delta P_k}|\ \sigma(k)/\sigma(\Delta P)$ for the respective data points. The model is verified by comparing the observed pressure drop and the predicted pressure drop by plotting them on the Y and X axis respectively. A linear relationship, $y(x) = y(x|a,b) = a + bx$ is considered, where y(x) is the predicted pressure drop; the fitting parameter "a" is the intercept and the fitting parameter "b" is the slope of the line. As the error in the observed pressure drop was not known, we assumed that all measurements have the same standard deviation. The formulae, derived from minimization of the chi-square merit function calculates the intercept, the slope and their respective standard deviations (Chapter 15, modeling of data from Numerical recipes [52]).

For validation, it is necessary to assume that the data points were independently and identically distributed. A bootstrap procedure involved drawing 157 data points at a time with replacement from the original set by independent random sampling. Because of the replacement, a data set is created using visual basic in Excel® in which a random fraction of the original points (typically $1/e$=37%) [52] are replaced by duplicated original points. Fifty such synthetic data sets, each with 157 data points are subjected to the same model

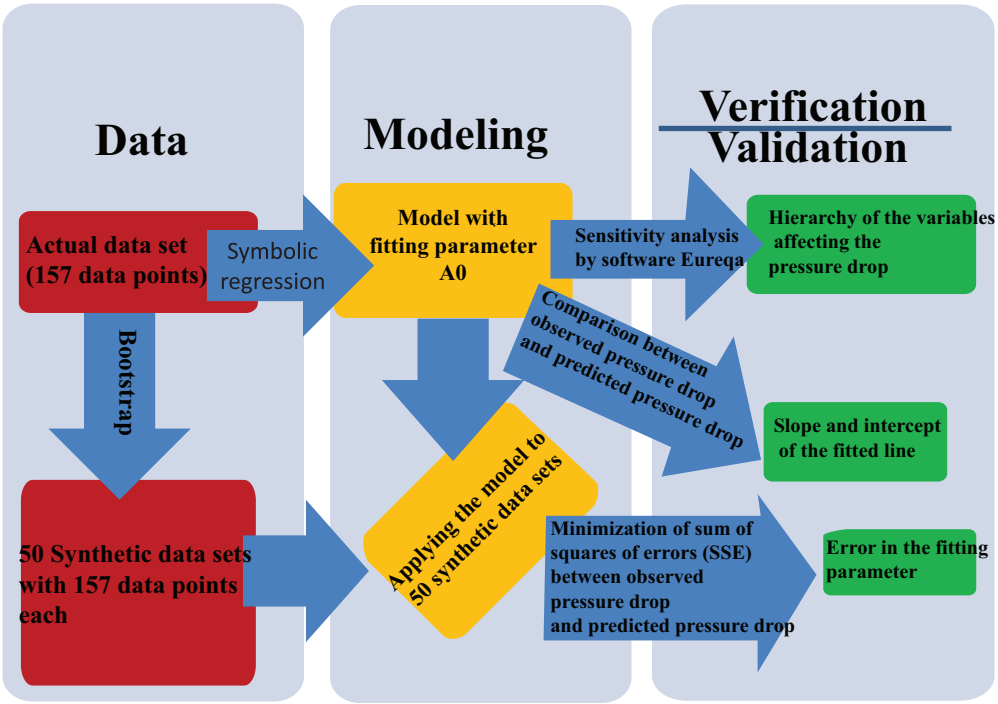

Figure 4.8: Statistical modeling of the data

Table 4.3: Variable sensitivity analysis for the selected model by Eureqa®

Variable	Sensitivity[1]	Positive[2] %	Positive[3] Magnitude	Negative[4] %	Negative[5] Magnitude
Permeability	148.79	0	0	100	148.79
Salinity	14.74	38	35.936	62	1.97
Water velocity	0.615	100	0.615	0	0

[1] The relative impact that a variable within the model has on the predicted pressure drop; [2] Percent data points, which show an increase in the predicted pressure drop with the increase in the variable; [3] Size of the positive impact; [4] Percent data points, which show a decrease in the predicted pressure drop with the increase in the variable; [5] Magnitude Size of the negative impact.

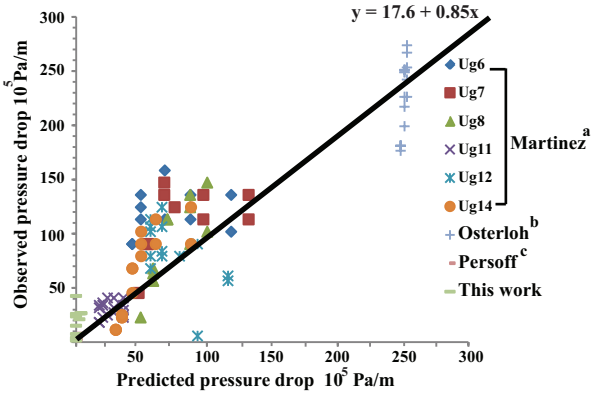

Figure 4.9: Precision of the predicted pressure drop from a model based on symbolic regression with the experimental pressure drop. The standard deviation in the values of the intercept and slope are 3.20×10^5 Pa/m and 0.03 respectively, calculated by fitting data to a straight line [52]. The mean absolute error in the predicted pressure drop is 21.6×10^5 Pa/m. Data from literature: (a) Martinez [24, 25], (b) Osterloh [48] and (c) Persoff [39]. The model fits better to the data from Martinez [24, 25] and Persoff [39] than to the data from Osterloh [48] and us. The experimental conditions for the data from the literature are given in appendix B.3.

$\Delta P = A_0 Nc\ u_w^{Nc}/\sqrt{k}$ as the original data. The fitting parameter for each simulated data set is found by minimizing the sum of squares of difference between predicted pressure drop and observed pressure drop by the Generalized Reduced Gradient (GRG) nonlinear engine in Excel®. To obtain the error, we compared the 50 values of the fitted parameters (A_1^s to A_{50}^s) for simulated data set to the original fitted parameter A_0.

4

4.3.2. STATISTICAL RESULTS

Table 4.3 shows the sensitivity analysis for the selected model Eq. 4.1. The relative impact of the permeability, salinity and surfactant solution velocity on the pressure drop is 148.8, 14.06 and 0.61 respectively. For all (100%) data points, an increase in the permeability leads to a decrease in the pressure drop with a negative impact of 148.8. For all (100%) data points, an increase in the surfactant solution velocity leads to an increase in the predicted pressure drop, albeit with a small positive impact of 0.61. The effect of salinity for the selected model is ambiguous. Indeed, the salinity (NaCl) for 38% of all data points shows a positive impact with a magnitude of 35.3. But for the remaining 62% of the data points, it decreases with a small negative magnitude of 1.97.

We calculated the predicted pressure drop values in Figure 4.9 by using Eq. 4.1 from set of equations (given in Appendix B) generated by symbolic regression using original experimental data from our work and from the literature (given in Appendix B). The procedure of generating these equations is briefly discussed in subsection statistical modeling, while readers can find the details of the procedure in the work by Schmidt [44]. Figure 4.9 shows the observed pressure drop from the experiments versus the predicted pressure drop from the Eq. 4.1. The observed pressure drop deviated from the predicted pressure drop by a mean absolute error of $2.16 \pm 0.03 \times 10^6$ Pa/m, which is 10 % error for a typical data point of 2.0×10^7 Pa/m. The intercept of the straight line is 17.6×10^5 Pa/m with

standard deviation of 3.22×10^5 Pa/m. The slope between the observed pressure drop and the predicted pressure drop data is 0.85 with a standard deviation of 0.03. When we applied the model to 50 data sets with the used bootstrap method, we observed a small error of 3% in the fitting parameter, i.e. $A_0 = 6078 \pm 163$.

The model does not match the experimental results on the contribution of surfactant concentration (Figure 4.7), where the observed pressure drop increases with an increase in the surfactant concentration while other variables (permeability, salinity, etc.) are constant. The model shows considerable discrepancy in the fit for the data points with the lowest observed pressure drop, i.e. our data points. The observed pressure drop in this work is higher than the predicted pressure drop. Moreover, the model also shows a large discrepancy for the data points with the highest observed pressure drop, i.e. the data points of Jante and Osterloh [48]. Although the model shows some agreement with the data from Martinez [24, 25], the interactive effect of gas and surfactant solution velocity on the pressure drop as explained in the original article is not observed.

4.4. DISCUSSION

We split the discussion in two parts, viz. (i) experimental analysis and (ii) statistical analysis. In the experimental analysis we discuss the variables affecting the time to reach the steady state pressure drop and the value of steady state pressure drop. In the statistical analysis we discuss quantitatively (i) the sensitivity of the pressure drop to the variables from the selected model and (ii) the difference between the predicted pressure drop and observed pressure drop for the data set.

4.4.1. EXPERIMENTAL ANALYSIS

We observed a "S"-shaped initial part of the pressure drop curve in all experiments, which represents foam displacing surfactant solution in the AOS saturated core. The gravitational effect due to direction of the flow is found negligible, i.e. $\rho\ g\ L \approx 98$ Pa compared to foam pressure, which is of the order 1×10^6 Pa. In case of the same permeability, the steady state pressure drop depended on the initial AOS saturation. For example, the first experiment "A" (Figure 4.1) for coarse sandpack, when we injected 0.54 pore volumes surfactant solution before gas, we observed the effect of foam formation only after 2.0 pore volumes of AOS and gas injection. However, the next experiment "B" (Figure 4.1), we observed an immediate increase in the pressure drop after the gas injection after injecting 2.5 pore volumes of AOS solution. The reason for the delay to reach the steady state pressure drop can be due to retardation effect caused by the adsorption of surfactant as noted by Chou [79]and by us in chapter 2. When other variables (permeability, AOS concentration and pore volumes of AOS before the gas injection) were the same, we achieved the steady state at different times for different superficial velocities, for example, Bentheimer core with 0.0375 w/w % AOS and ≈ 4.0 pore volumes AOS before gas injection. Experiment "M" took 10 pore volumes to attain the steady state pressure drop, while experiment "N" took 20.0 pore volumes, which used one-fourth of the total superficial velocity of experiment "M". From the simulations in our first paper [73] and in chapter 3, the capillary end effects occur well outside the region where we measure the pressure drop. The simulated saturation during steady state flow for Bentheimer

(Expt "M" in the current chapter) is almost equal between the measurement points. We can show similar results for the sandpack experiments as well. With other variables kept constant (*c.p.*), we observed the steady state pressure drop to increase with increasing surfactant concentration or with increasing total superficial velocity. The low permeability cases, as shown for Bentheimer (Figure 4.6) has by far the highest pressure drop, even with the lowest surfactant concentrations and low superficial velocities. In the case of unconsolidated coarse sandpacks (Figure 4.2 [73]) and the fine sandpack (Figure 4.4), the steady state pressure drop increased with the increase in the total superficial velocity for constant AOS concentration and constant permeability. In addition, this trend was not affected by the foam quality change. At a high surfactant concentration (0.15 w/w % AOS : Figure 4.5) for the case of the fine sandpack and at low concentration for Bentheimer (0.0375w/w % AOS : Figure 4.6), the steady state pressure drop increased with a decrease in the total superficial velocity. We can associate the effect to the low gas velocity and due to the high concentration creating numerous thick lamellae. For the same superficial velocities, the increase in AOS concentration (0.0375 w/w% to 0.15 w/w%) resulted in an increase in the pressure drop across the fine sandpack. Therefore we have not found the limit after which the pressure drop does not increase with an increase in the surfactant concentration while maintaining the other variables (permeability, gas velocity and surfactant superficial velocity) constant. We did not have common cases where only pH and the salinity of the water was modified. Therefore we cannot explain their effect on the observed pressure drop. We could not compare our results directly with the results from the literature because the exact combination of the variables we used (permeability, surfactant concentration, gas and surfactant solution velocities, salinity and pH) are not reported by them.

4.4.2. STATISTICAL ANALYSIS

The arithmetic expressions given by the symbolic regression allow to express the observed pressure drop in terms of only three variables, viz. permeability, salinity and surfactant solution velocity. Equations with less number of variables, e.g. only permeability, show a worse match as given in supporting information (Section B.2 in Appendix B). If we include more data in the symbolic regression, we might have to include other physical parameters like the gas velocity to explain the observed pressure drop. Extending the data set would also force to consider more parameters (for instance, presence of oil (aromatic or aliphatic) and soil content, etc.) on which the predicted pressure drop depends. However, it is not possible to include each data set which might give the predicted results closer to the experimental results. The generated trend by the symbolic regression for the used data suggests that the gas velocity has no significant effect on the predicted pressure drop for the entire data set as opposed to the pressure drop to a reduced data set [1]. This is because the data from Jante and Osterloh [48] and our data considered in this study are at low foam quality. The data from the high quality regime from Persoff [39] and from Martinez [24, 25] fits the model better than the data from the low quality regime. The large discrepancy for the data points with the highest observed pressure drop, i.e. Jante and Osterloh [48] obtained data points for foams by mixing two surfac-

[1] Shear-thickening may be obtained in the high-quality regime, while shear-thinning behavior is found in the low-quality regime.

tants, viz. AOS (Alpha Olefin Sulfonate) and SDS (Sodium Dodycyl Sulfonate), which is not considered in the equation. Although the equation shows some agreement with the data from Martinez [24, 25], the interactive effect of gas and surfactant solution velocity on the pressure drop as explained in the original article is not observed. Therefore, a relatively important variable such as the permeability masks the relationships between the variables in the subsets of data. We need more experiments for conditions for which large deviations between observed and predicted pressure drop occur, i.e. for the extremely low and high experimental pressure drop.

The DLVO theory [36] can explain the possible physical mechanism with which salinity affects the foam pressure drop, i.e. stability of foam films. The DLVO theory describes the interaction between double layer forces, Van der Waals forces and steric forces. When surfactant is absent (i.e. no steric forces), an increase in the NaCl concentration would decrease the foam stability as a result of double-layer compression [126]. However, when surfactant is present, with other variables kept constant (*c.p.*),"We expect that (i) a low salt concentration salt mainly affects the charging of a film interface, whereas (ii) a high salt concentration salt mainly affects the screening of the electrostatic repulsion between the two interfaces of the film" [127].Therefore, the effect of salt concentration can only be observed in limited parameter spaces. In addition, we interpret Equation 4.1 in a statistical sense, where, for the available data points, the effect of salinity on the predicted pressure drop cannot be viewed in an isolated sense. The only clear trend that we observed from the equation is that lower permeable media shows higher pressure drop. If we consider Darcy's formula to explain the physical mechanism, higher permeability leads to the lower pressure drop and an increase in water velocity would increase the pressure drop. Equation 4.1 is therefore a data driven equation and not based on physical mechanism, as explicitly stated.

4.5. CHAPTER SUMMARY

- We measured fourteen pressure drop histories before and after injection of an Alpha Olefin Sulfonate solution (AOS) with nitrogen gas (N_2) across measurement points in various porous media. When we added nitrogen in the flowing surfactant solution, we observed an increase in pressure drop in all experiments. The initial conditions of the core (gas content, adsorption) influenced the foam generation in the core. It is possible to obtain a steady state pressure drop from the pressure drop histories.

- We measured the steady state pressure drop for unconsolidated sand packs (1860 and 130 Darcy) and a Bentheimer sand stone core (3 Darcy) for various surfactant concentrations (0.0375, 0.075 and 0.15 w/w %), for various gas and surfactant solution velocities (0.27-3.97 m/day), for two salinities (0, 0.5M NaCl) and for two pHs (6.5, 3.0). We varied the above six variables simultaneously to obtain their interactive effects on the steady state pressure drop. We refer to the pressure drop divided by the distance between the measurement points as the pressure drop (Pa/m). The pressure drop increased with an increase in the total superficial velocity and the AOS concentration while keeping other variables constant (ceteris paribus *c.p.*). For the concentration range studied by us, a limiting surfactant concentration that

gives a maximum pressure drop was not observed.

- We can apply symbolic regression to our data along with 143 data points from the literature to produce a number of analytical expressions without prior knowledge of an underlying physical process. A simple model with a single fitting parameter can describe the pressure drop with three out of the six variables, viz. the permeability, the salinity and the surfactant solution velocity. We used a sensitivity analysis to modify the model, which shows that for the chosen model the variables in order of importance are the permeability, the salinity and the surfactant solution velocity. We validated the model by estimating the error in the model parameter ($A_0 = 6078 \pm 163$) by the applied bootstrap method. The purpose of the derived data driven model is not to replace the models based on physical processes, i.e. mechanistic models.

- The observed pressure drop was of the order of 2.00×10^7 Pa/m and deviated from the predicted pressure drop by a mean absolute error of 2.16×10^6 Pa/m. The intercept and the slope between the observed pressure drop and the predicted pressure drop data are $17.6 \pm 3.22 \times 10^5$ Pa/m and 0.85 ± 0.03 respectively. Our data set and the data set of Jante and Osterloh [48] show significant deviation from the chosen symbolic regression model, which shows that the model has limitations. Jante and Osterloh [48] use mixtures of surfactants and we confine our data set to conditions that lead to a low pressure drop. Both our data and of Jante and Osterloh have the low foam quality in common. It is not clear to us whether the low foam quality can explain the deviation from the symbolic regression model.

- The model from symbolic regression is only able to explain the general behavior and hierarchy of the variables affecting the steady state pressure drop. The model gives the variable spaces for which we need more experiments. Considering an entire data set shows that the trends obtained from a subset of the data are not necessarily valid for the complete data set.

5

COAGULATION AND SEDIMENTATION OF POLYMER TREATED ASH PARTICLES IN DOUBLY DISTILLED WATER WITH AND WITHOUT SURFACTANT

God made the bulk; the surface was invented by the devil.

Wolfgang Pauli

This chapter investigates the colloidal stability of polymer treated ash particles, a waste product from a power plant in aqueous dispersion. We study coagulation and sedimentation of the dispersion for various pH values with and without the surfactant, Alpha Olefin Sulfonate (AOS, 0.0375 w/w%). We consider the relative sedimentation rate as the main criterion for stability optimization. The zeta potential, the particle size distribution, the ultra violet - visible light absorption and transmission of laser light is measured. Based on the analysis of the tests, when surfactant is absent, an alkaline medium stabilizes the ash particle dispersion. Addition of surfactant counteracts coagulation and later sedimentation of the ash particles for the observed period of one hour. When surfactant is present, an acidic medium stabilizes ash particles for applications in porous media.

5.1. INTRODUCTION

The study of particle flow in porous media is important for several applications: contaminant flow [7], aquifer remediation [8], enhanced oil recovery [16] and ground water flow [47]. A prerequisite to apply particles for various applications in porous media is that they should be stable, i.e. neither conglomerate nor sediment in the aqueous dispersion before injection. In addition, the particles should be able to flow through the porous medium excluding inaccessible parts [128]. Therefore, the mobility of particles in natural formations is strongly influenced by their dispersion stability [32, 129]. Due to gravity segregation, there will be a preponderance of large particles in the dispersed phase at the lower part of the vessel and a preponderance of small particles in the dispersed phase at the upper part of the vessel. In the extreme case all the dispersed mass is at the bottom due to sedimentation. In addition, the particles have the tendency to aggregate (stick together), which is called coagulation. A relation between coagulation and sedimentation of the particles is given by Smoluchowski's theory of rapid and slow coagulation [36]. Large particles of size one micron and above take the order of minutes to coagulate [36]. In order to decide whether the particles are suitable for the applications mentioned at the start of the paragraph, we can use the settling rate as a screening criterium.

The balance between gravity forces and viscous forces determines the settling velocity of the particles in the bulk aqueous phase [130]. For constant viscosity and density of the water and for constant density of the particles, the radius of the particles affects the settling velocity. Therefore, if the particles are small enough, effectively they would not sediment during the experimentation time, i.e. 24 hours. In addition, electrokinetic effects slow down the settling rate [36]. In particular for smaller particles the surface plays a more important role with respect to the bulk. In such a system, mainly H^+ and OH^- (due to pH) and ions constituting the solid [131] determine surface charge and potential. The charged surface of the particles along with the counter ions from the solution close to the surface forms an electric double layer [29], which leads to repulsive forces between the particles. These electrostatic repulsive forces can be increased by manipulating pH or by decreasing the ionic strength, thereby stabilizing the suspension [132]. In addition, the dipole-dipole interactions between molecules consist Van der Waals forces, which are attractive or repulsive in nature [30]. The theory, which considers the net force acting on two particles as a sum of the double layer forces and the Van der Waals forces is named DLVO theory, after Derjaguin, Landau, Verwey and Overbeek [31]. However, the interaction between two particles in a medium is not independent of the surrounding medium interactions [32]. The adjacent water molecules form hydrogen bonds with the surface groups of the particle, and are therefore rendered immobile. The interactions lead to structural forces, significant at surface separations less than 2 nm [33, 34]. In addition, when a polymer is present in the solution at high concentration, complete particle surface coverage by absorbed or anchored polymer can produce a steric layer that prevents particle coagulation, which is called steric repulsion [35, 55, 55]. To calculate the fraction of particle collisions that lead to coagulation, it is necessary to sum the interparticle forces, i.e. the double layer, Van der Waals and Steric forces. These forces determine the activation barrier ($k_B T$) particles need to cross before coagulation can occur. As explained above, the pH, the ionic strength of the solution and the surfactant

affects these forces. Therefore, to establish whether the particles are suitable for the applications mentioned in the first paragraph, it is necessary to determine the effect of pH, ionic strength and surfactant on the stability of the particles in a dispersion.

Useful measurements that we address in this paper are (a) zeta potential, (b) particle size and (c) scattered/absorbed light intensity. Researchers measure forces in the double layer experimentally in terms of potential at the hydrodynamic slipping plane [133]. This potential is known as the zeta potential. A large zeta potential means a high surface charge around the particles leading to an insurmountable barrier preventing the particles to coagulate [32]. If the zeta potential is small, the repulsion is also small. In such case, the Van der Waals attraction may dominate and cause particles to agglomerate. However, when surfactants are present, the zeta potential alone cannot be considered as a criterium for colloidal stability [134]. For example, even at the isoelectric point (the pH, at which a net surface potential approaches zero), a surfactant can stabilize the particles [135]. The stability of particles in surfactant solutions depends on many properties of the adsorbed surfactants, such as their charge, hydrophobicity and structure [134]. Consequently, the hydrodynamic diameter [71] of the particle including the solvation layers becomes important. The hydrodynamic diameter is a diameter of a sphere that has same translational diffusion coefficient as the particle [136, 137] and can be derived from the diffusion coefficient of the particle [70]. As the hydrodynamic diameter affects the interaction of colloidal particles with light [53, 138], the absorbed/scattered light intensity with respect to observed time during experiments can be used to qualitatively determine the sedimentation rate of the particles.

In summary, the aim of this work is to establish an experimental procedure with which we can quantify the coagulation and sedimentation rates of ash particle dispersions for various pH values with and without surfactant. We hypothesize for the given particles that the surfactant can improve their stability in a dispersion. If the surfactant increases the stability of the particles in the bulk dispersion, the particles will be less adsorbed while flowing through porous media. In order to check the hypotheses, we measure zeta potential, particle size and particle size distribution of ash particles in the dispersions with and without the surfactant. In addition, we use an absorption test set up and an in-house built laser transmission set up to estimate the sedimentation rate. We measured radius of the particles by the Malvern "Zeta sizer" to calculate the number of particles for each size, i.e. by dividing mass of particles of a particular size by the number average "molecular weight" [36]. We used the number of particles per cubic micron and the particle size to estimate the attenuation constant, α (per mm), by Mie scattering [53].
We organize the chapter as follows: Section 5.2 explains the theory of interparticle forces in an aqueous medium (subsection 5.2.1) and the relation between coagulation and sedimentation (subsection 5.2.2). Subsection 5.3.1 describes the preparation of the dispersions with and without surfactant. Subsection 5.3.2 describes the zeta potential and the particle size measurement. We study the laser transmission and absorption in subsection 2.3.3 to establish sedimention rate of particles with and without AOS for various pH values. The zeta potential and particle size of the dispersions are given in section 5.4. In section 5.5 we relate the mechanism of coagulation and sedimentation of the ash particles to the zeta potential, the particle size, the scattering of light and absorption of

light. We end with some conclusions about the procedure used, about the stability of the dispersions and about its implication to subsurface flow.

5.2. THEORY

5.2.1. FORCES BETWEEN POLYMER TREATED PARTICLES IN A DISPERSION

The interaction energy between polymer treated spherical particles (V) of identical radius R in an aqueous medium as a function of inter particle distance H can be written as [56]:

$$V = V_{VdW} + V_{Edl} + V_s. \tag{5.1}$$

where, V_{VdW} is the Van der Waals energy, V_{Edl} is the electric double layer energy and V_s is the energy due to steric forces [54, 55].
The electric double layer energy is based on the DLVO theory and given by

$$V_{Edl} = 2\pi\epsilon\epsilon_o R\psi^2 \ln[1 + exp(-\kappa H)], \tag{5.2}$$

where, ϵ is dielectric constant of water, ϵ_o the permittivity of free space and ψ is the surface potential. The Debye length, κ^{-1} is referred to as the thickness of the double layer. The region of varying potential extends to a distance of about $3/\kappa$ before the potential has decayed to about 2 % of its value at the surface [56]. The Debye length is given by,

$$\kappa^{-1} = \sqrt{\frac{\epsilon\epsilon_o k_B T}{2e^2 N_A I}}, \tag{5.3}$$

where k_B is the Boltzmann's constant, e is the electric charge, T is the absolute temperature and N_A is Avogadro's number. I is the ionic strength of the solution and can be calculated by

$$I = \frac{1}{2}\sum_{i=1}^{n} c_i z_i^2, \tag{5.4}$$

where c_i is the molar concentration of ion component i (mol dm^{-3}), z_i is the charge number of that ionic component. The Debye length (meter) for 1:1 electrolyte [32] can be simplified by the linear Debye-Hückel approximation to

$$\kappa^{-1} = \frac{0.304 \times 10^{-9}}{\sqrt{I}}. \tag{5.5}$$

The Van der Waals energy can be given by

$$V_{VdW} = -\frac{A\,R}{12H} \tag{5.6}$$

where, A, Hamaker constant is $\pi^2 q^2 \lambda = 6.31 \times 10^{-19}$ J, where q is number of atoms per cubic meter, 8×10^{28} [30]. The London-Van der Waals constant, $\lambda = 10^{-77}$ J m^6 depends

on the polarizability of the atoms [32]. The more polarizable the atoms are, the more easily are the electrons displaced that produces a larger induced dipole causing a larger interaction force [131].
The steric energy of interaction due to polymer treatment of the particles can be given [35, 139] by

$$V_S = 2\pi kTR\Gamma^2 N_A \left(\frac{\omega_p}{\omega_s}\right)(0.5-\chi)\left(1-\frac{H}{2\delta}\right)^2 + V_{elastic} \tag{5.7}$$

where Γ is the amount of adsorbed polymer [mg/m^2], ω_p is the specific partial volume of the polymer, ω_s is the molar volume of the solvent [m^3 per mole] and χ is the Flory-Huggins parameter. δ is the maximum extent of the adsorbed layer [nm]. $V_{elastic}$ takes account of the compression of polymer chains on close approach.
The Debye–Hückel equation cannot be used to calculate the surface charge in the surfactant solutions, where micelles influence the electrochemical properties of the system (even rough judgment overestimates activity coefficient by 50%) [140]. The reactions on the surface of the particles due to adsorption of surfactant determine the charge and therefore, the surface potential. Surface complexation models consider the charge on both the adsorbing ion and the solid adsorbent surface [141]. The surface complexation models demand tedious surface charge calculation on the polymer treated particles in a surfactant solution. Therefore, we consider surface complexation modeling outside the scope of the present work.

5.2.2. PARTICLE SIZE AND NUMBER DISTRIBUTION DURING SEDIMENTATION

We can calculate the number of particles of a radius r_i for a given time during a sedimentation test from the particle size distribution and the corresponding number/volume fraction, given by the zeta sizer [70]. For an assumed spherical shape, the volume (Ω_i) and mass (M_i) of the particles is calculated by $\Omega_i = \frac{4\pi}{3}\, r_i^3$ and $M_i = \Omega_i\, \rho_i$, respectively. As the concentration density of the particles is fixed, i.e. 0.4 kg/m^3, we assume that the relationship between particle size and the number of particles is inversely proportional, i.e. the smaller the particle size, the higher the number of particles in a dispersion. We can establish a settling velocity, v_i of the particle with a hydraulic radius, r_i, falling in the water under its own weight due to gravity by balancing the buoyant force with the friction force [36],

$$v_i = \frac{2}{9} {r_i}^2 \frac{(\rho_i - \rho_w)g}{\mu_w}, \tag{5.8}$$

where, ρ_i is density of the particle, ρ_w is density of the water, g is acceleration due to gravity and μ_w is viscosity of the water.

5.3. EXPERIMENTS

5.3.1. DISPERSIONS

Chapter 2 describes ash particles (subsection 2.1.3) and surfactant (subsection 2.1.2) used to prepare ash dispersions with and without surfactant as shown in Table 5.1. We used 0.1M HCl and 0.1M NaOH to change the pH of the dispersions. Calibration and procedure for the pH measurement is given in Appendix A.

Name	DD water	Ash dispersion 0.05 g/ ml	0.1M HCl	Dispersion 0.04 w/w % Ash	
	ml	ml (pH 11)	ml	ml	pH
Ash	88.29	0.71	1.2	90.29	2.88
Ash	79.00	0.64	0.1	79.75	4.62
Ash	82.80	0.40	0.2	83.40	6.00
Ash	79.20	0.40	0.1	79.70	6.90
Ash	52.00	0.50	0.0	52.50	9.09
Ash	77.00	0.62	1.5 (0.1M NaOH)	79.12	11.19
Name	**Ash dispersion** 0.08 w/w %	**AOS** 0.075 w/w %	**0.1M HCl**	**AOS-Ash dispersion** 0.0375 & 0.04 w/w%	
	ml (pH 9.83)	ml (pH 6.53)	ml	ml	pH
Mix	38.30	38.30	1.4	78.00	2.92
Mix	38.20	38.20	0.5	77.00	4.12
Mix	41.90	39.50	0.2	81.60	5.20
Mix	39.90	39.60	0.1	79.60	7.20
Mix	40.00	40.00	0.0	80.00	9.36
Mix	38.50	38.50	1.0 (0.1M NaOH)	78.00	11.05

Table 5.1: We mixed doubly distilled water with the ash dispersion and further added HCl or NaOH to prepare the dispersions with various pH. Similarly, we mixed 0.075 w/w% AOS, 0.08 w/w% ash dispersion, HCl or NaOH to prepare the dispersions with the surfactant. We obtained dispersions with and without surfactant of comparable pH values.

5.3.2. ZETA POTENTIAL AND PARTICLE SIZE

We treated the individual dispersions in an ultrasonic bath for 20 minutes. We measured zeta potential, particle size and particle size distribution by the Malvern "Zeta Sizer" ZS (subsection 2.3.2) at various times (immediately after ultrasonification, after 2 min and after 4 min).

5.3.3. SEDIMENTATION MEASUREMENTS

We measured the sedimentation of the dispersions with and without surfactant using an inhouse built Laser set up, shown in chapter 2, subsection 2.3.3. We studied light absorption (range 1000 nm to 200 nm) of the dispersions by ultra violet visible (UV-vis) light 1800 Shimadzo Spectrophotometer, shown in chapter 2, subsection 2.3.3. A computer program recorded the corresponding absorption spectrum at 0, 20 and 40 minutes.

5

5.4. RESULTS

5.4.1. ZETA POTENTIAL AND PARTICLE SIZE

Table 5.2 shows the zeta potential (mV) and particle sizes (nm) of the dispersions with and without surfactant for different pH values. Figure 5.1 and Figure 5.2 show the effect of pH on the zeta potential and on the hydrodynamic particle diameter of the dispersions respectively. The zeta potential in case of ash dispersions without surfactant decreases from acidic to alkaline pH with an isoelectric point (IEP) around 3.5. The zeta potential for surfactant added dispersions is negative with high values at extreme pH values. For the conditions studied, the particle hydrodynamic diameter is lower in case of dispersions with surfactant compared to dispersions without surfactant. The change in pH in case of ash-AOS dispersions has a negligible effect on the hydrodynamic diameter except at a pH of 9.09.

Table 5.2: Zeta potential and particle sizes of ash particle dispersions with and without surfactant for different pHs. The dispersions "Ash" are without surfactant and the dispersions "Mix" are with surfactant. The table reads from left to right.

Zeta potential (mV)							
pH	**Ash-0 min**	**Ash-2min**	**Ash-4min**	**pH**	**Mix-0min**	**Mix-2min**	**Mix-4min**
2.82	23.20	23.70	22.50	**2.92**	-46.80	-44.90	-46.00
4.62	-20.70	-21.80	-20.80	**4.12**	-74.60	-74.60	-72.20
6.00	-18.50	-18.10	-18.70	**5.20**	-38.40	-37.80	-35.30
7.00	-16.70	-16.50	-17.90	**7.20**	-35.50	-34.90	-36.50
9.09	-40.20	-40.60	-40.30	**9.36**	-69.00	-70.20	-74.00
11.19	-61.20	-62.10	-64.60	**11.05**	-51.70	-50.40	-53.00

Particle size (nm)							
pH	**Ash-0 min**	**Ash-2min**	**Ash-4min**	**pH**	**Mix-0min**	**Mix-2min**	**Mix-4min**
2.82	341.00	458.00	396.00	**2.92**	32.00	43.00	91.00
4.62	1100.00	955.00	531.00	**4.12**	91.00	91.00	122.00
6.00	1363.00	1013.00	970.00	**5.20**	378.00	153.00	120.00
7.00	851.00	791.00	883.00	**7.20**	216.20	316.70	176.70
9.09	78.00	122.00	222.00	**9.36**	396.00	824.00	824.00
11.19	530.00	141.00	122.00	**11.05**	141.00	164.00	122.00

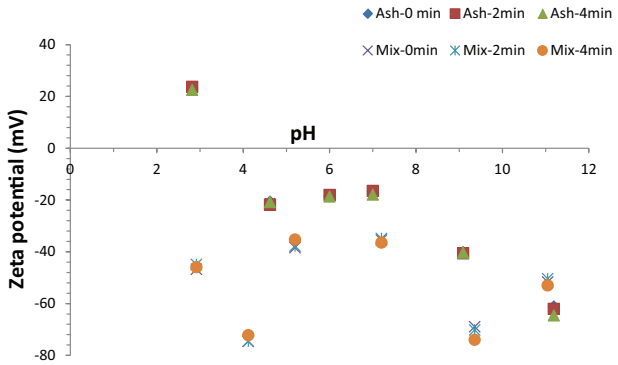

Figure 5.1: Effect of pH on zeta potential of the particles in doubly distilled water. The dispersions "Ash" are without surfactant and the dispersions "Mix" are with surfactant.

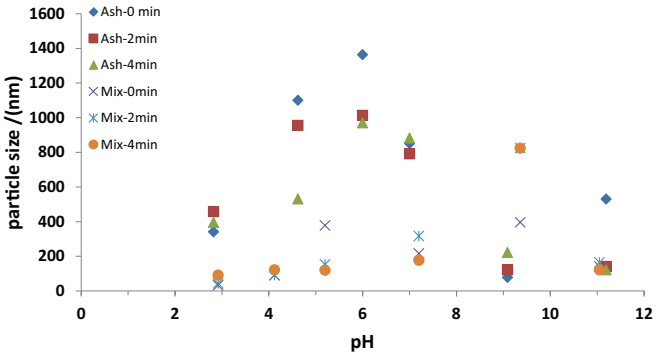

Figure 5.2: Effect of pH on the hydrodynamic diameter of the particles. The dispersions "Ash" are without surfactant and the dispersions "Mix" are with surfactant.

5.4.2. SEDIMENTATION STUDIES

Figure 5.3 and 5.4 show the signal received on the photocell (V) due to the transmitted light for ash dispersions without and with surfactant respectively. Figure 5.3 shows a higher light intensity for an ash particle dispersion with an alkaline nature (9.09 and 11.09 pH) compared to an acidic nature (2.82 and 4.62 pH). We observed a faster increase in light intensity for the ash dispersion with a pH of 2.82 and for the ash dispersion with a pH of 4.62 than the other dispersions. Figure 5.4 shows a higher light intensity for the ash particle-surfactant dispersion with an alkaline nature (9.09 and 11.09 pH) compared to the ash particle-surfactant dispersion with acidic nature (2.82 and 4.62 pH). We observed the lowest transmitted light intensity in case of the ash-AOS dispersion with acidic pH 2.92. Figure 5.5 shows the absorption spectra of ash dispersions without surfactant for the time interval 0, 20 and 40 minutes at four different pH values. We observed a decrease in absorption with respect to time in all dispersions. In addition, we observed a maximum absorption around 950 nm and a minimum absorption around 250 nm. We observed the highest absorption in case of the ash dispersion of 4.62 pH , followed by the dispersion of 2.82 pH, the second highest absorption. The alkaline pH dispersions (9.09 and 11.09) show a lower absorption than the acidic dispersions. Figure 5.6 shows the absorption spectra of ash dispersions with surfactant for the time interval 0, 20 and 40 minutes at four different pH values. The absorption spectra decrease with respect to time when surfactant is present albeit at a lower rate than the ash dispersions without surfactant. Dispersions at pH 9.36 and 11.19 have similar absorption spectra. The rate of change of absorption is higher in acidic dispersions (2.92 and 4.12) than in alkaline dispersions (9.36 and 11.05). The rate of change of absorption is the lowest for the dispersion with 9.36 pH. Figure 5.7 shows the effect of pH on the absorption of all dispersions at the wavelength of maximum absorption, i.e. 975 nm.

We used values from the literature in equations from theory discussed in section 5.2 to calculate DLVO forces given in nomenclature. The Hamaker constant [30] is 6.31×10^{-19} J. The Flory-Huggins parameter, χ, is 0.3. Polymer layer thickness on the particles, δ, is considered to be 0.2 nm and its adsorbed weight, Γ, is 1 mg/m^2. Figure 5.8 shows the

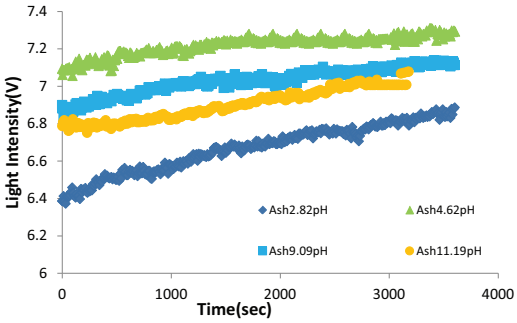

Figure 5.3: Signal detected by the photo cell in the laser set up through the ash dispersions for various pHs

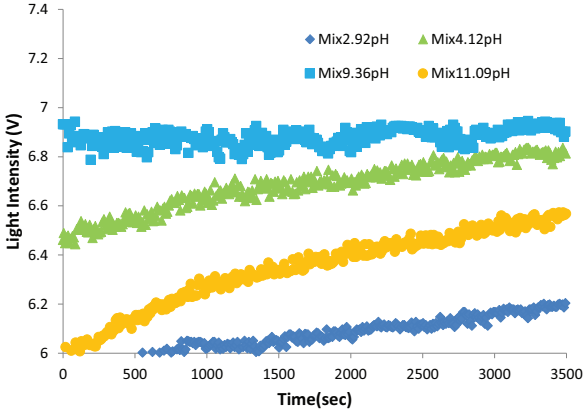

Figure 5.4: Signal detected by the photo cell in the laser set up through the ash-AOS dispersions for various pHs

profile of the calculated DLVO forces for various pH values.

5.5. DISCUSSION

5.5.1. COLLOIDAL STABILITY OF ASH PARTICLES WITHOUT SURFACTANT

In case of ash particle dispersions without surfactant in doubly distilled water (pH 5.5), the particles have a slightly negative zeta potential (Figure 5.1). The surface of a silica particle contains a high density of Silanol groups (about 1 per 25 Å), which dissociate to some extent in water to give a negatively charged surface. Adding HCl, Si-OH + H^+ gives $SiOH_2^+$, which makes the zeta potential less negative. Further addition of HCl reduces the zeta potential to zero at the isoelectric point of pH 3.5. Researchers observe similar values for fly ash [142] and SiO_2 (3.5) [129, 143]. Further addition of HCl causes a build up of positive charges. On the other side of the pH 5.0, i.e. when we add NaOH, Si-OH + OH^- gives SiO^- + H_2O, the particles tend to acquire more negative charges. We observed

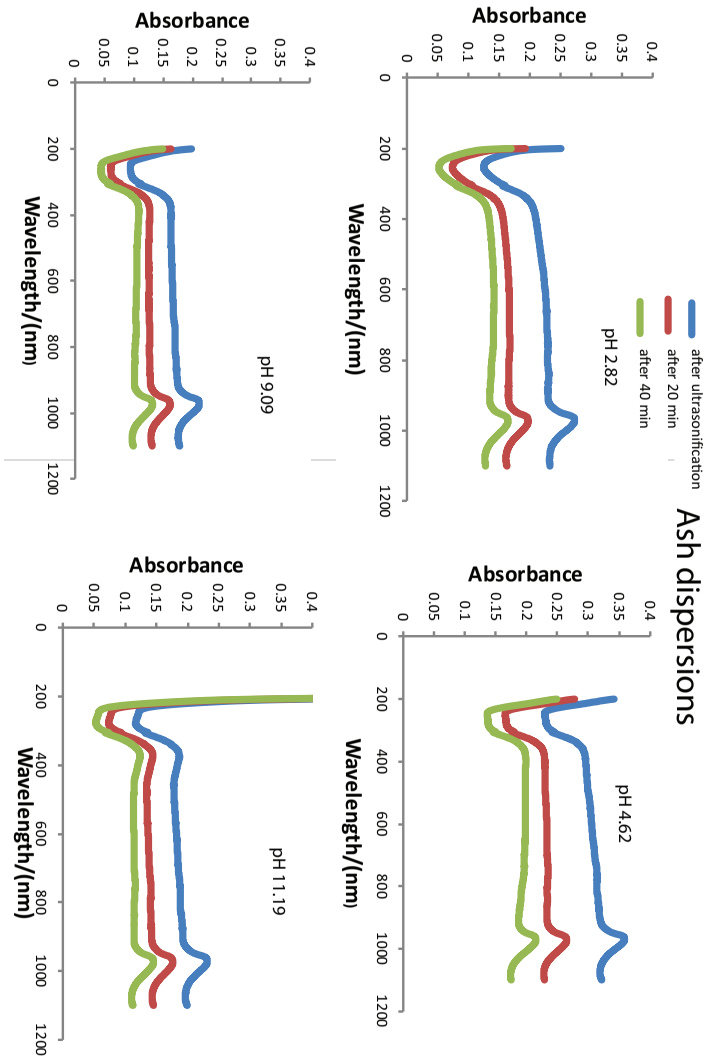

Figure 5.5: Effect of pH on colloidal stability of ash dispersions with respect to time

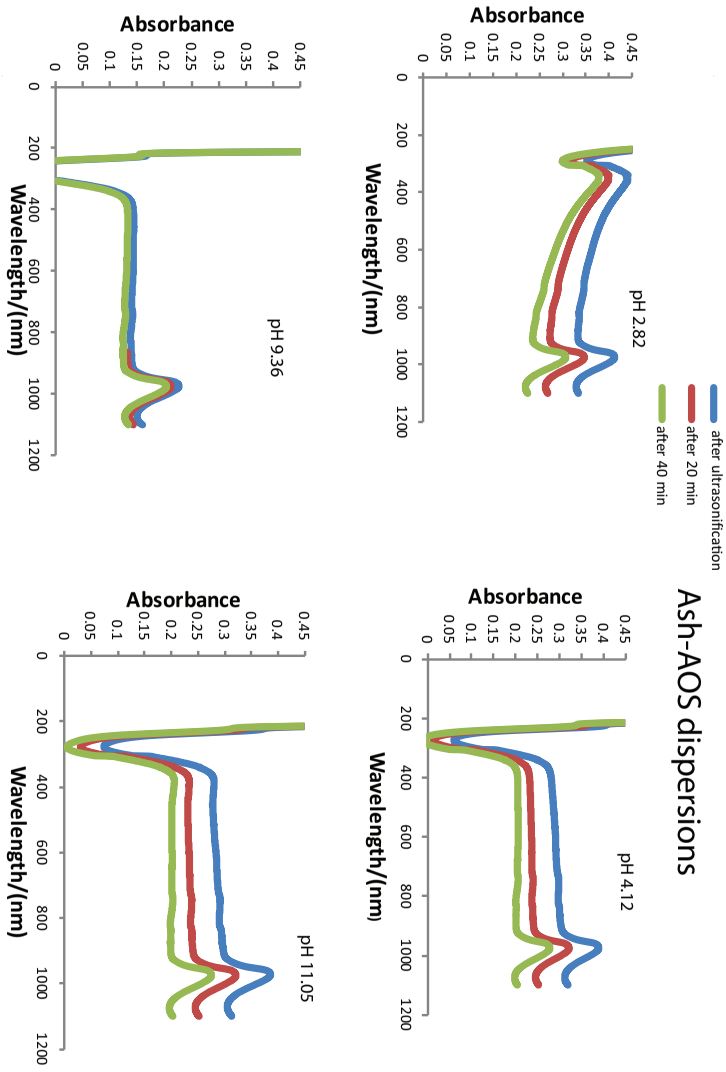

Figure 5.6: Effect of pH on colloidal stability of mix dispersions with respect to time

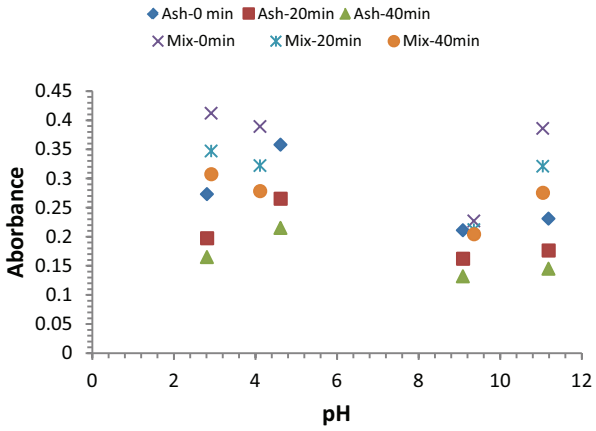

Figure 5.7: Effect of pH on the absorption of the dispersions at wavelength 975 nm

that for the pH values (pH 4.5 -9.0), the attenuation and the rate of change of attenuation of transmitted light is smaller than at extreme pH values. Figure 5.8 shows the interparticle energy estimated from the equations in subsection 5.2.1 for ash dispersions without surfactant for various pH values. The X axis indicates the inter particle distance in nm and the Y axis indicates the net interparticle energy in terms the activation barrier, k_BT. The plot shows the barrier required for particles to overcome before they coagulate. Due to the steric energy of the polymer treatment of particles, the particles repel each other at a small distance of 0.5 nm. The coagulation manifests itself in a larger hydrodynamic radius measured by Malvern zeta sizer [70]. Coagulation increases the attenuation due to constructive interference of scattered light. Sedimentation decreases the attenuation because particles moved out of domain of incident light. A decrease in attenuation, observed in the experiments implies prevalence of sedimentation over coagulation. Sedimentation increases with the weight of the particles. Therefore, coagulated particles sediment faster than non-coagulated particles. A large barrier implies slower coagulation, i.e. not all particle collisions lead to coagulation.

We explain here the effect of pH on coagulation and sedimentation of ash dispersions with respect to the observed particle size, zeta potential and light intensity profiles as follows. (a) The dispersion of pH 2.82 shows a smaller hydrodynamic diameter (300 nm) relative to other dispersions. Therefore at the start of the sedimentation studies, the attenuation constant is smaller due to smaller particle diameter [144]. As shown in Figure 5.8, it crosses a lower activation barrier k_BT, causing a high rate of successful collision that results in coagulation. Therefore, as time passes there is a higher sedimentation rate, i.e. instability of the dispersion. (b) The dispersion of pH 4.62 shows the highest hydrodynamic diameter (1200 nm). Therefore, we observed the highest transmitted light as large number of particles sedimented before the start of the test. The particles crosses a lower activation barrier k_BT (Figure 5.8), causing a high rate of successful collisions. The large hydrodynamic diameter results in initial coagulation. Therefore, as time passes the particles show a higher sedimentation rate, resulting in an unstable dispersion. (c)

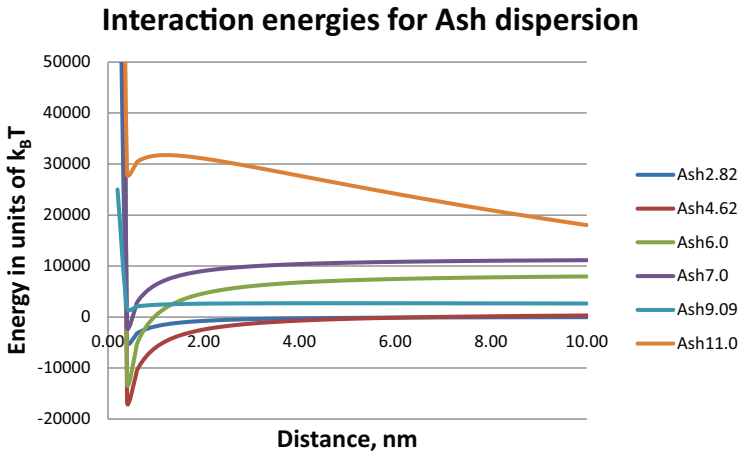

Figure 5.8: Interaction energies for ash dispersions. An alkaline medium (pH bigger than 9.0) can be used to get the optimum stability of ash dispersions.

The dispersion at pH 9.09 shows a hydrodynamic diameter of 200 nm; the dispersion has larger number of particles and absorbs more light. A higher activation barrier k_BT needs to be crossed by the particles; the dispersion has a lower rate of successful collisions than the acidic dispersion of 2.82 pH. Therefore, the sedimentation rate for the dispersion of pH 9.09 is lower than the sedimentation rate for the dispersion of pH 2.82. (d) The particles in a dispersion of a pH of 11.09 have a hydrodynamic diameter of 450 nm; the dispersion has a smaller number of particles and absorbs less light. We observed a higher transmitted light intensity at the start of the sedimentation studies. However, the particles must cross the highest activation barrier k_BT compared to the other dispersions; therefore, the dispersion has the lowest rate of successful collisions. This results in a low coagulation rate and a slightly lower sedimentation rate than the other dispersions.

In summary, we recommend an alkaline medium (pH higher than 9.0) for the colloidal stability of given ash particles without surfactant.

5.5.2. COLLOIDAL STABILITY OF ASH PARTICLES BY THE SURFACTANT

The zeta potential alone cannot explain the colloidal stability of the particles when a surfactant is present (discussed in Section 5.1). Therefore, we use the transmitted light intensity profiles in Figure 5.4 and the light absorption profiles in Figure 5.6 alongwith the zeta potential (Figure 5.1) and the particle size (Figure 5.2) to explain the effect of pH on the coagulation and sedimentation of ash particles when AOS is present: (a) The ash dispersion at pH 2.92 with surfactant shows the smallest observed hydrodynamic diameter (32 nm) and a negative zeta potential (-46.80 mV). When surfactant is not present, the zeta potential at this pH is positive. Comparing Figure 5.3 and 5.4, the ash dispersion at 2.92 pH has a larger number of particles, which absorb more light at the start of the light transmission tests. This observation is also supported by Figure 5.6, where the

dispersion at 2.92 pH has a larger volume of particles compared to the dispersions at other pH values. Furthermore, Figure 5.7 shows that the dispersion with surfactant at a pH of 2.92 has the highest absorption among the dispersions at a wavelength of maximum absorption (975 nm). Therefore, the dispersion at pH 2.92 with surfactant has the largest number of particles at a height where the light intensity was measured. (b) The ash dispersion with surfactant at a pH 4.12 has a hydrodynamic diameter of 91 nm and a zeta potential of -74.60 mV. The dispersion has, therefore, at the start of the measurement, many small size particles and consequently a high transmitted light signal (Figure 5.6). The dispersion shows a sedimentation rate that is slightly higher than that of the ash dispersion with surfactant at a pH 2.92. (c) The particles in the ash dispersion with surfactant at a pH 9.36 have a hydrodynamic diameter of 396 nm and a zeta potential of -69.00 mV. As the hydrodynamic diameter is large (Figure 5.2), part of the particles already sedimented. Therefore the dispersion at a pH 9.36 has a higher transmitted light intensity (Figure 5.4). Furthermore, the dispersion does not show a time dependence absorption (Figure 5.6) indicating a low rate of successful collisions, i.e. no further coagulation and no further sedimentation. (d) The ash dispersion with surfactant at pH 11.09 shows a hydrodynamic diameter of 141 nm and a zeta potential of -51.70 mV. Therefore it has a larger number of particles, which absorb more light and consequently leading to a lower transmitted light immediately after the start of the measurement. This observation is also observed in Figure 5.6, where the dispersion has a larger volume of particles compared to the dispersions at the other pH values.

In summary, when surfactant is present in ash dispersions, a reduction in the transmitted light intensity is observed compared to the ash dispersions without surfactant for similar pH values. This effect is clearer in extreme acidic and alkaline environments (pH of 2.92 and 11.09) compared to intermediate pH conditions (pH 4-8). The dispersion with a pH of 2.92 shows a lower sedimentation rate compared to the dispersion with a pH of 11.09. Therefore, we recommend acidic pH (2.92) in case of ash dispersions with surfactant to maintain the colloidal stability.

5.6. CHAPTER SUMMARY

- To use ash particles in foam flow through porous media we investigated their dispersion stability when a surfactant is present or absent for pH values ranging from 3 to 11. We measured two properties, viz. the zeta potential and the particle size. An inhouse built laser transmission set up can be used to measure the attenuation coefficient of the dispersions as a function of time. An ultra violet - visible light absorption instrument can be used to detect the maximum wavelength of absorption of 975 nm for the dispersions as a function of time.

- We observed an increase in transmitted light intensity (a decrease in attenuation coefficient) with respect to time for all dispersions, showing that a sedimentation effect prevails over a coagulation effect.

- When surfactant is absent, a high absolute value of the zeta potential of the particles in the dispersion leads to repulsion between particles and a high $k_B T$ barrier, which opposes coagulation. In such cases, a large hydrodynamic diameter

indicates that the particles have coagulated. When surfactant is absent, we recommend an alkaline medium for optimal stability of ash dispersion.

- Adding surfactant in ash dispersions leads to a more negative zeta potential, while decreasing the hydrodynamic diameter independently of the pH. This effect is more evident in extreme acidic and alkaline environments compared to the environments at moderate conditions (pH 4-8). Addition of surfactant counteracts coagulation and subsequent sedimentation for the observed period of one hour. To retain ash particles at their initial size in a surfactant solution for applications in porous media, we recommend an acidic medium.

6

EFFECT OF THE STABILITY OF THE ASH PARTICLES DISPERSION WITH/WITHOUT SURFACTANT ON THE FOAM PRESSURE DROP

I do not mind if you think slowly, but I do object when you publish more quickly than you think.

Wolfgang Pauli

The chapter summarizes experimental work to prove the connection between colloidal stability of ash dispersions and their effect on the pressure drop during foam flow in porous media. The mixtures of nitrogen gas and surfactant AOS (Alpha Olefin Sulfonate solution of 0.0375 and 0.15 w/w %) of a pH of 6.5 with and without 0.04 w/w % ash particles are passed through a sandpack of 130 Darcy. Similarly, we passed mixtures of nitrogen gas and 0.0375 w/w % AOS solution at a pH of 3.0, i.e. at the optimal stability condition for ash particles, with and without particles through a Bentheimer consolidated core of 3 Darcy. A foam flow experiment is conducted by injecting a particle dispersion and nitrogen gas without surfactant. We compared the pressure drop profile measured across the porous media for the dispersion with particles to that for the dispersion without particles. We attribute the pressure drop increase across the porous medium during foam flow to the increased stability of foam films. If the porous medium is thoroughly cleaned after each experiment, no permanent permeability deterioration is observed. When the surfactant is absent, the pressure drop across the core during experiments with particle dispersion and

nitrogen gas is very small (one percent) compared to the foam experiments when surfactant is present. In case of the sandpack for a dispersion at a pH of 6.5, the addition of ash particles does not influence the pressure drop during foam flow. Possibly particles from the unstable dispersion are not able to enter the sandpack. In case of the Bentheimer core using a dispersion at a pH of 3.0, the addition of particles increases the pressure drop by 10-15 %. Therefore, the effect of ash particles on the pressure drop during foam flow in both porous media (sandpack and Bentheimer) is related to the colloidal stability of the ash dispersions.

6.1. INTRODUCTION

Foam in porous media suffers from the adsorption losses [145] and the chemical instability of the surfactant [146]. Osmotic pressure [147] causes drainage from a foam film between foam bubbles, i.e. from the lamellae to the Plateau borders[1] due to internal concentration differences. Gravity causes drainage of liquid from the Plateau border to the foam base, where the foam film touches the surface of the medium. In addition, the Laplace pressure[2] causes diffusion of gas from smaller to larger bubbles. The trapping of nanoparticles in the Plateau borders as well as in the lamellae retards liquid drainage and bubble coalescence as observed in bulk foam with clay [12] or silica [13] particles. Such particle enhanced foam flow can increase the pressure gradient across a porous medium [14–16] and can change the wettability of the inner pore walls [5, 148, 149]. In addition, foam can promote deeper penetration of the particles (e.g. haemetite[10]), delaying particle cake formation. However, particles can change the wettability of the inner pore walls and decrease the permeability of the porous medium [148, 149]. To understand the pros and cons of particle enhanced foam flow through porous media, more study is necessary.

Possible mechanisms of liquid film stabilization due to particles involve (a) a monolayer of bridging particles, (b) a bilayer of close-packed particles and (c) a network of particle aggregates (gel) inside the film [150, 151]. The presence of particles can hamper the drainage of the liquid film or enhance repulsion between two film interfaces. Completely hydrophilic or completely hydrophobic particles will not get at the interface between gas and water. Therefore, wettability is an important property to consider in the particle stabilized bulk foam [152–156]. The forces acting at the gas-liquid interface affect the wettability. For example, Van der Waals forces tend to make films thin but the electrostatic double layer repulsion force counteracts the thinning of films. The surface tension gradient (Marangoni effect) counteracts further stretching [36]. Forces due to short-range interactions, capillary action, thermal fluctuation and solvation have been recently considered for wettability change due to particle adsorption at the interfaces [157]. The forces are influenced by the particle size, the surface properties of particles, the pH of the solution and the salinity of the solution as discussed in the previous chapter 5. If the particle size is small enough compared to the film thickness, the particles connect the two liquid-gas interfaces and stabilize the foam film [158]. Further, treatment of the particles with polymer or surfactant changes the surface properties of the hydrophilic

[1] An edge, where the three soap films always meet at an angle of 120 degrees.
[2] The pressure difference between the inside and the outside of a curved surface.

particles. The polymer treatment of particles leads to an increase in their hydrophobic nature, which promotes particle adsorption on the bubble surfaces [154, 156, 159–163]. For example, Espinosa [164] used a polymer, PolyEthylene Glycol (PEG), to convert hydrophlic silica into hydrophobic silica.
The effect of silica particles on the pressure drop in the presence or absence of surfactant during two-phase (foam) flow in porous media is well-studied [14, 159, 161, 162, 164–167]. Surfactants and particles are primarily screened before their further use in foam flow experiments, e.g., in beadpack [15, 16]. However, the studies discuss particle added foam flow without accounting for the stability of the particles in a dispersion. In addition they did not extensively discuss the effect of particle flow along with the surfactant solution on the permeability of porous media. In addition, most studies use high concentrations of surfactants, e.g. Wang [12] and Singh [13] used 0.4 wt % and 0.5 wt % of surfactants respectively. The pressure drop during foam flow due to particles in a surfactant solution with a concentration near the critical micelle concentration (CMC) has not been studied.
Fly ash particles, i.e. a waste from coal-fired power plants have physical and chemical properties like silica particles as observed previously in subsection 5.3.1 chapter 5. The purpose of the current chapter is to prove or disprove the effect of ash particles on the increase of the pressure gradient during foam flow in porous media. Our hypothesis is that ash particles stabilize foam in porous media by slowing down the drainage of liquid from lamellae. Such an enhanced stabilization will reduce the relative gas permeability [168] and will be observed as an increased pressure gradient in foam flow tests. However, a larger pressure gradient can also be caused by swelling of clay particles due to surfactant adsorption [169] on the porous medium. Therefore we refer to chapter 2 for the adsorption of surfactant at a critical micelle concentration for further details. In addition, we conducted auxiliary experiments measuring the surface tension and "foamability" of the dispersions in a test tube. The particle retention in the porous medium would also change the permeability of the medium. We hypothesize that such a change in the permeability can be detected by pressure drop measurements before and after the foam flow experiment.
The main emphasis in this chapter is on flow experiments. In order to attach a particle to a bubble, the surfactant needs to lower the contact angle between solid and gas but not overload the interface to prevent aggregation. Therefore we selected a concentration for flow experiments, which is close to the critical micelle concentration. Chapter 2 describes the experimental set-up used for the foam flow tests. We describe the colloidal stability of ash dispersion with and without surfactant in chapter 5. We study the effect of particle addition on the stability of foam flow through porous media with combinations of particles and Alpha Olefin Sulfonate (AOS) in acidic water as documented in the following sections. In subsection 6.2.2 of this chapter we describe long duration foam flow experiments (maximum 30 pore volumes). There are five foam experiments with the fine sandpack of 130 Darcy that allow a comparison between ash free and ash-added dispersions (pH 6.5) at atmospheric back pressure. There are five foam experiments with the Bentheimer sandstone of 3 Darcy that allow a comparison between ash free and ash-added dispersions at conditions where the ash particles are most stable, i.e. at an acidic pH of 3 with 0.0375 w/w % AOS. We conducted the tests before and after

Solution ml	Ash dispersion ml	HCl 0.1M ml	Final dispersion	pH
795 (0.0375 w/w % AOS)	-	4.6	0.0375 w/w %AOS	3.07
785 (DD water)	6.4	4	0.04 w/w %Ash	2.83
785 (0.0375 w/w%AOS)	6.4	7	0.0375 w/w% AOS + 0.04 w/w % Ash	2.92

Table 6.1: Samples for flow experiments with Bentheimer. pH is changed by adding HCl.

the foam flow experiments to measure the effect of particles on the permeability of the porous medium. The main experimental result, shown in subsection 6.3, is the pressure drop history between two measurement points and the time required to get a stationary value. Section 6.4 compares the effect on the pressure gradient due to addition of ash particles in the AOS solution for experiments with an unconsolidated sandpack and Bentheimer. Appendix C describes auxiliary experiments measuring the surface tension, the zeta potential and "foamability" in a test tube, used to support the conclusions.

6.2. EXPERIMENTS

6.2.1. POROUS MEDIA, DISPERSIONS

We used two porous media, namely an unconsolidated sandpack of 130 Darcy (Figure 2.4) and a Bentheimer core of 3 Darcy (Figure 2.5) to observe the effect of foam flow with and without particles on the pressure drop. We used Bio-TERGE® AS-40, an Alpha Olefin Sulfonate (AOS) solution, with 39.1 w/w % active content in doubly distilled water. We received ash particles (0.05 g/ml, 250 ml) from the power plant Kraftwerk Altbach/Deizisau near Stuttgart in Germany. Subsection 2.1.2 and subsection 2.1.3 describe the surfactant and ash particles respectively. Ash particles were surface treated with PolyethyleneImine (PEI) as described in Appendix C. Table C.2 from Appendix C shows the effect of treatment of ash particles on their zeta potential in doubly distilled water. For experiments with the sandpack, we used a surfactant solution in doubly distilled water (pH = 6.0 ± 0.5) with two concentrations (0.0375 and 0.15 w/w %). We prepared a 610 ml dispersion containing 0.0375 w/w % AOS and 0.04 w/w % ash particles by mixing 600 ml of a 0.0375 w/w % AOS solution with 10 ml of a 2.5 w/w% ash particle dispersion. For the experiments with Bentheimer, we prepared a 0.0375 w/w % AOS solution by diluting the solution of 0.3 w/w % AOS in doubly distilled water with dissolved HCl (pH = 3.0 ± 0.3). Table 6.1 shows the AOS-Ash dispersion with 0.04 w/w % ash and 0.0375 w/w % AOS, prepared by adding the ash particle dispersion to the 0.0375 w/w % AOS solution. We treated the dispersion ultrasonically after preparation and used it for the experiments after one hour at the earliest and after one day at the latest.

6.2.2. FOAM FLOW EXPERIMENTS

Chapter 2, section 2.2 describes the flow set up used for foam experiments. The flow was from top to bottom in the porous media in all experiments. Table 6.2 gives the conditions before the start of the experiments and the conditions during the steady state flow of a single phase AOS solution before gas injection. Table 6.3 gives the steady state conditions

after gas injection. We proposed to study the effect of particles for two AOS concentrations, at CMC (0.0375 w/w %) and well above CMC (0.15 w/w %). We used magnetic stirring (300 rpm) to keep the particles suspended in the injection vessel during the experiments. We conducted five experiments with the sandpack of 130 Darcy, one for each case, i.e. a solution of 0.0375 w/w % AOS (Expt "K0"), a solution of 0.15 w/w % AOS (Expt "L"), a dispersion containing 0.04 w/w % ash and 0.0375 w/w % AOS (Expt "L1"), a dispersion containing 0.04 w/w % ash particles without surfactant (Expt "L2") and a dispersion containing 0.04 w/w % ash and 0.15 w/w % AOS (Expt "L3"). The flow rate was kept constant in all five experiments (Liquid: 1.03 m/d and Nitrogen gas: 4.14 m/d). The back pressure during the experiments was at 1.03 barA. We did not measure the temperature during experiments. After experiment "L3", we carried out a test to measure the permeability of the sandpack as described in Appendix A. We conducted five experiments with the Bentheimer core of 3 Darcy: two for 0.0375 w/w % of AOS solution, one for 0.04 w/w % ash particle dispersion and two for ash (0.04 w/w %) in 0.0375 w/w % AOS dispersion. We measured the permeability of the core before and after each foam flow experiment as described in Appendix A. The measurements for the foam experiment with the Bentheimer core started at t=0 seconds by flushing a 0.0375 w/w % AOS ($\approx$ CMC). We waited to achieve a steady liquid pressure drop between measurement points. After achieving a steady state pressure drop for single phase flow, we injected N_2 gas in the already flowing AOS solution. The inlet and outlet pressure at the time of gas injection were 4.22 and 4.18 barA respectively. After injection of approximately 600 ml of AOS solution with a corresponding amount of gas, we stopped the measurements by closing the gas and liquid flow. We repeated the foam experiment "M0" with AOS solution under the name "M" and the foam experiment "M2" with AOS-ash particle dispersion under the name "M4". The temperature in the laboratory measured during the spring season fluctuated between 16 and 17 °C. Before and after each flow test, we measured the surface tension of the dispersion samples and the solution used for permeability tests.

6.3. RESULTS

The permeability of the sandpack changed from 130 Darcy to 112 Darcy (Appendix A) after conducting foam experiment "L3" with AOS-ash dispersion at pH 6.5 on 13^{th} September 2011. The permeability of the Bentheimer remains unchanged after foam flow experiments with ash-particles at pH 3, which is an optimum stability condition as shown in chapter 5. Bentheimer requires 20-25 pore volumes of 0.0375 w/w % AOS solution to satisfy the adsorption condition as shown in chapter 2. The permeability test for Bentheimer conducted after the first foam flow experiment without ash particles shows a decrease in the permeability of the core, which will be discussed in discussion section.

6.3.1. SANDPACK

Figure 6.1 shows a comparison of three pressure drop profiles during the experiments with the sandpack. The red triangles show the pressure drop due to foam flow containing 0.0375 w/w% AOS and 0.04 w/w % ash particles. The blue diamonds show the pressure drop due to foam flow of a solution of 0.0375 w/w % AOS without ash particles. The fluctuation observed in the experiments with the sandpack is due to the atmospheric back

Table 6.2: Experimental details before the gas injection

Porous media	Test	Date	Time started	Medium	AOS	Initial conditions before start			Steady State Single phase AOS				AOS solution before gas injection
						P_{in}	P_{out}	Δ P × 10^4	u_w	P_{in}	P_{out}	Δ P × 10^4	
		dd/mm/yy	hh:mm		w/w%	barA	barA	Pa/m	m/d	barA	barA	Pa/m	PV
Sandpack	K0	24/08/11	15:39	pH 6.5	0.0375	0.97	1.05	0.17	1.03	1.66	1.14	1.48	4.38
130 Darcy	L	29/08/11	10:02	pH 6.5	0.15	0.93	1.04	-1.96	1.09	1.04	1.05	4.80	1.43
	L1	30/08/11	14:20	pH 6.5	0.0375	0.97	1.05	0.02	1.03	1.03	1.07	4.53	0.7
	L2	03/09/11	09:28	pH 6.5	0	0.96	1.04	-0.36	1.03	1.00	1.06	0.36	3.10
	L3	13/09/11	15:26	pH 6.5	0.15	0.91	0.99	0.00	1.03	0.97	1.05	0.34	2.58
Bentheimer	M0	27/03/12	10:44	pH 3.0[b]	0.0375	3.36	3.35	0.01	3.28	4.18	4.12	1.36	4.5
3 Darcy	M1	30/03/12	15:55	pH 3.0[b]	0	0.95	0.94	0.01	3.24	4.28	4.18	1.46	4.6
	M2	05/04/12	08:24	pH 3.0[b]	0.0375	2.21	2.20	0.01	3.24	4.23	4.21	1.30	4.6
	M	19/04/12	10:44	pH 3.0[b]	0.0375	3.36	3.30	0.00	3.20	4.20	4.13	1.30	5.0
	M4	26/04/12	10:24	pH 3.0[b]	0.0375	4.03	4.02	0.00	3.25	4.26	4.21	1.01	4.7

$^{P_{in}}$Pressure at inlet manometer, $^{P_{out}}$Pressure at outlet manometer, ^{u_w}Surfactant solution velocity, ^{AOS}Alpha Olefin Sulfonate, $^{\Delta P}$Pressure drop across the measuring points, ^{PV}Pore volume of surfactant solution, [a]pH value fluctuated ± 0.2 in doubly distilled water, [b]pH value fluctuated ± 0.3 in doubly distilled water with HCl. Further details are described in the text.

Table 6.3: Experimental conditions during the steady state foam flow after gas injection

Porous media	Test	BP	u_g^{st}	P_1^{ss}	u_g^{ss}	u_w	u_t^{ss}	η^{ss}	AOS	Ash	ΔP_f $\times 10^5$
		barA	m/d	Pa	m/d	m/d	m/d	quality	w/w%	w/w%	Pa/m
Sandpack	K0	1.03	4.14	1.20	3.63	1.03	4.66	0.77	0.0375	0	0.8±0.05
130 Darcy	L	1.03	4.15	2.22	1.24	1.09	2.33	0.53	0.15	0	26.0±0.70
	L1	1.03	4.14	1.47	3.97	1.03	5.00	0.80	0.0375	0.04	0.65±0.06
	L2	1.03	4.14	1.02	4.02	1.03	5.05	0.79	0	0.04	0.4±0.20
	L3	1.03	4.14	3.18	1.30	1.03	2.38	0.57	0.15	0.04	26.5
Bentheimer	M0	4.2	3.62	7.65	1.68	3.25	4.93	0.34	0.0375	0	22.5
3 Darcy	M1	4.1	3.62	4.22	1.68	3.25	4.93	0.34	0	0.04	0.03
	M2	4.1	3.62	8.65	1.68	3.25	4.93	0.34	0.0375	0.04	28.9
	M	4.2	3.62	6.66	1.68	3.25	4.93	0.34	0.0375	0	23.7±0.05
	M4	4.1	3.62	4.22	1.68	3.25	4.93	0.34	0.0375	0.04	28.7±0.15

u_g^{st} Gas velocity at the start, u_w Surfactant solution velocity; ^{BP}Back pressure, ^{AOS}Alpha Olefin Sulfonate, $^{\Delta P_f}$ Foam pressure drop, Steady state conditions: i. P_1^{ss} Pressure at the inlet, ii. u_g^{ss} Gas velocity iii. u_t^{ss} total velocity iv. η^{ss} foam quality. Experiments "L" and "M" are described in chapter 4.

pressure and it increases with the increase in the measured foam pressure drop as shown in Figure 6.1. The green squares show the effect of foam flow on the pressure drop across the sand pack due to the flow of 0.04 w/w% ash particles in water and nitrogen gas without surfactant. As in the foam flow experiments described in Chapter 4, we observed a sharp increase in the pressure drop when we introduced gas in the porous medium. The experiments did not show a change in the pressure drop due to ash particles in the AOS solution compared to the "surfactant only" solution. When surfactant is not present, the ash particle dispersion and nitrogen gas ("L2") shows no change in the pressure drop before and after gas injection except for the initial fluctuation. We observed that the particles are visibly clogging the cylinder in the pump. In addition when we opened the gas valve for the flow (ash particle dispersion and gas), foam was not observed at the exit. The experiments show that ash particles indeed do not increase the pressure gradient in the case of "low concentration and low flow rate". Figure 6.2 shows the comparison of the pressure drop profile due to flow of a 0.15 w/w % AOS solution (blue diamonds) to the pressure drop profile due to flow of a solution containing 0.15 w/w % AOS and 0.04 w/w % ash particles dispersion (red triangles). The high pressure drop with a gradual increase during the single phase flow for a solution without particles suggest that the gas is present from an earlier experiment. This is in contrast to the result with particles, where apparently there is no evidence of gas in the single phase dispersion part of the experiment. The profiles show a sudden increase in pressure drop as a result of the injection of nitrogen gas. The pressure drop is high in both cases, i.e. approximately 28 × 10^5 Pa/m. The result shows a stable foam flow with no signs of instability for the period of experimentation (12 hours). From Figure 6.2, there was no effect of addition of ash particles on the pressure drop across the sand pack for the "high concentration and low flow rate" cases. Figure 6.3 shows a summary of the foam pressure drop values for the sandpack.

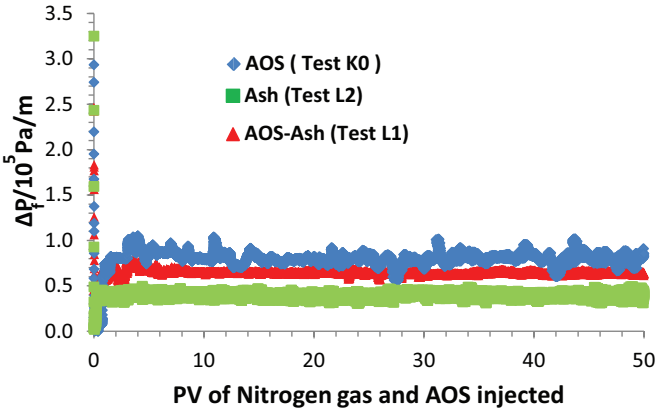

Figure 6.1: Comparison among the pressure drop values due injection of (1) 0.0375 w/w % AOS (Blue diamonds), (2) 0.0375 w/w % AOS and 0.04 w/w % ash particles (red triangles), (3) 0.04 w/w % ash particles (green squares) after nitrogen gas injection in case of a sandpack of 130 Darcy permeability. See Table 6.3 for further details.

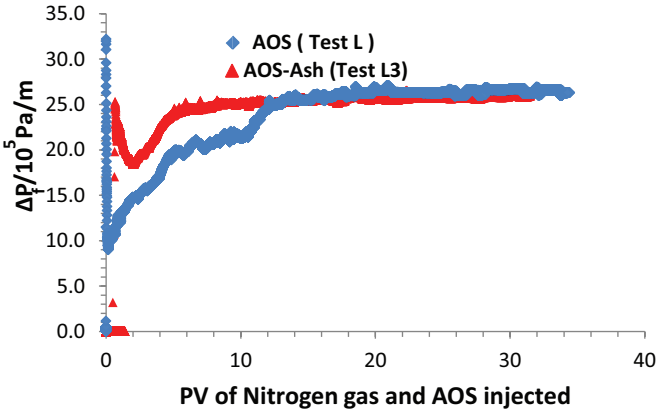

Figure 6.2: Comparison among the pressure drop values due injection of (1) 0.15 w/w % AOS (Blue diamonds) and (2) 0.15 w/w % AOS and 0.04 w/w % ash particles (red triangles) after nitrogen gas injection in case of a sandpack of 130 Darcy permeability. See Table 6.3 for further details.

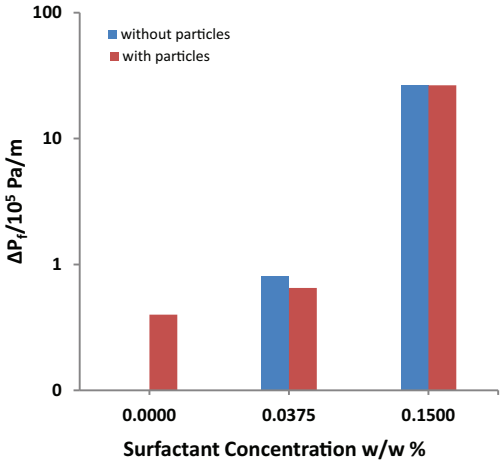

Figure 6.3: Pressure drop across the sand pack for 0.0375 w/w % and 0.15 w/w% AOS with and without 0.04 w/w % ash particles.

6.3.2. BENTHEIMER

Figure 6.4 compares the pressure drop values due to foam flow of an AOS solution, of an ash dispersion and of an AOS-ash dispersion in case of Bentheimer. Similar to the sand-pack experiments, the red triangles show the pressure drop due to 0.0375 w/w % AOS and 0.04 w/w % ash particles. The blue diamonds show the pressure drop due to foam flow of 0.0375 w/w % AOS without ash particles. The green squares show the pressure drop due to 0.04 w/w % ash particles in water and nitrogen gas without the surfactant. The steady state flow rate was kept constant for all three experiments (liquid: 3.25 m/d and nitrogen gas: 1.68 m/d). We observed a sharp increase in the pressure drop when we mixed gas with the solution. The slope of foam generation is higher in case of particle added dispersions. The experiment with a particle-AOS ("M2") dispersion shows a slight increase in the steady state pressure drop due to the presence of ash particles in the AOS solution (28.90×10^5 Pa/m) compared to "surfactant only" experiment ("M0") (26.90×10^5 Pa/m). We observed stable foam flow with no signs of instability for the subsequent period of experimentation (2 hours). The repeated experiments of an AOS only solution, "M" and an AOS solution with particles, "M4" show similar results to their predecessor experiments. Test "M" (shown in chapter 4, Figure 4.6) develops into building pressure drop of 28×10^5 Pa/m till around 20 pore volumes and then fluctuates around 26.90×10^5 Pa/m for the rest of the experiment. In case of experiments with ash particles and nitrogen gas without AOS (Experiment "M1"), particles along with gas produced an immediate pressure drop of 0.03×10^5 Pa/m. "Ash particle only" dispersion show no foam after interaction with gas. We observed severe fluctuations in the pressure difference (averaged to 0.03×10^5 Pa/m), because the particles are visibly clogging the cylinder in the pump.

Table 6.4 shows the pH and the surface tension of dispersions before and after the

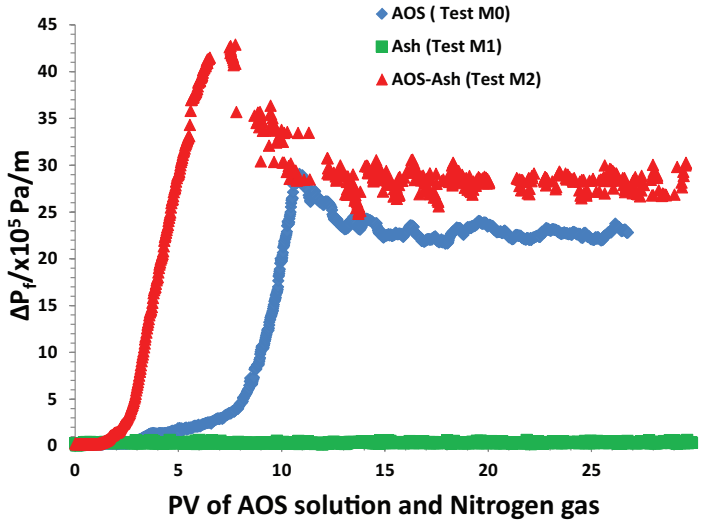

Figure 6.4: Comparison among the pressure drop due injection of (1) 0.0375 w/w % AOS (Blue diamonds), (2) 0.0375 w/w % AOS and 0.04 w/w % ash particles (red triangles) and (3) 0.04 w/w % ash particles (green squares) after nitrogen gas injection in case of a Bentheimer core of 3 Darcy permeability. See Table 6.3 for further details.

flow experiments. In all cases where we use a surfactant, the pH of effluents is higher than the pH of the inlet solutions. When AOS is not present, the pH of the inlet solutions and effluents do not defer significantly. The effluents, which are obtained after foam experiments show an increase in the surface tension. The doubly distilled water with added HCl (pH 3.0) used for the permeability tests after foam experiments show a decrease in the surface tension after passing through the core, which will be discussed in discussion section.

6.4. DISCUSSION

Four aspects are discussed here, viz. (1) interaction between polymer treated ash particles and the gas/water interface without surfactant, (2) interaction between polymer treated ash particles and the gas/water interface with surfactant, (3) adsorption of surfactant on the porous medium and (4) adsorption of particles on the porous medium. In all of these cases a generic mechanism plays a role. Particles that are not completely hydrophobic or hydrophilic attach at the gas/water interface of foam. Indeed, accumulation of these particles at the interface between gas and liquid decreases the free energy [170]. Possible configurations include particles at liquid/gas interface on one side of the film, encompassing both sides of the film or forming a network of particle aggregates (gel) inside the film [150, 151]. The presence of particles can hamper the drainage of the liquid film or enhance repulsion between two film interfaces. All of these mechanisms increase the stability of the foam film.

Table 6.4: pH and surface tension of injecting and effluent dispersions in case Bentheimer experiments. The temperature during measurement was 21 – 22 °C.

Test	**Permeability measured** Darcy	**Experiment date** dd/mm/yy	**pH** inlet	**pH** outlet	**ST**[1] inlet mN/m	**std**[2] inlet mN/m	**ST** outlet mN/m	**std** outlet mN/m
Permeability	3.28	23/03/12	2.86	3.93	69.22	0.10	58.24	0.40
M0	-	27/03/12	3.10	3.65	28.67	0.07	27.80	0.04
Permeability	2.49	29/03/12	2.93	3.22	67.37	0.17	31.79	0.46
M1	-	30/03/12	3.93	3.82	62.10	0.19	58.08	0.41
Permeability	3.18	04/04/12	3.06	3.48	70.37	0.07	30.47	0.14
M2	-	05/04/12	3.17	3.71	25.69	0.15	29.04	0.05
Permeability	3.20	11/04/12	2.95	3.50	70.32	0.09	59.17	0.37
M	-	19/04/12	3.16	3.95	27.77	0.12	28.83	0.05
Permeability	3.27	24/04/12	2.98	3.47	70.18	0.07	55.81	0.29
M4	-	26/04/12	3.12	4.20	31.19	0.22	28.68	0.11
Permeability	3.37	11/05/12	-	-	-	-	-	-

[1]Surface Tension, [2]Standard Deviation

6.4.1. INTERACTION BETWEEN ASH PARTICLES AND THE GAS/WATER INTERFACE WITHOUT SURFACTANT

A strong analogy exists between an emulsion of oil in water and a foam of air in water [36]. To create foam, we need work (W) to increase the surface area (ΔA) of liquid, i.e. $W = 2\sigma\Delta A$, where, σ is the surface tension between gas and water. The factor of two arises as there are two surfaces. From the bulk dispersion studies in Table 6.4 without surfactant, the surface tension between water and gas decreases due to addition of polymer treated ash particles, i.e., 70 mN/m of DD water to 62 mN/m for 0.04 w/w% Ash dispersion. However, we cannot assert if the decrease in the surface tension of the liquid air interface is due to adsorption of polymer from the treated ash particles or adsorption of ash particles with polymer at its surface. In addition, the lowering surface tension cannot be explained by the Gibbs adsorption formula [36]. The adsorption of the particle at the interface is related to the contact angle. We used PEI treated ash particles that were unable to foam as shown in Appendix C. Therefore, the decrease in the surface tension of the ash particle dispersion with N_2 gas is not enough to produce foam without surfactant. Consequently they were not able to enhance the pressure difference across the core as shown in Figure 6.4.

6.4.2. INTERACTION BETWEEN ASH PARTICLES AND THE GAS/WATER INTERFACE WITH SURFACTANT

If the particles were stable in a suspension (not sediment or coalesce), they would be adsorbed at the air/water interface with surfactant while flowing with foam in porous media. With a thicker air/water interface due to the particles and surfactant, the foam film would be stronger leading to a higher pressure gradient across the measuring points. Chapter 5 shows that when a surfactant is present, coagulation and sedimentation of ash particles in the bulk dispersion may or may not occur. If the particles were unstable in a suspension, they would not be adsorbed at the air/water interface and we would not measure a change in the pressure gradient as explained in the previous subsection. For instance, in the case of an unstable dispersion (pH 6.5), addition of particles did not increase the foam pressure drop for 0.0375 w/w % and 0.15 w/w % AOS solutions

in the sandpack. A similar relationship between colloidal stability of ash particles in a dispersion and their flow with foam is also observed in the Bentheimer sandstone core. When the particles are present, the foam steady state pressure drop in case of a stable dispersion of pH 3.0 is 10-15 % higher than the foam steady state pressure drop when the particles are absent. Therefore, the flow of ash particles with foam in porous media is related to the colloidal stability of the ash dispersion.

6.4.3. ADSORPTION OF SURFACTANT ON THE POROUS MEDIUM

A larger pressure gradient can also be caused by surfactant adsorption on, or particle retention in, the porous medium. When we injected gas with a 0.0375 w/w% AOS solution without particles ("M0") in Bentheimer sandstone, it took 10 to 15 pore volumes to reach the steady state pressure drop due to adsorption of surfactant on the pore wall as shown in chapter 3. We observed no significant change in the surface tension of the effluent liquid with respect to the injected dispersion. The pH of AOS containing effluents changed from 3.1 to 3.6 after passing through the core ("M0"), which indicates adsorption of H^+ ions on the pore walls. We measured a decrease in the permeability of the Bentheimer sandstone in a test conducted after a foam experiment of 0.0375 w/w% AOS without particles ("M0"). Washing the core with ethanol and water before the permeability test did not remove adsorbed AOS from the core.

6.4.4. ADSORPTION OF THE PARTICLES ON THE POROUS MEDIUM

The permeability of the porous media (sandpack and Bentheimer) slightly changed after a foam flow experiment with particles. The permeability of the sandpack was decreased, i.e. from 130 Darcy to 112 Darcy (Appendix A), but we cannot confirm that particle adsorption caused the permeability change. The permeability of the Bentheimer did not change significantly after foam flow experiments with ash particles at a pH of 3.0.

6.5. CHAPTER SUMMARY

- We conducted foam flow experiments in a sandpack of 130 Darcy and in a Bentheimer core of 3 Darcy to prove or disprove the effect of an ash dispersion on the foam flow in porous media. We conducted three cases with the sandpack, where we injected a 0.04 w/w % ash dispersion (a) without surfactant, (b) containing 0.0375 w/w % AOS solution and (c) containing 0.15 w/w % AOS solution. In the same way, we conducted three cases with the Bentheimer core with a 0.04 w/w % ash dispersion; one without surfactant and two with 0.0375 w/w % AOS solution. The pH of the injected dispersion for sandpack experiments was 6.5. For experiments with Bentheimer we selected a dispersion at a pH of 3.0, i.e. at the optimal stability condition for ash particles.

- We compared the pressure drop profile for both porous media of ash-AOS experiments with the pressure drop profile of AOS experiments without ash particles. When the surfactant is absent, the pressure drop across the core during the experiments with a particle dispersion and nitrogen gas is very small (0.03×10^5 Pa/m) compared to the foam experiments when surfactant is present (26×10^5 Pa/m). In addition, no foam formation is observed at the outlet of the set up. Therefore, we

conclude that an ash particle dispersion alone with nitrogen gas cannot generate foam in porous media.

- The effect of ash particles on foam in porous media (Bentheimer and sandpack) is related to the colloidal stability of the ash dispersion. In the case of an unstable dispersion (pH 6.5) in a sandpack, we did not observe a difference in pressure drop between cases where particles are absent or present. In case of a stable dispersion at a pH of 3.0 in Bentheimer, we observed that a foam steady state pressure drop in the presence of particles is 10-15 % higher than the pressure drop in the absence of particles. Indeed, in the experiments performed by us, the effect of ash particles on the pressure drop was noticable but relatively small.
- We observed slight change in the permeability of the porous media (sandpack and Bentheimer) after foam flow experiments with ash particles.

7

THESIS SUMMARY AND CONCLUSIONS

This concluding chapter summarizes the scientific and technical implications of the research findings in considerable detail. The general and specific ideas that the thesis brings forth are as follows:

- We measured pressure drop histories before and after injection of an Alpha Olefin Sulfonate solution (AOS) with nitrogen gas (N_2) across two measurement points in unconsolidated sand packs (1860 and 130 Darcy) and a Bentheimer sand stone core (3 Darcy) for various surfactant concentrations (0.0375, 0.075 and 0.15 w/w %), for various gas and surfactant solution velocities (0.27-3.97 m/day), for two salinities (0, 0.5M NaCl) and for two pH values (6.5, 3.0). We refer to the pressure divided by the distance between the measurement points as the pressure drop (Pa/m). When we added nitrogen in the flowing surfactant solution, we observed an increase in pressure drop across the porous media in all experiments. The pressure drop increased with an increase in the total superficial velocity and the AOS concentration while keeping other variables constant (ceteris paribus *c.p.*). For the concentration range studied by us, a limiting surfactant concentration that gives a maximum pressure drop was not observed. The initial conditions of the core (gas content, surfactant adsorption) expedited the foam generation in the core.

- We used the experimental pressure drop during foam flow to obtain a first estimate of the average bubble density in a bubble population model. The model contained four equations, viz. a pressure equation, a water saturation equation, a bubble density equation and a surfactant transport-adsorption equation. We estimated the viscosity coefficient α in the Hirasaki-Lawson equation from the surfactant concentration to relate the foam viscosity to the estimated bubble density. The modeled bubble density can take into account the trapped gas fraction and the water saturation.

- Simulations for a 0.0375 w/w % AOS-nitrogen gas flow in a Bentheimer core indicate that the maximum in the pressure drop corresponds to a minimum in the water saturation. With the assumption that all gas is foamed and foam is the only phase in the porous medium, the dependence between the source term and bubble density is approximate. The difference between the simulated and experimental pressure drop is less than 10 %, which suggests the usefulness of first estimate of the bubble generation coalescence function.

- The numerical study separates the overall bubble generation-coalescence function, $R(n_f)$ into contributions of accumulation, convection and dispersion (diffusion) of bubbles. As we approximated the viscosity coefficient α as a resistance per lamella in the capillary tube, the generation-coalescence function can only be obtained within a factor. If we consider water saturation (two-phase flow) and the flowing fraction of foam, the rate of change of bubble density during transient state is equal to the bubble density generation function plus the terms that account for bubble transport by convection and diffusion divided by porosity and saturation.

- We considered fourteen experiments with simultaneous variations in six variables viz. the permeability, the salinity, the gas velocity, pH of the solution, the surfactant concentration and the surfactant solution velocity to obtain their interactive effects on the steady state pressure drop. We applied symbolic regression to our data along with 143 data points from the literature to produce a number of analytical expressions without prior knowledge of an underlying physical process. We can describe the pressure drop with three out of six variables, viz. the permeability, the salinity and the surfactant solution velocity by a simple model with a single fitting parameter. A sensitivity analysis of the model shows that the variables in order of importance for the chosen model are the permeability, the salinity and the surfactant solution velocity. We validated the model by estimating the error in the model parameter ($A_0 = 6078 \pm 163$) by the bootstrap method. The predicted pressure drop deviated from the observed pressure drop by 10-15 %. Our data set and the data set of Jante and Osterloh [48] show significant deviation from the chosen symbolic regression model, which shows that the model has limitations. Jante and Osterloh [48] use mixtures of surfactants and we confine our data set to conditions that lead to a low pressure drop. Both our data and of Jante and Osterloh have the low foam quality in common. It is not clear to us whether the low foam quality can explain the deviation from the symbolic regression model.

- The purpose of the derived data driven model is not to replace the models based on physical processes, but to find the underlying physics of the foam flow through porous media. The model from symbolic regression is able to explain the general behavior and hierarchy of the variables affecting the steady state pressure drop. The model gives the variable spaces for which we need more experiments. Considering an entire data set shows that the trends obtained from a subset of the data are not necessarily valid for the complete data set.

- For the applications of ash particles in foam flow through porous media we studied their dispersion stability when surfactant is present or absent for pH values rang-

ing from 3 to 11. We measured two properties, viz. , zeta potential and the particle size. An inhouse built laser transmission set up can be used to measure the attenuation coefficient of the dispersions as a function of time. An ultra violet - visible light absorption instrument can be used to detect that the maximum absorption occurs at 975 nm, i.e. in the infrared region. Therefore, the light transmission is influenced by both, light absorption and light scattering.

- We observed an increase in transmitted light intensity (a decrease in attenuation coefficient) with respect to time for all dispersions, showing that a sedimentation effect prevails over a coagulation effect. We validated using Mie scattering that coagulation for relevant particles sizes leads to increased scattering intensity.

- When a surfactant is absent, a high absolute value of the zeta potential of the particles in the dispersion leads to repulsion between particles and a high $k_B T$ barrier, which opposes coagulation. In such cases, a large hydrodynamic diameter indicates that the particles already have coagulated. In such cases, we recommend an alkaline medium for optimal stability of the ash dispersion.

- Adding surfactant in ash dispersions leads to a more negative zeta potential, while decreasing the hydrodynamic diameter independent of the pH. This effect is more evident in extreme acidic and alkaline environments compared to the moderate conditions (pH 4-8). Addition of a surfactant counteracts coagulation and subsequent sedimentation for the observed period of one hour. To retain ash particles at their initial size in a surfactant solution for application in porous media, we recommend an acidic medium.

- We conducted foam flow experiments in a sandpack of 130 Darcy and in a Bentheimer core of 3 Darcy to prove or disprove the effect of an ash dispersion on the foam flow in porous media. We conducted three experiments with the sandpack, where we injected a 0.04 w/w % ash dispersion (a) without surfactant, (b) containing 0.0375 w/w % AOS solution and (c) containing 0.15 w/w % AOS solution. In the same way, we conducted three experiments with the Bentheimer core with a 0.04 w/w % ash dispersion; one without surfactant and two with 0.0375 w/w % AOS solution. The pH of the injected dispersion for sandpack experiments was 6.5. For experiments with Bentheimer we selected a dispersion at a pH of 3.0, i.e. at the optimal stability condition for ash particles.

- For both porous media, we compared the pressure drop profiles of ash-AOS experiments with the pressure drop profiles of AOS experiments without ash particles. When the surfactant is absent, the pressure drop across the core during the experiments with a particle dispersion and nitrogen gas is very small (0.03×10^5 Pa/m) compared to the foam experiments when surfactant is present (26×10^5 Pa/m) . In addition, no foam formation is observed at the outlet of the set up. Therefore, we conclude that an ash particle dispersion alone with nitrogen gas cannot generate foam in porous media.

- The effect of ash particles on foam in porous media (Bentheimer and sandpack) is related to the colloidal stability of the ash dispersion. In the case of an unstable

dispersion (pH 6.5) in a sandpack, we did not observe a difference in pressure drop between cases where particles are absent or present. In case of a stable dispersion at a pH of 3.0 in Bentheimer, we observed that a foam steady state pressure drop in the presence of particles is 10-15 % higher than the pressure drop in the absence of particles. Indeed, in the experiments performed by us, the effect of ash particles on the pressure drop is noticed albeit relatively small. If this is to be considered as practically viable, more research is needed to get optimal conditions.

- We observed tiny change in the permeability of the porous media (sandpack and Bentheimer) after foam flow experiments with ash particles. Therefore we conclude that when the ash particle suspension is unstable, the particles are not able to inject in the porous media and when the ash particle suspension is stable, the particles donot clog the pores, but flow along with the foam bubbles.

REFERENCES

[1] D. Bond and O. Holbrook, *Gas drive oil recovery process,* (1958), US Patent 2,866,507.

[2] F. Craig Jr. and J. Lummus, *Oil recovery by foam drive,* (1965), US Patent 3,185,634.

[3] L. Holm, *The mechanism of gas and liquid flow through porous media in the presence of foam,* SPE Journal **8**, 359 (1968).

[4] R. Farajzadeh, A. Andrianov, R. Krastev, G. J. Hirasaki, and W. R. Rossen, *Foam-oil interaction in porous media: implications for foam assisted enhanced oil recovery,* Advances in Colloid and Interface Science **183-184**, 1 (2012).

[5] A. M. Sani and K. K. Mohanty, *Investigation of VOC emission control by the use of clay aqueous foams,* in *SPE Annual Technical Conference and Exhibition, 21-24 September, Denver, Colorado, USA* (Society of Petroleum Engineers, 2008).

[6] Q. Xu and W. Rossen, *Effective viscosity of foam in periodically constricted tubes,* Colloids and Surfaces A: Physicochemical and Engineering Aspects **216**, 175 (2003).

[7] M. A. Dria, S. L. Bryant, R. S. Schechter, and L. W. Lake, *Interacting precipitation/dissolution waves: The movement of inorganic contaminants in groundwater,* Water Resources Research **23**, 2076 (1987).

[8] W.-x. Zhang, *Nanoscale iron particles for environmental remediation: An overview,* Journal of Nanoparticle Research **5**, 323 (2003).

[9] S. Wang and C. N. Mulligan, *An evaluation of surfactant foam technology in remediation of contaminated soil,* Chemosphere **57**, 1079 (2004).

[10] Q. Nguyen, P. Currie, and P. S. Bouzanga, *The effect of gas on the injectivity of particles in sandstone,* SPE Journal (2011), 10.2118/121637-PA.

[11] F. Tang, Z. Xiao, J. Tang, and L. Jiang, *The effect of SiO_2 particles upon stabilization of foam,* Journal of Colloid and Interface Science **131**, 498 (1989).

[12] D. Wang, Q. Hou, Y. Luo, Y. Zhu, and H. Fan, *Stability comparison between particles-stabilized foams and polymer-stabilized foams,* Journal of Dispersion Science and Technology **36**, 268 (2015).

[13] R. Singh and K. K. Mohanty, *Synergy between nanoparticles and surfactants in stabilizing foams for oil recovery,* Energy & Fuels **29**, 467 (2015).

[14] A. Aroonsri, A. J. Worthen, T. Hariz, K. P. Johnston, C. Huh, and S. L. Bryant, *Conditions for generating nanoparticle-stabilized CO_2 foams in fracture and matrix flow,* (Society of Petroleum Engineers, 2013).

[15] A. J. Worthen, S. L. Bryant, C. Huh, and K. P. Johnston, *Carbon dioxide-in-water foams stabilized with nanoparticles and surfactant acting in synergy,* AIChE Journal **59**, 3490 (2013).

[16] A. Worthen, P. Parikh, Y. Chen, S. Bryant, C. Huh, and K. Johnston, *Carbon dioxide-in-water foams stabilized with a mixture of nanoparticles and surfactant for CO_2 storage and utilization applications,* Energy Procedia **63**, 7929 (2014).

[17] F. Trogus, T. Sophany, R. Schechter, and W. Wade, *Static and dynamic adsorption of anionic and nonionic surfactants,* SPE Journal **17**, 337 (1977).

[18] G. Hirasaki and J. Lawson, *Mechanisms of foam flow in porous media: Apparent viscosity in smooth capillaries,* SPE Journal **25**, 176 (1985).

[19] A. R. Kovscek, P. Persoff, and C. J. Radke, *A mechanistic population balance model for transient and steady-state foam flow in Boise sandstone,* Chemical Engineering Science **50**, 3783 (1995).

[20] A. Falls, G. Hirasaki, T. Patzek, D. Gauglitz, D. Miller, and T. Ratulowski, *Development of a mechanistic foam simulator: The population balance and generation by snap-off,* SPE Reservoir Engineering **3**, 884 (1988).

[21] W. R. Rossen, *A critical review of Roof snap-off as a mechanism of steady-state foam generation in homogeneous porous media,* Colloids and Surfaces A: Physicochemical and Engineering Aspects **225**, 1 (2003).

[22] P. L. J. Zitha, D. X. Du, M. Uijttenhout, and Q. P. Nguyen, *Numerical analysis of a new stochastic bubble population foam model,* in *SPE/DOE Symposium on Improved oil recovery, 22-26 April, Tulsa, USA* (Society of Petroleum Engineers, 2006) pp. 1–14.

[23] O. Fergui, H. Bertin, and M. Quintard, *Transient aqueous foam flow in porous media: experiments and modeling,* Journal of Petroleum Science and Engineering **20**, 9 (1998).

[24] J. Martinez, *Foam-Flow Behaviour in Porous Media: Effects of Flow Regime and Porous-Medium Heterogeneity*, Ph.D. thesis, University of Texas at Austin (1998).

[25] J. Martinez, H. J. Rivas, and W. R. Rossen, *Unified model for steady-state foam behavior at high and low foam qualities,* SPE Journal **6**, 325 (2001).

[26] A. R. Kovscek, T. W. Patzek, and C. J. Radke, *Mechanistic foam flow simulation in heterogeneous and multidimensional porous media,* SPE Journal **2**, 511 (1997).

[27] W. Rossen, S. Zeilinger, J.-X. Shi, and M. Lim, *Simplified mechanistic simulation of foam processes in porous media,* SPE Journal **4**, 279 (1999).

[28] R. Mason, R. Gunst, and J. Hess, *Statistical Design and Analysis of Experiments*, 2nd ed. (John Wiley & Sons, Inc., Hoboken, New Jersey, 2003).

[29] H. Helmholtz, *Ueber einige gesetze der vertheilung elektrischer ströme in körperlichen leitern mit anwendung auf die thierisch-elektrischen versuche,* Annalen der Physik **165**, 211 (1853).

[30] H. Hamaker, *The London-Van der Waals attraction between spherical particles,* Physica **4**, 1058 (1937).

[31] E. J. W. Verwey, *Theory of the stability of lyophobic colloids.* The Journal of Physical and Colloid Chemistry **51**, 631 (1947).

[32] J. N. Israelachvli, *Intermolecular and Surface Forces* (Elsevier, 2011) p. 674.

[33] W. A. Ducker, T. J. Senden, and R. M. Pashley, *Direct measurement of colloidal forces using an atomic force microscope,* Nature **353**, 239 (1991).

[34] J. Forsman, C. Woodward, and B. Jönsson, *The origins of hydration forces:Monte Carlo simulations and density functional theory,* Langmuir **13**, 5459 (1997).

[35] F. T. Hesselink, A. Vrij, and J. T. G. Overbeek, *Theory of the stabilization of dispersions by adsorbed macromolecules. II. Interaction between two flat particles,* The Journal of Physical Chemistry **75**, 2094 (1971).

[36] J. Overbeek, *Colloid and Surface Chemistry,* Lyophobic Colloids, Vol. 2 (Massacheusetts Institute of Technology, Cambridge, Massacheusetts, 1971).

[37] M. Simjoo, *Immiscible foam for Enhanced Oil Recovery,* Ph.D. thesis, Delft University of Technology (2012).

[38] A. Falls, J. Musters, and J. Ratulowski, *The apparent viscosity of foams in homogeneous bead packs,* SPE Reservoir Engineering **4**, 155 (1989).

[39] P. Persoff, C. Radke, K. Pruess, S. Benson, and P. Witherspoon, *A laboratory investigation of foam flow in sandstone at elevated pressure,* SPE Reservoir Engineering **6**, 365 (1991).

[40] F. Friedmann, W. Chen, and P. Gauglitz, *Experimental and simulation study of high-temperature foam displacement in porous media,* SPE Reservoir Engineering **6**, 37 (1991).

[41] D. Liu, L. M. Castanier, and W. E. Brigham, *Displacement by foam in porous media,* in *Annual Technical Conference and Exhibition, 4-7 October, Washington, DC, USA* (Society of Petroleum Engineers, 1992).

[42] M. Carretero-Carralero, R. Farajzadeh, D. Du, and P. Zitha, *Modeling and CT-scan study of foams for acid diversion,* in *European Formation Damage Conference, 30 May-1 June, Scheveningen, The Netherlands*, Vol. 2 (Society of Petroleum Engineers, 2007) pp. 769–779.

[43] D. Du, P. Zitha, and F. Vermolen, *Numerical analysis of foam motion in porous media using a new stochastic bubble population model,* Transport in Porous Media **86**, 461 (2011).

[44] M. Schmidt and H. Lipson, *Distilling free-form natural laws from experimental data,* Science **324**, 81 (2009).

[45] K. Vladislavleva, K. Veeramachaneni, U.-M. O'Reilly, M. Burland, and J. Parcon, *Learning a lot from only a little: Genetic programming for panel segmentation on sparse sensory evaluation data,* in *Genetic Programming*, Lecture Notes in Computer Science, Vol. 6021, edited by A. Esparcia-Alcázar, A. Ekárt, S. Silva, S. Dignum, and A. Uyar (Springer Berlin Heidelberg, 2010) pp. 244–255.

[46] C. E. Renshaw, G. D. Zynda, and J. C. Fountain, *Permeability reductions induced by sorption of surfactant,* Water Resources Research **33**, 371 (1997).

[47] L. Chen, D. A. Sabatini, and T. C. G. Kibbey, *Retention and release of TiO_2 nanoparticles in unsaturated porous media during dynamic saturation change,* Journal of Contaminant Hydrology **118**, 199 (2010).

[48] W. Osterloh and M. Jante Jr., *Effects of gas and liquid velocity on steady-state foam flow at high temperature,* in *SPE/DOE Enhanced Oil Recovery Symposium, 22-24 April, Tulsa, Oklahoma* (Society of Petroleum Engineers, 1992) pp. 237–248.

[49] Nutonian, *Eureqa® Desktop,* (2015), www.nutonian.com/products/eureqa/.

[50] H. Akaike, *A new look at the statistical model identification,* IEEE Transactions on Automatic Control **19**, 716 (1974).

[51] B. Efron and R. Tibshirani, *An Introduction to the Bootstrap*, Monographs on Statistics and Applied Probability, Vol. 57 (Chapman Hall CRC, 1993).

[52] H. Press, S. A. Teukolsky, W. Vetterling, and B. Flannery, *Numerical Recipes*, 3rd ed. (Cambridge university press, New York, 2007).

[53] G. Mie, *Beiträge zur optik trüber medien, speziell kolloidaler metallösungen,* Annalen der Physik **330**, 377 (1908).

[54] R. Evans and D. Napper, *Steric stabilization I,* Kolloid-Zeitschrift und Zeitschrift für Polymere **251**, 409 (1973).

[55] R. Evans and D. Napper, *Steric stabilization II,* Kolloid-Zeitschrift und Zeitschrift für Polymere **251**, 329 (1973).

[56] R. J. Hunter, *Zeta Potential in Colloid science* (Academic Pr, 1981) p. 386.

[57] S. E. Buckley and M. C. Leverett, *Mechanism of fluid displacement in sands,* Transactions of the AIME **146**, 107 (1942).

[58] Z. Zhou and W. R. Rossen, *Applying fractional-flow theory to foam processes at the "limiting capillary pressure",* SPE Advanced Technology Series **3**, 154 (1995).

[59] R. H. Brooks and A. Corey, *Properties of porous media affecting fluid flow,* Journal of the Irrigation and Drainage Division **92**, 61 (1966).

[60] Reviewer, *Review "Determination of the most significant variables affecting the steady state pressure drop in selected foam flow experiments",* (2015), manuscript number PETROL6802.

[61] H. Salimi and J. Bruining, *Upscaling in partially fractured oil reservoirs using homogenization,* SPE Journal **16**, 273 (2011).

[62] M. N. Panda and L. W. Lake, *Estimation of single-phase permeability from parameters of particle-size distribution,* AAPG Bulletin **78**, 1028 (1994).

[63] R. Chhabra and J. Richardson, *Chapter 2 - rheometry for non-newtonian fluids,* in *Non-Newtonian Flow and Applied Rheology (Second Edition)*, edited by R. C. Richardson (Butterworth-Heinemann, Oxford, 2008) second edition ed., pp. 56 – 109.

[64] K. Wolf, *The interaction between coal fires and their roof rocks,* Ph.D. thesis, Delft University of Technology (2006).

[65] B. Furniss, A. Hannaford, P. Smith, and A. Tatchell, *Vogel's Textbook of Practical Organic Chemistry,* 5th ed. (Longman Group UK Limited, U.K, 1989).

[66] R. Wygal, *Construction of models that simulate oil reservoirs,* SPE Journal **3**, 281 (1963).

[67] M. J. Rosen, *Surfactants and Interfacial Phenomena,* 3rd ed. (John Wiley & Sons, New Jersey, 2004).

[68] R. A. Ettinger and C. J. Radke, *Influence of texture on steady foam flow in Berea sandstone,* SPE Reservoir Engineering **7**, 83 (1992).

[69] T. Ransohoff and C. Radke, *Mechanisms of foam generation in glass-bead packs,* SPE Reservoir Engineering **3**, 573 (1988).

[70] Malvern, *Zetasizer nano ZS :when your laboratory needs the best.* (2011).

[71] R. Pecora, *Dynamic light scattering: Applications of photon correlation spectroscopy* (Plenum, 1985).

[72] M. I. Kuhlman, A. M. Falls, S. K. Hara, T. G. Monger-McClure, and J. K. Borchardt, *CO_2 foam with surfactants used below their critical micelle concentrations,* SPE Reservoir Engineering **7**, 445 (1992).

[73] R. Thorat and H. Bruining, *Foam flow experiments. I. estimation of the bubble generation-coalescence function,* Transport in Porous Media **112**, 53 (2016).

[74] G. E. P. Box, *Science and statistics,* Journal of the American Statistical Association **71**, pp. 791 (1976).

[75] Z. Khatib, G. Hirasaki, and A. Falls, *Effects of capillary pressure on coalescence and phase mobilities in foams flowing through porous media,* SPE Reservoir Engineering **3**, 919 (1988).

[76] K. Ma, G. Ren, P. R. Cordelier, K. Mateen, and D. C. Morel, *Literature review of modeling techniques for foam flow through porous media,* in *SPE Improved Oil Recovery Symposium, 12-16 April, Tulsa, Oklahoma, USA* (Society of Petroleum Engineers, 2014).

[77] O. Apaydin and A. Kovscek, *Surfactant concentration and end effects on foam flow in porous media,* Transport in Porous Media **43**, 511 (2001).

[78] D. Huh and L. Handy, *Comparison of steady and unsteady-state flow of gas and foaming solution in porous media,* SPE Reservoir Engineering **4**, 77 (1989).

[79] S. Chou, *Conditions for generating foam in porous media,* in *SPE Annual Technical Conference and Exhibition, 6-9 October, Dallas, Texas* (Society of Petroleum Engineers, 1991) pp. 353–364.

[80] K. Aziz and A. Settari, *Petroleum reservoir simulation* (Applied Science Publishers Ltd., 1979).

[81] F. P. Bretherton, *The motion of long bubbles in tubes,* Journal of Fluid Mechanics **10**, 166 (1961).

[82] G. Q. Tang and A. R. Kovscek, *Trapped gas fraction during steady-state foam flow,* Transport in Porous Media **65**, 287 (2006).

[83] R. Haberman, *Applied partial differential equations* (Pearson, 2004) pp. 267–270.

[84] L. Lake, *Enhanced oil recovery* (Prentice Hall, 1989).

[85] P. V. Danckwerts, *Continuous flow systems,* Chemical Engineering Science **2**, 1 (1953).

[86] K. E. Jansen, C. H. Whiting, and G. M. Hulbert, *A generalized-α method for integrating the filtered Navier–Stokes equations with a stabilized finite element method,* Computer Methods in Applied Mechanics and Engineering **190**, 305 (2000).

[87] F. Dullien, *Porous Media-Fluid Transport and Pore Structure* (Academic Press, INC, 1992).

[88] R. Thorat and H. Bruining, *Determination of the most significant variables affecting the steady state pressure drop in selected foam flow experiments,* Journal of Petroleum Science and Engineering , (2016).

[89] F. Dyson, *A meeting with Enrico Fermi,* Nature **427**, 297 (2004).

[90] F. Friedmann and A. Jensen, *Some parameters influencing the formation and propagation of foams in porous media,* in *SPE California Regional Meeting, 2-4 April, Oakland, California* (Society of Petroleum Engineers, 1986) pp. 441–454.

[91] W. R. Rossen and P. A. Gauglitz, *Percolation theory of creation and mobilization of foams in porous media,* AIChE Journal **36**, 1176 (1990).

[92] D. Cohen, T. Patzek, and C. Radke, *Onset of mobilization and the fraction of trapped foam in porous media,* Transport in Porous Media **28**, 253 (1997).

[93] Q. Nguyen, P. K. Currie, M. Buijse, and P. L. J. Zitha, *Mapping of foam mobility in porous media,* Journal of Petroleum Science and Engineering **58**, 119 (2007).

[94] H. Balan, M. T. Balhoff, Q. P. Nguyen, and W. Rossen, *Network modeling of gas trapping and mobility in foam enhanced oil recovery,* Energy & Fuels **25**, 3974 (2011).

[95] G. Barenblatt, V. Entov, and V. Ryzhik, *Theory of fluid flows through natural rocks* (Kluwer, Dordrecht, 1989).

[96] Y. Yortsos and J. Chang, *Capillary effects in steady-state flow in heterogeneous cores,* Transport in Porous Media **5**, 399 (1990), cited By 38.

[97] J. S. Osoba, J. G. Richardson, J. K. Kerver, J. A. Hafford, and P. M. Blair, *Laboratory measurements of relative permeability,* Journal of Petroleum Technology **3** (1951), 10.2118/951047-G.

[98] Z.-X. Pang, *The blocking ability and flowing characteristics of steady foams in porous media,* Transport in Porous Media **85**, 299 (2010).

[99] M. Simjoo, Y. Dong, A. Andrianov, M. Talanana, and P. L. J. Zitha, *Novel insight into foam mobility control,* SPE Journal **18**, 416 (2013).

[100] E. E. Isaacs, F. C. McCarthy, and J. D. Maunder, *Investigation of foam stability in porous media at elevated temperatures,* SPE Reservoir Engineering **3**, 565 (1988).

[101] J. E. Hanssen, *Foam as a gas-blocking agent in petroleum reservoirs I: Empirical observations and parametric study,* Journal of Petroleum Science and Engineering **10**, 117 (1993).

[102] H. J. Bertin, O. G. Apaydin, L. M. Castanier, and A. R. Kovscek, *Foam flow in heterogeneous porous media: Effect of cross flow,* SPE Journal **4**, 75 (1999).

[103] J. S. Solbakken, A. Skauge, and M. G. Aarra, *Foam performance in low permeability laminated sandstones,* Energy & Fuels **28**, 803 (2014).

[104] L. Kapetas, S. Vincent Bonnieu, S. Danelis, R. Farajzadeh, A. Eftekhari, S. R. Mohd Shafian, R. Z. Kamarul Bahrim, and W. R. Rossen, *Effect of temperature on foam flow in porous media,* in *SPE Middle East Oil & Gas Show and Conference, 8-11 March, Manama, Bahrain* (Society of Petroleum Engineers, 2015) pp. 1–16.

[105] A. S. de Vries and K. Wit, *Rheology of gas/water foam in the quality range relevant to steam foam,* SPE Reservoir Engineering **5**, 185 (1990).

[106] W. R. Rossen, Z. H. Zhou, and C. K. Mamun, *Modeling foam mobility in porous media,* SPE Advanced Technology Series **3**, 146 (1995).

[107] W. R. Rossen and M. W. Wang, *Modeling foams for acid diversion,* SPE Journal **4**, 92 (1999).

[108] E. Ashoori, D. Marchesin, and W. Rossen, *Roles of transient and local equilibrium foam behavior in porous media: travelling wave,* Colloids and Surfaces A: Physicochemical and Engineering Aspects **377**, 228 (2011).

[109] K. Ma, J. L. Lopez-Salinas, C. A. Miller, S. L. Biswal, and G. J. Hirasaki, *Non-uniqueness, numerical artifacts, and parameter sensitivity in simulating steady-state and transient foam flow through porous media,* Transport in porous media **102**, 325 (2014).

[110] W. R. Rossen and C. S. Boeije, *Fitting foam-simulation-model parameters to data: II. Surfactant-Alternating-Gas foam applications,* SPE Reservoir Evaluation & Engineering **18**, 273 (2015).

[111] C. Boeije and W. Rossen, *Fitting foam-simulation-model parameters to data: I. coinjection of gas and liquid,* SPE Reservoir Evaluation & Engineering **18**, 264 (2015).

[112] H. Bertin, M. Quintard, and L. Castanier, *Development of a bubble-population correlation for foam-flow modeling in porous media,* SPE Journal **3**, 356 (1998).

[113] S. I. Kam and W. R. Rossen, *A model for foam generation in homogeneous media,* SPE Journal **8**, 417 (2003).

[114] K. Ma, G. Ren, K. Mateen, D. Morrel, P. Cordelier, and G. J. Hirasaki, *Modeling techniques for foam flow in porous media,* SPE Journal **20**, 453 (2015).

[115] L. Zhao, A. Li, K. Chen, J. Tang, and S. Fu, *Development and evaluation of foaming agents for high salinity tolerance,* Journal of Petroleum Science and Engineering **81**, 18 (2012).

[116] D. Montegomery, *Design and Analysis of Experiments*, 7th ed. (John Wiley & Sons, Inc., Hoboken, New Jersey, 2007).

[117] J. Wang, H. Liu, Z. Ning, and H. Zhang, *Experimental research and quantitative characterization of nitrogen foam blocking characteristics,* Energy & Fuels **26**, 5152 (2012).

[118] Q. Nguyen, P. Zitha, and P. K. Currie, *Effect of foam films on gas diffusion,* Journal of Colloid and Interface Science **248**, 467 (2002).

[119] R. Farajzadeh, R. M. Muruganathan, W. R. Rossen, and R. Krastev, *Effect of gas type on foam film permeability and its implications for foam flow in porous media,* Advances in Colloid and Interface Science **168**, 71 (2011).

[120] K. Ma, J. L. Lopez-Salinas, M. C. Puerto, C. A. Miller, S. L. Biswal, and G. J. Hirasaki, *Estimation of parameters for the simulation of foam flow through porous media. part 1: The dry-out effect,* Energy & Fuels **27**, 2363 (2013).

[121] C. Boeije and W. Rossen, *Fitting foam simulation model parameters to data,* in *IOR 2013: 17th European Symposium on Improved Oil Recovery, St. Petersburg, Russia, 16-18 April* (EAGE, 2013) pp. 1–16.

[122] J. D. Olden and D. A. Jackson, *Torturing data for the sake of generality: How valid are our regression models?* Ecoscience **7**, 501 (2000).

[123] E. Vittinghoff, D. Glidden, S. Shiboski, and C. McCulloch, *Basic statistical methods,* in *Regression Methods in Biostatistics*, Statistics for Biology and Health (Springer US, 2012) pp. 27–67.

[124] K. Veeramachaneni, E. Vladislavleva, and U. M. O'Reilly, *Knowledge mining sensory evaluation data: Genetic programming, statistical techniques, and swarm optimization,* Genetic Programming and Evolvable Machines **13**, 103 (2012).

[125] A. Raynolds, *Sensitivity interpretation,* (2014), formulize.nutonian.com/forum.

[126] L. Wang and R.-H. Yoon, *Effect of pH and NaCl concentration on the stability of surfactant-free foam films,* Langmuir **25**, 294 (2009).

[127] N. Schelero, G. Hedicke, P. Linse, and R. v. Klitzing, *Effects of counterions and coions on foam films stabilized by anionic dodecyl sulfate,* The Journal of Physical Chemistry B **114**, 15523 (2010).

[128] K. S. Sorbie, *Polymers in improved oil recovery* (Boca Raton, FL (USA); CRC Press Inc., 1990).

[129] C. Metin, L. W. Lake, C. Miranda, and Q. Nguyen, *Stability of aqueous silica nanoparticle dispersions,* Journal of Nanoparticle Research **13**, 839 (2011).

[130] G. K. Batchelor, *An introduction to fluid dynamics* (Cambridge University Press, 1967).

[131] R. J. Hunter, *Introduction to Modern Colloid Science* (Oxford University Press, 2002) p. 344.

[132] H. Yotsumoto and R.-H. Yoon, *Application of extended DLVO theory: II. stability of silica suspensions,* Journal of Colloid and Interface Science **157**, 434 (1993).

[133] A. W. Adamson and A. P. Gast, *Physical chemistry of surfaces*, sixth ed. (Wiley, 1997).

[134] M. Hosokawa, K. Nogi, M. Naito, and T. Yokoyama, *Nanoparticle technology handbook,* (Elsevier Science, Amsterdam, 2007) Chap. Characteristics and behavior of nanoparticles and its dispersion systems.

[135] J. Lyklema, F. Dumont, A. Watillon, T. F. Tadros, M. A. Malati, S. F. Estefan, T. W. Healy, S. G. Dick, G. D. Parfitt, and J. A. Kitchener, *General discussion,* Discuss. Faraday Soc. **52**, 372 (1971).

[136] J. Bruining and H. M. Fijnaut, *A rotational diffusion coefficient of the 70s ribosome determined by depolarized laser light scattering,* Biophysical Chemistry **9**, 345 (1975).

[137] P. Atkins and D. P. Julio, *Physical Chemistry*, 9th ed. (Oxford UP, 2010).

[138] J. Strutt, *On the scattering of light by small particles,* Philosophical Magazine 2, **41**, 447 (1871).

[139] P. de Gennes, *Polymers at an interface; a simplified view,* Advances in Colloid and Interface Science **27**, 189 (1987).

[140] Wikipedia, *Debye–Hückel equation — wikipedia, the free encyclopedia,* (2015), [Online; accessed 21-December-2015].

[141] S. Goldberg, *Surface complexation modeling,* Environmental Toxicology and Chemistry **33**, 2172 (2014).

[142] E. Nagele and U. Schneider, *The zeta-potential of blast furnace slag and fly ash,* Cement and Concrete Research **19**, 811 (1989).

[143] M. Kosmulski, *pH-dependent surface charging and points of zero charge. III. update,* Journal of Colloid and Interface Science **298**, 730 (2006).

[144] S. Prahl, *Mie scattering calculator,* `http://omlc.org/calc/mie_calc.html` (2015), accessed: 2010-10-20.

[145] R. B. Grigg and A. A. Mikhalin, *Effects of flow conditions and surfactant availability on adsorption,* (Society of Petroleum Engineers, 2007).

[146] R. M. Enick, D. K. Olsen, J. R. Ammer, and W. Schuller, *Mobility and conformance control for CO_2 EOR via thickeners, foams, and gels – a literature review of 40 years of research and pilot tests,* in *SPE Improved Oil Recovery Symposium, 14-18 April, Tulsa, Oklahoma, USA* (Society of Petroleum Engineers, 2012).

[147] J. H. van 't Hoff, *The role of osmotic pressure in the analogy between solutions and gases,* Journal of Membrane Science **100**, 39 (1995), The early history of membrane science, selected papers celebrating vol. 100.

[148] B. Ju and T. Fan, *Experimental study and mathematical model of nanoparticle transport in porous media,* Powder Technology **192**, 195 (2009).

[149] R. D. Kaminsky, R. C. Wattenbarger, J. Lederhos, and S. A. Leonardi, *Viscous oil recovery using solids-stabilized emulsions,* in *SPE Annual Technical Conference and Exhibition, 19-22 September, Florence, Italy* (Society of Petroleum Engineers, 2010).

[150] S. Ali, P. Gauglitz, and W. Rossen, *Stability of solids-coated liquid layers between bubbles,* Industrial and Engineering Chemistry Research **39**, 2742 (2000), cited By (since 1996): 8 Export Date: 21 June 2011 Source: Scopus.

[151] T. S. Horozov, *Foams and foam films stabilised by solid particles,* Current Opinion in Colloid & Interface Science **13**, 134 (2008).

[152] B. P. Binks, *Particles as surfactants - similarities and differences,* Current Opinion in Colloid and Interface Science **7**, 21 (2002).

[153] A. C. Martinez, E. Rio, G. Delon, A. Saint-Jalmes, D. Langevin, and B. P. Binks, *On the origin of the remarkable stability of aqueous foams stabilised by nanoparticles: link with microscopic surface properties,* Soft Matter **4**, 1531 (2008).

[154] B. P. Binks, S. Campbell, S. Mashinchi, and M. P. Piatko, *Dispersion behavior and aqueous foams in mixtures of a vesicle-forming surfactant and edible nanoparticles,* Langmuir **31**, 2967 (2015).

[155] P. M. Kruglyakov, S. I. Elaneva, and N. G. Vilkova, *About mechanism of foam stabilization by solid particles,* Advances in Colloid and Interface Science **165**, 108 (2011).

[156] F. AttarHamed, M. Zoveidavianpoor, and M. Jalilavi, *The incorporation of silica nanoparticle and alpha olefin sulphonate in aqueous CO_2 foam: Investigation of foaming behavior and synergistic effect,* Petroleum Science and Technology **32**, 2549 (2014).

[157] F. Bresme and M. Oettel, *Nanoparticles at fluid interfaces,* Journal of Physics: Condensed Matter **19**, 1 (2007).

[158] M. P. Aronson, *Influence of hydrophobic particles on the foaming of aqueous surfactant solutions,* Langmuir **2**, 653 (1986).

[159] T. Zhang, M. Roberts, S. L. Bryant, and C. Huh, *Foams and emulsions stabilized with nanoparticles for potential conformance control applications,* in *SPE International Symposium on Oilfield Chemistry, The Woodlands, Texas* (Society of Petroleum Engineers, 2009).

[160] Z.-G. Cui, Y.-Z. Cui, C.-F. Cui, Z. Chen, and B. P. Binks, *Aqueous foams stabilized by in situ surface activation of $CaCO_3$ nanoparticles via adsorption of anionic surfactant,* Langmuir **26**, 12567 (2010).

[161] T. Zhang, D. Davidson, S. L. Bryant, and C. Huh, *Nanoparticle-stabilized emulsions for applications in enhanced oil recovery,* in *SPE Improved Oil Recovery Symposium, 24-28 April, Tulsa, Oklahoma, USA* (Society of Petroleum Engineers, 2010).

[162] T. Zhang, D. Espinosa, K. Y. Yoon, A. R. Rahmani, H. Yu, F. M. Caldelas, S. Ryoo, M. Roberts, M. Prodanovic, K. P. Johnston, T. E. Milner, S. L. Bryant, and C. Huh, *Engineered nanoparticles as harsh-condition emulsion and foam stabilizers and as novel sensors,* in *Offshore Technology Conference, 2-5 May, Houston, Texas, USA* (Society of Petroleum Engineers, 2011).

[163] R. G. Alargova, D. S. Warhadpande, V. N. Paunov, and O. D. Velev, *Foam superstabilization by polymer microrods,* Langmuir **20**, 10371 (2004).

[164] D. A. Espinosa, F. M. Caldelas, K. P. Johnston, S. L. Bryant, and C. Huh, *Nanoparticle-stabilized supercritical CO_2 foams for potential mobility control applications,* in *SPE Improved Oil Recovery Symposium, 24-28 April, Tulsa, Oklahoma, USA* (2010).

[165] J. Yu, N. Liu, L. Li, and R. L. Lee, *Generation of nanoparticle-stabilized supercritical CO_2 foams,* in *Carbon Management Technology Conference, 7-9 February, Orlando, Florida, USA* (Carbon Management Technology Conference, 2012).

[166] J. Yu, M. Khalil, N. Liu, and R. Lee, *Effect of particle hydrophobicity on CO_2 foam generation and foam flow behavior in porous media,* Fuel **126**, 104 (2014).

[167] H. ShamsiJazeyi, C. A. Miller, M. S. Wong, J. M. Tour, and R. Verduzco, *Polymer-coated nanoparticles for enhanced oil recovery,* Journal of Applied Polymer Science **131**, 1 (2014).

[168] D. A. DiCarlo, B. Aminzadeh, M. Roberts, D. H. Chung, S. L. Bryant, and C. Huh, *Mobility control through spontaneous formation of nanoparticle stabilized emulsions,* Geophysical Research Letters **38**, n/a (2011).

[169] K. H. Gardner and M. S. Arias, *Clay swelling and formation permeability reductions induced by a nonionic surfactant,* Environmental Science & Technology **34**, 160 (2000).

[170] W. Ramsden, *Separation of solids in the surface-layers of solutions and 'Suspensions' (observations on surface-membranes, bubbles, emulsions, and mechanical coagulation). – Preliminary account,* Proceedings of the Royal Society of London **72**, 156 (1903).

[171] G. O. Brown, *Henry Darcy and the making of a law,* Water Resources Research **38**, 11 (2002).

[172] S. Abaci, J. Edwards, and B. Whittaker, *Relative permeability measurements for two phase flow in unconsolidated sands,* Mine Water and the Environment **11**, 11 (1992).

[173] R. Mészáros, L. Thompson, M. Bos, I. Varga, and T. Gilányi, *Interaction of sodium dodecyl sulfate with polyethyleneimine:? surfactant-induced polymer solution colloid dispersion transition,* Langmuir **19**, 609 (2003).

[174] B. S. Necula, I. Apachitei, L. E. Fratila-Apachitei, C. Teodosiu, and J. Duszczyk, *Stability of nano-/microsized particles in deionized water and electroless nickel solutions,* Journal of Colloid and Interface Science **314**, 514 (2007).

A

APPENDIX : SUPPLEMENTARY INFORMATION FOR CHAPTER 2

In 1856, Henry Darcy [171] investigated the flow of water through sand filters by conducting a series of experiments. He determined that the rate of flow of water through a sand column could be described by the equation

$$Q = KA\frac{\Delta h}{\Delta L}, \tag{A.1}$$

where Q is the flow rate of water, K is the hydraulic conductivity, A is the cross - sectional area of the sand column, $h = (p/\rho g) + z$ is the total head, p is pressure and $(\frac{\Delta h}{\Delta L})$ is the hydraulic gradient. In differential form, the equation can be written as

$$u = \frac{q}{A} = \frac{k\rho g}{\mu}\frac{dh}{dx}, \tag{A.2}$$

where x is the coordinate in the flow direction, u is the Superficial velocity, μ is the viscosity of the fluid and q is the volumetric flow rate [172]. The hydraulic conductivity is $K = \frac{k\rho g}{\mu}$ and g is the acceleration due to gravity.

A.1. PERMEABILITY OF BENTHEIMER

The flow set up (Figure 2.6) is used to measure the permeability of the Bentheimer core. When there is no flow, the manometers indicate zero pressure difference across the measuring points of the core. We injected CO_2 gas in the flow set up for five minutes. Then we saturated the core with doubly distilled water at a flow velocity of 0.61 m/d. We filled the core, manometers and the tubes with water. Doubly distilled water of pH 3 was injected at a velocity 0.61 m/d. We increased the injection velocity stepwise every 30 minutes to twice, thrice of original velocity, etc.. As indicated in the results given in chapters 3, 4, and chapter 6, the permeability of Bentheimer core used by us is 3.1±0.2 Darcy.

Test	Date dd/mm/yy	Sand type	Slope($Q/\Delta P$) $(m^3/s)/(N/m^2)$	Intercept N/m^2	Permeability $10^{-12}m^2$
Test104	19/09/11	Fine	6.85×10^8	313	62.1

Table A.1: Single phase (water) flow experiment with fine sand d_{avg} = 0.38 mm in the sand pack.

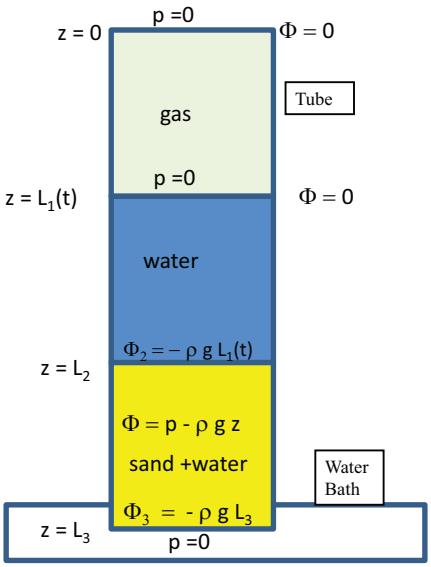

Figure A.1: Outlay of gravity cell, top open to atmosphere (built with the help from Karel Heller, Laboratory Technician).

A.2. PERMEABILITY OF SANDPACKS

A.2.1. FLOW TESTS

We conducted initial permeability studies on sandpacks prepared with a coarse sand (Figure 2.1) or a fine sand (Figure 2.2). The permeability experiment for a sandpack with fine sand started on 19^{th} September 2011, 11 : 40 by passing ethanol at a rate of 1.08 m/d. After 2.5 pore volumes of ethanol, CO_2 from the laboratory lines at a pressure of 8.1 barA was passed for next fifteen minutes. At 13 : 15, we started to inject water at a rate of 1.08 m/d. After 20 minutes, we measured the steady state pressure drop across the measurement points of the sandpack. We increased the velocity stepwise in the same way as in Bentheimer and noted the pressure drop corresponding to the Darcy velocities of water. We used Darcy's law Eq. A.1 to relate potential difference across the sand pack to the velocity to calculate the permeability of the sandpack. The potential difference is measured by the manometer. Table A.1 shows the slope, the intercept and calculated permeability.

A.2.2. GRAVITY CELL

We carried experiments in the gravity displacement set-up (Figure A.1) to determine the single-phase permeability of sandpacks containing coarse or fine sand. The gravity displacement set-up consists of a graded glass cylinder with an inner diameter of 0.02 m and a length of 1.0 m. The top of the cylinder is indicated by $z = 0$. The bottom position is indicated by $z = L_3 = 1$ m, and the top of the sand by $z = L_2 \approx 0.69$ m. The top of the water column is indicated by $z = L_1(t)$ which starts from 0.31 m and reaches to L_2 with respect to time. The potential is defined as $\phi = p - \rho g z$, where the minus sign arises because z is pointing vertically downward. At the inlet and outlet, the pressure is atmospheric, indicated by $p = 0$. We disregarded the density of gas at atmospheric pressure. Therefore at $z = L_1(t)$ the pressure is equal to zero. At $z = L_2$, the pressure is $p_2 = 0 + \rho g(L_2 - L_1(t))$ and the potential is $\phi_2 = p_2 - \rho g L_2 = -\rho g L_1(t)$. At the bottom, the pressure is zero and the potential $\phi_3 = p_3 - \rho g L_3$. Application of Darcy's law leads to

$$u = \frac{k}{\mu} \rho g \frac{L_3 - L_1(t)}{L_3 - L_2} \tag{A.3}$$

The rate of change of the liquid level $dL_1(t)/dt$ is equal to the volumetric flux in the sand pack. So we find

$$\frac{dL_1(t)}{dt} = \frac{k}{\mu} \rho g \frac{L_3 - L_1(t)}{L_3 - L_2}. \tag{A.4}$$

The solution of Eq. A.4 is

$$\ln \frac{L_3 - L_1(0)}{L_3 - L_1(t)} = \frac{Kt}{L_3 - L_2} \tag{A.5}$$

where, $L_1(0)$ is the position of the water column at $t = 0$. The procedure to conduct an experiment with the gravity tube is as follows:

- Close the bottom end of the tube with a small filter paper/cloth using glue to allow passage of water but not of the sand. Fill the tube with sand till L_2.
- Place the tube vertically in a water bath (mineralized water or DD water depending on your preference) just 2 cm below the water level (to enable to suck the water in the tube). Fix the position of the tube by a holding stand.
- Connect the vacuum pump and tubing to the valve. The other end of the tube is open to the atmosphere.
- Start the vacuum pump using the needle valve to very slowly suck the air from the tube, thus sucking water in the tube from the water bath. Wait until the water eventually builds a column above the sand column.
- Stop the vacuum pump and make sure that the tube end is not open to the atmosphere. Note down the water level L_1 at $t = 0$, and have the video camera parallel to the water level.
- Open the valve to the atmosphere and at the same time start recording on the camera. The top of the water column changes with time, which starts from $L_1(t)$ and reaches L_2.

- Go back to computer system and observe the video. From the video, note down the water level change in meters and the corresponding seconds. Use these two parameters ($L_1(t)$ and t) in Eq. A.4 to plot a graph of $\ln \frac{L_3-L_1(0)}{L_3-L_1(t)}$ vs $t(sec)$ to the slop $\frac{K}{L_3-L_2}$.

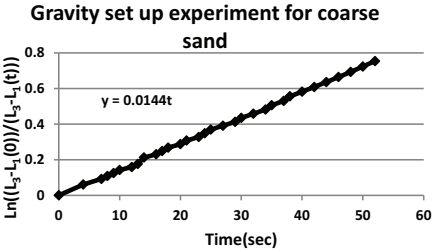

Figure A.2: Time vs. the gravity drainage: slope gives the hydraulic conductivity divided by the length of the coarse sand column (see Eq. A.5).

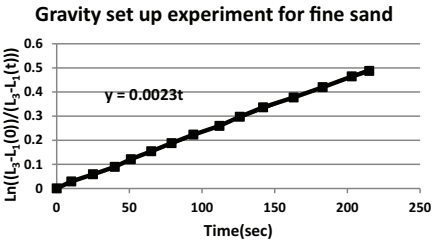

Figure A.3: Time vs. the gravity drainage: slope gives the hydraulic conductivity divided by the length of the fine sand column(see Eq. A.5).

Figure A.2 and Figure A.3 show left side ($\frac{L_3-L_1(0)}{L_3-L_1(t)}$) vs. right side ($t$) of the Eq. A.5 for coarse and fine sand columns during gravity drainage experiments. The water level satisfied Eq. A.5 as the data for water level fall on a straight line (on a log scale).

A.2.3. KOZENY-CARMAN EQUATION

In order to validate the experimental permeabilities we use an equation derived by Panda and Lake [62] to calculate Kozeny-Carman permeabilities with the equation

$$k = \frac{D_p^2 \varphi^3}{150(1-\varphi)^2} \frac{(\gamma C_{D_p}^3 + 3C_{D_p}^2 + 1)^2}{(1-C_{D_p}^2)^2}, \tag{A.6}$$

where φ is the porosity, $D_p \leq 2\sqrt{2\,A/\pi}$ is the number averaged particle diameter, A is the sand particle area, γ is the skewness and C_{D_p} is the coefficient of variation, i.e. the standard deviation divided by the average. We calculated the heterogeneity factor for the coarse sand (1.48) and for the fine sand (1.26). We obtained Kozeny-Carman permeability of 1770 Darcy for the coarse sand and of 137 Darcy for the fine sand. The data are summarized in Table A.2. The flow experiments show that the permeability of the fine sand is 80±20 Darcy as shown in Table A.2. The permeability values for the fine sand in all three cases (sand pack, gravity set up and theoretical Kozeny-Carman) vary between samples. For the coarse sandpack the applicability range of the manometer prevented to get useful results with the sand pack. For calculations in the thesis, we selected the average values, i.e. 1860 Darcy for coarse sandpack and 130 Darcy for fine sandpack.

	Description	Coarse sand	Fine sand
	Mean area of the particles (mm^2)	1.11	0.12
	Diameter of the particles (mm)	1.12	0.38
Permeability, Darcy	a		80±20
	b	470±50	70±15
	c	1193	137
	d	1770[e]	173[f]

Table A.2: Permeability calculation for sandpacks with coarse and fine sand by : [a]Flow setup, [b]Gravity tube, [c] Kozeny-Carman Eq. A.6 without Panda Lake factor, [d] Kozeny-Carman Eq. A.6 with Panda Lake factor. Panda Lake factor [e]for coarse sand: 1.48, [f] for fine sand: 1.26

A.3. CALIBRATION CURVE FOR PRESSURE DIFFERENCE MANOMETER

A

Figure A.4 and Figure A.5 show calibration curves for the pressure manometer 0-3 bar and the pressure manometer 0-0.1 bar used to measure the pressure difference across the measuring points in the porous media (point 19 in Figure 2.6).

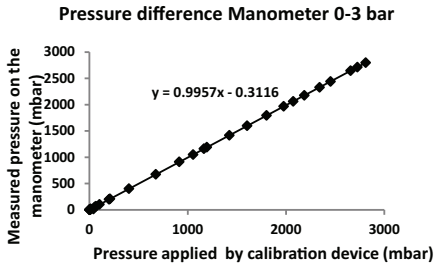

Figure A.4: Calibration curve for pressure difference manometer 0-3 bar used for experiments with Bentheimer core.

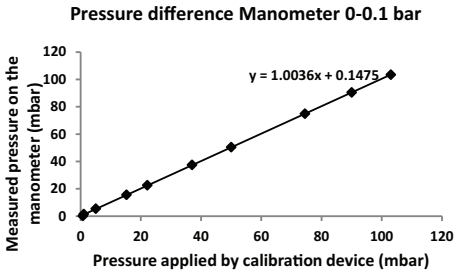

Figure A.5: Calibration curve for pressure difference manometer 0-0.1 bar used for experiments with Bentheimer core.

A.4. GENERAL CALIBRATION OF A pH METER

We used a two point calibration with 2 buffers, one at pH 7 and one at pH 4. The electrode is rinsed with deionized water and dried carefully with some paper. Then the electrode is first immersed in the buffer solution with pH 7. The meter calibrates automatically by reading a potential (mV) value. Subsequently the electrode is rinsed, dried and immersed in the second buffer solution with pH 4. After calibration the electrode is ready to be used. The pH values of the solutions are measured with a combined pH electrode, i.e. we measure a difference between an internal reference electrode with a fixed potential and a H^+ sensitive electrode. The difference in potentials (mV) between the reference and the H^+ sensitive electrode is converted into a pH value.

B

APPENDIX : SUPPLEMENTARY INFORMATION FOR CHAPTER 4

B.1. COMPILATION OF DATA FROM THE LITERATURE AND OUR DATA IN THE SYMBOLIC REGRESSION

	Surfactant	NaCl	pH	Permeability	Velocity		Pressure drop
					Gas	Surfactant	
	10^{-5} mol/l	10^{-5} mol/l	10^{-5} mol/l	10^{-12} m^2	10^{-5} m/s	10^{-5} m/s	10^{5} Pa/m
Ug6[a]	3170.000	50000.000	1.000	0.532	1.588	0.106	90.480
	3170.000	50000.000	1.000	0.532	0.265	0.106	90.480
	3170.000	50000.000	1.000	0.532	1.323	0.141	135.720
	3170.000	50000.000	1.000	0.532	0.794	0.141	113.100
	3170.000	50000.000	1.000	0.532	0.529	0.141	124.410
	3170.000	50000.000	1.000	0.532	0.265	0.265	113.100
	3170.000	50000.000	1.000	0.532	0.794	0.265	158.340
	3170.000	50000.000	1.000	0.532	0.529	0.441	135.720
	3170.000	50000.000	1.000	0.532	0.265	0.441	113.100
	3170.000	50000.000	1.000	0.532	0.265	0.811	101.790
	3170.000	50000.000	1.000	0.532	0.529	0.811	135.720
Ug7[a]	793.700	50000.000	1.000	0.430	2.029	0.106	45.240
	793.700	50000.000	1.000	0.430	0.353	0.106	45.240
	793.700	50000.000	1.000	0.430	1.588	0.141	90.480
	793.700	50000.000	1.000	0.430	0.970	0.141	90.480
	793.700	50000.000	1.000	0.430	0.617	0.141	90.480
	793.700	50000.000	1.000	0.430	0.794	0.212	147.030
	793.700	50000.000	1.000	0.430	0.529	0.212	135.720
	793.700	50000.000	1.000	0.430	0.265	0.265	124.410
	793.700	50000.000	1.000	0.430	0.529	0.441	135.720
	793.700	50000.000	1.000	0.430	0.353	0.441	113.100
	793.700	50000.000	1.000	0.430	0.353	0.811	113.100
	793.700	50000.000	1.000	0.430	0.617	0.811	135.720
Ug8[a]	158.730	50000.000	1.000	0.535	0.141	0.141	22.620
	158.730	50000.000	1.000	0.535	0.176	0.201	67.860
	158.730	50000.000	1.000	0.535	0.212	0.201	63.336
	158.730	50000.000	1.000	0.535	0.706	0.201	56.550
	158.730	50000.000	1.000	0.535	1.147	0.201	56.550
	158.730	50000.000	1.000	0.535	0.176	0.282	113.100
	158.730	50000.000	1.000	0.535	0.247	0.282	113.100
	158.730	50000.000	1.000	0.535	0.176	0.441	90.480

	158.730	50000.000	1.000	0.535	0.247	0.441	124.410
	158.730	50000.000	1.000	0.535	0.617	0.441	135.720
	158.730	50000.000	1.000	0.535	0.176	0.582	101.790
	158.730	50000.000	1.000	0.535	0.617	0.582	147.030
Ug11[a]	3170.000	50000.000	1.000	3.110	0.882	0.106	18.096
	3170.000	50000.000	1.000	3.110	3.881	0.106	31.668
	3170.000	50000.000	1.000	3.110	5.292	0.106	33.930
	3170.000	50000.000	1.000	3.110	6.703	0.106	18.096
	3170.000	50000.000	1.000	3.110	0.882	0.141	22.620
	3170.000	50000.000	1.000	3.110	3.881	0.141	33.930
	3170.000	50000.000	1.000	3.110	5.292	0.141	36.192
	3170.000	50000.000	1.000	3.110	1.588	0.194	24.882
	3170.000	50000.000	1.000	3.110	5.292	0.194	40.716
	3170.000	50000.000	1.000	3.110	1.588	0.282	27.144
	3170.000	50000.000	1.000	3.110	2.470	0.282	31.668
	3170.000	50000.000	1.000	3.110	5.292	0.282	40.716
	3170.000	50000.000	1.000	3.110	0.882	0.441	22.620
	3170.000	50000.000	1.000	3.110	1.588	0.441	24.882
	3170.000	50000.000	1.000	3.110	2.470	0.441	29.406
	3170.000	50000.000	1.000	3.110	3.881	0.441	33.930
	3170.000	50000.000	1.000	3.110	5.292	0.441	40.716
	3170.000	50000.000	1.000	0.302	0.353	0.106	67.860
	3170.000	50000.000	1.000	0.302	0.882	0.106	79.170
	3170.000	50000.000	1.000	0.302	1.499	0.106	101.790
	3170.000	50000.000	1.000	0.302	2.293	0.106	106.314
	3170.000	50000.000	1.000	0.302	3.175	0.106	113.100
	3170.000	50000.000	1.000	0.302	0.706	0.141	79.170
ug12[a]	3170.000	50000.000	1.000	0.302	0.882	0.141	83.694
	3170.000	50000.000	1.000	0.302	1.411	0.141	106.314
	3170.000	50000.000	1.000	0.302	2.117	0.141	124.410
	3170.000	50000.000	1.000	0.302	0.706	0.205	79.170
	3170.000	50000.000	1.000	0.302	0.353	0.282	5.655
	3170.000	50000.000	1.000	0.302	1.058	0.282	90.480
	3170.000	50000.000	1.000	0.302	0.353	0.441	56.550
	3170.000	50000.000	1.000	0.302	0.706	0.441	61.074
	3170.000	50000.000	1.000	0.527	0.088	0.053	11.310
	3170.000	50000.000	1.000	0.527	0.247	0.053	11.310
	3170.000	50000.000	1.000	0.527	0.600	0.053	11.310
	3170.000	50000.000	1.000	0.527	0.088	0.071	22.620
	3170.000	50000.000	1.000	0.527	0.247	0.071	22.620
Ug14[a]	3170.000	50000.000	1.000	0.527	0.529	0.071	24.882
	3170.000	50000.000	1.000	0.527	0.635	0.071	24.882
	3170.000	50000.000	1.000	0.527	0.212	0.106	45.240
	3170.000	50000.000	1.000	0.527	0.529	0.106	67.860
	3170.000	50000.000	1.000	0.527	0.635	0.106	67.860
	3170.000	50000.000	1.000	0.527	0.176	0.141	79.170
	3170.000	50000.000	1.000	0.527	0.353	0.141	90.480
	3170.000	50000.000	1.000	0.527	0.564	0.141	101.790
	3170.000	50000.000	1.000	0.527	0.141	0.212	90.480
	3170.000	50000.000	1.000	0.527	0.353	0.212	113.100
	3170.000	50000.000	1.000	0.527	0.141	0.441	90.480
	3170.000	50000.000	1.000	0.527	0.353	0.441	124.410
	3170.000	0.010	1.000	270.000	1.058	0.035	2.262
	3170.000	0.010	1.000	270.000	1.058	0.155	2.262
	3170.000	0.010	1.000	270.000	1.058	0.176	2.262
	3170.000	0.010	1.000	270.000	1.058	0.212	2.262
	3170.000	0.010	1.000	270.000	1.058	0.247	2.262
	3170.000	0.010	1.000	270.000	1.058	0.282	2.262
	3170.000	0.010	1.000	270.000	2.293	0.035	6.786
	3170.000	0.010	1.000	270.000	2.293	0.071	6.786
	3170.000	0.010	1.000	270.000	2.293	0.106	6.786
	3170.000	0.010	1.000	270.000	2.293	0.141	6.786
	3170.000	0.010	1.000	270.000	2.293	0.212	6.786
	3170.000	0.010	1.000	270.000	2.293	0.247	6.786
	3170.000	0.010	1.000	270.000	2.293	0.282	6.786
	3170.000	0.010	1.000	270.000	2.293	0.353	6.786
	3170.000	0.010	1.000	270.000	2.293	0.529	6.786

B

	3170.000	0.010	1.000	270.000	2.293	0.706	6.786
	3170.000	0.010	1.000	270.000	2.293	0.776	6.786
	3170.000	0.010	1.000	270.000	2.293	0.988	6.786
	3170.000	0.010	1.000	270.000	2.293	1.058	6.786
	3170.000	0.010	1.000	270.000	2.293	1.129	6.786
	3170.000	0.010	1.000	270.000	2.293	1.764	6.786
	3170.000	0.010	1.000	270.000	2.293	1.940	6.786
	3170.000	0.010	1.000	270.000	4.269	0.035	11.310
	3170.000	0.010	1.000	270.000	4.269	0.071	11.310
	3170.000	0.010	1.000	270.000	4.269	0.106	11.310
	3170.000	0.010	1.000	270.000	4.269	0.353	11.310
	3170.000	0.010	1.000	270.000	4.269	0.706	11.310
	3170.000	0.010	1.000	270.000	4.269	0.988	11.310
	3170.000	0.010	1.000	270.000	4.269	1.588	11.310
Jante[b]	1587.400	1197.810	1.000	6.200	4.699	0.587	226.200
	1587.400	1197.810	1.000	6.200	6.462	0.587	242.034
	1587.400	1197.810	1.000	6.200	7.613	0.587	253.344
	1587.400	1197.810	1.000	6.200	10.280	0.587	266.916
	1587.400	1197.810	1.000	6.200	10.573	0.587	273.702
	1587.400	1197.810	1.000	6.200	4.088	0.305	199.056
	1587.400	1197.810	1.000	6.200	4.699	0.305	217.152
	1587.400	1197.810	1.000	6.200	5.874	0.305	226.200
	1587.400	1197.810	1.000	6.200	7.636	0.305	248.820
	1587.400	1197.810	1.000	6.200	10.338	0.305	248.820
	1587.400	1197.810	1.000	6.200	11.983	0.305	251.082
	1587.400	1197.810	1.000	6.200	13.276	0.305	251.082
	1587.400	1197.810	1.000	6.200	16.448	0.305	251.082
	1587.400	1197.810	1.000	6.200	19.972	0.305	251.082
	1587.400	1197.810	1.000	6.200	4.088	0.117	176.436
	1587.400	1197.810	1.000	6.200	6.109	0.117	180.960
	1587.400	1197.810	1.000	6.200	7.613	0.117	180.960
	1587.400	1197.810	1.000	6.200	9.963	0.117	180.960
	1587.400	1197.810	1.000	6.200	12.336	0.117	180.960
	1587.400	1197.810	1.000	6.200	13.487	0.117	180.960
	1587.400	1197.810	1.000	6.200	15.837	0.117	180.960
Persoff[c]	3170.000	100000.000	1.000	1.000	2.350	0.180	1.824
	3170.000	100000.000	1.000	1.000	7.049	0.180	1.824
	3170.000	100000.000	1.000	1.000	1.175	0.217	3.039
	3170.000	100000.000	1.000	1.000	2.350	0.217	3.039
	3170.000	100000.000	1.000	1.000	5.287	0.217	3.039
	3170.000	100000.000	1.000	1.000	9.399	0.217	3.039
	3170.000	100000.000	1.000	1.000	12.923	0.217	3.039
	3170.000	100000.000	1.000	1.000	15.273	0.217	3.039
	3170.000	100000.000	1.000	1.000	2.350	1.035	7.598
	3170.000	100000.000	1.000	1.000	7.049	1.035	7.598
This work	1900.000	50000.000	1.000	1860.000	1.046	1.692	17.000
	1900.000	50000.000	1.000	1860.000	0.869	1.692	26.500
	1900.000	50000.000	1.000	1860.000	0.388	1.281	21.000
	1900.000	50000.000	1.000	1860.000	1.245	3.243	26.600
	1900.000	50000.000	1.000	1860.000	1.245	3.243	26.800
	190.000	0.010	0.030	130.000	0.916	1.281	7.500
	95.000	0.010	0.030	130.000	1.833	1.281	1.530
	95.000	0.010	0.030	130.000	4.112	1.281	1.600
	95.000	0.010	0.030	130.000	4.664	2.032	3.700
	380.000	0.010	0.030	130.000	2.925	2.032	15.000
	95.000	0.010	0.030	130.000	4.664	2.032	3.710
	380.000	0.010	0.030	130.000	1.433	1.281	26.000
	95.000	0.010	100.000	3.000	1.046	3.818	23.700
	95.000	0.010	100.000	3.000	0.317	0.952	42.500

[a]Martinez [24, 25], [b]Jante and Osterloh [48], [c]Persoff [39]

B.2. CANDIDATE EXPRESSIONS FROM SYMBOLIC REGRESSION

Table B.3: Candidate expressions from symbolic regression

No[a]	MAE[b] 10^6 Pa/m	Equation for ΔP Pa/m
45	1.38915	$377681.4327 + 1.114365938 \times 10^{15}\ k + (6823.26519\ Nc\ 6.497605885 \times 10^{-6\,Nc}/\sqrt{k}) - 0.002971262642\ Nc\ 8.425572656 \times 10^{-6\,Nc}/(u_w\ \sqrt{k})$
43	1.43048	$1.315789606 \times 10^{15}\ k + 6910.710854\ Nc\ 6.797525275 \times 10^{-6\,Nc}/\sqrt{k} - 0.002971977144\ Nc\ 8.501011606 \times 10^{-6\,Nc}/(u_w\ \sqrt{k})$
41	1.43888	$678560.5061 + 6797.25261\ Nc\ 6.221372108 \times 10^{-6\,Nc}/\sqrt{k} - 0.003019722055\ Nc\ 8.150821468 \times 10^{-6\,Nc}/(u_w\ \sqrt{k})$
39	1.53871	$6938.775192\ Nc\ 6.725976843 \times 10^{-6\,Nc}/\sqrt{k} - 0.003001926342\ Nc\ 8.30778555 \times 10^{-6\,Nc}/(u_w\ \sqrt{k})$
36	1.60824	$4.843955836 \times 10^{14}\ k + (7.875908381 \times 10^{-6})/(1.944280258 \times 10^{-13} + k) - (3.21637241 \times 10^{-12})/(k\ u_w) + (2532457.026\ \sqrt{Nc} - 800.781136)/(Nc) - 7339893.971\ Nc^2$
34	1.61347	$(7.875893003 \times 10^{-6})/(1.946096741 \times 10^{-13} + k) - (3.21637241 \times 10^{-12})/(2.44611893 \times 10^{-22} + k\ u_w) + (2531207.834\ \sqrt{Nc} - 800.3728314)/(Nc) - 7337312.339\ Nc^2$
32	1.61356	$(7.875893198 \times 10^{-6})/(1.946096741 \times 10^{-13} + k) - (3.214191759 \times 10^{-12}/k\ u_w) + (2531335.569\ \sqrt{Nc} - 800.4132249)/(Nc) - 7338278.044\ Nc^2$
30	1.62838	$(-8.633964039/Nc) + (7.70832884 \times 10^{-6})/(1.656584668 \times 10^{-13} + k) - (3.154482163 \times 10^{-12})/(k\ u_w) - 4856154.908\ Nc - 5397158.539\ logNc$
28	1.68529	$(5.133531253 \times 10^{-6}/k) - (8.567627227/Nc) - (2.950808877 \times 10^{-12})/(k\ u_w) - 3470357.199\ Nc - 5356695.802\ logNc$
26	1.76764	$(5.171882559 \times 10^{-6}/k) - (9.358540701/Nc) - (2.931315393 \times 10^{-12})/(k\ u_w) - 2321051.989 - 5991421.158\ logNc$
24	1.82686	$678562.2683 + (319699.2982\ Nc(2.262195156 \times 10^{-6} + u_w)^{0.3403830017+Nc})/(\sqrt{k})$
22	1.91764	$678565.7035 + (5635.492471\ Nc(1.41585097 \times 10^{-6} + u_w)^{Nc})/(\sqrt{k})$
21	1.93234	$678573.9922 + (836.9748199\ Nc\ k^{-0.573999548}\ u_w^{Nc}$
20	1.99975	$678564.3434 + (5858.987646\ Nc\ u_w^{Nc})/\sqrt{k}$
19	2.07161	$798.8460475\ Nc\ k^{-0.5769082117}\ u_w^{Nc}$
18	2.19567	$6078.006267\ Nc\ u_w^{Nc}/(\sqrt{k})$
17	2.32027	$(2.155817858 \times 10^{-6}/k) - (8.052079115/Nc) - 5037282.84\ logNc$
16	2.36424	$(2.953499141 \times 10^{-6}/k) + 2289147862\ Nc\ u_w^N c$
14	2.40236	$1885581.344 + (1.539841872 \times 10^{-6}\ Nc)/(k\ Nc^2 - 1.275960317 \times 10^{-19})$
12	2.55063	$(1.797981544 \times 10^{-6}\ Nc)/(2.649518112 \times 10^{-19} + k\ Nc^2)$
11	2.84359	$2276025767\ Nc\ (4.838808504 \times 10^{-5\,Nc})$
10	3.0249	$18318407.5 - (1.763980564/Nc) - (18540807.94\ Nc)$
8	3.23147	$(6219360.129\ Nc)/(Nc - 0.008900178241)$
6	3.6694	$4.44689799 \times 10^{-5}/(8.165912625 \times 10^{-12} - k)$
4	5.3185	$3.576222 \times 10^{-6}/k$
3	5.97989	$4453146.402 + Nc$
1	5.97989	4466958.902

[a]Relative Complexity Rank, [b]Mean Absolute Error
^{Nc}NaCl (mol/l), u_w Surfactant solution velocity (m/s), ^{k}Permeability (m^2)

B.3. FLOW CONDITIONS FOR THE DATA POINTS USED FROM THE LITERATURE

In a paper by Persoff [39], the core was initially vacuum saturated with brine and displaced by at least 10 pore volumes of the foaming solution. After the steady state pressure drop has been reached, the gas and liquid flow rates were varied independently to reach a series of steady states. In a paper by Jante and Osterloh [48], all the core flooding experiments were conducted at 150°C and with a back pressure of 1379 kPa (≈ 14 bar). Nitrogen and synthetic Kern River softened water (KRSW) were simultaneously injected at various rates. Before flooding while the core is still warm, the sandpack was evacuated and resaturated with KRSW until the original saturated weight was attained. Next, the KRSW was displaced from the sandpack with 2 pore volumes of surfactant solution. Nitrogen and surfactant were then simultaneously injected until a steady state pressure drop has been obtained. Like in case of Persoff [39], the gas and liquid flow rates were varied independently to reach a series of steady states. Separate core floods were conducted to obtain water saturation data at several steady-state conditions. In case of Martinez [25], all experiments were conducted at room temperature and at back pressure of 600 psi (≈41 bar). The core was initially vacuum saturated with brine. After a period of brine injection, surfactant solution and gas was injected to obtain the steady state pressure drop. After the steady state is maintained for some time, the liquid flow rate, the gas flow rate or both are changed to obtain new steady state pressure drop values. For complete information on the flow conditions we refer to the respective references.

C

APPENDIX : SUPPLEMENTARY INFORMATION FOR CHAPTER 5 AND CHAPTER 6

C.1. SURFACE ENERGY CHANGE FOR A PARTICLE AT AN INTERFACE

The energy required to detach a particle from the interface of the fluid-fluid can be given by [152]

$$V = \pi r^2 \sigma_{gw}(1 - |cos\theta|)^2, \tag{C.1}$$

where r is a radius of the particle, σ_{gw} is an interfacial tension between the fluids, θ is the contact angle between the particle and the fluid-fluid interface. In curved surfaces the wetting fluid will be on the external side. Therefore hydrophilic particles will form an oil in water emulsion whereas hydrophobic particles will form an water in oil emulsion. We compute the surface energy change (ΔV) when a particle is transferred from a single fluid to the interface between the fluids. The energy change when a particle is adsorbed at the water-gas interface is given by the sum of the following energies: the surface energy of a droplet sticking out of the water plus the surface energy of the part of the droplet immersed in water minus the surface energy of the full particle immersed in a gas phase minus surface area of the original water/gas interface that is now occupied by the particle. Indeed, when the particle is at the gas/water interface, it occupies the area that originally was at the boundary between water and gas. We describe the energy change $\Delta V(cos\theta)$ as a function of the cosine of the contact angle θ in the gas/surfactant-water/particle system with an expression that is unconditionally negative, unless the contact angle indicates a complete wetting condition, in which case it is zero. The equation reads

$$\frac{\Delta V\ cos\theta}{4\sigma_{gw} r^2} = -\frac{1}{4}(1 \pm cos\theta). \tag{C.2}$$

The minus sign is for the case, when the full particle is immersed in the water phase and the plus sign is for the case, when the full particle is immersed in the gas phase. In the case of complete wetting, the particle does not prefer to stay at the surface, but to be fully immersed in the wetting fluid. This corresponds to the situation using a minus sign in equation C.2 and that $cos\theta = 1$, i.e. $\theta = 0$ or for complete wetting [159].

C.2. TREATMENT OF PARTICLES

Polyethylene-imine (PEI) $NH_2-(CH2-CH2-N^+H)_n-$ neutralizes anionic colloids and ion-exchange resins [32, 173]. We used the following procedure to prepare the treatment of the ash particle in a dispersion:

- Mix 0.48 g of PEI in 100 ml[1] water.
- Apply ultrasonic treatment for 30 min to dissolve the PEI.
- Put the dispersion in a beaker and put it on the weighing scale. Take out a small amount of solution from the beaker by a syringe until the weighing scale reads 99.75 g and put 0.25 g of ash particles so that the total solution would weigh 100 g.
- Put the dispersion into an ultrasonic bath for 20 minutes.
- Put the dispersion bottle into tumbler for 30 minutes for mixing.
- Put the dispersion into two 50 ml bottles and centrifuge it at 3500 rpm for 30 min.
- Discard all the water. Add 50 ml of water to the precipitate so that the solution has the same mass as before.
- Put the solution in a bath for ultrasonic treatment for 5 minutes.
- Vibrate it on the vibrating machine for 10 minutes with speed level 3 out of 5.
- Centrifuge it for 5 minutes at 3500 rpm.
- Repeat step 7 to 10 (discarding the water, putting fresh water and ultrasonication) for another 2 times.

C.3. COLLOIDAL DISPERSION STABILITY AND BULK FOAM STABILITY

Table C.1 shows the sedimentation behavior of the as received (untreated) ash particles in water with average values of the zeta potential and the particle size. Each experiment was repeated three times and the values were averaged over the measurements. We measured the size and the zeta potential of the particles by the Malvern Zeta sizer described in subsection 2.3.2 chapter 2 after ultrasonication at a predetermined time interval. We repeated the observations after two days. Table C.1 shows an increase in the average size of the particles in the dispersion as time proceeds, indicating agglomeration. The

[1] We assumed 100 ml = 100 g of water

Table C.1: Sedimentation behavior of the untreated ash particles in the doubly distilled water. We observed the particle size and zeta potential of the dispersions after ultrasonication and after two days.

Time (min)	**Avg. Size** nm		**Avg. Zeta potential** mV	
	0^a	2^b	0	2
2	8.13	16.3	0.23	0.27
10	14.56	-	0.66	0.10
20	-	-	0.09	0.13
40	18.72	-	-0.41	0.49
80	11.04	26.68	0.07	0.33

^{a}Immediately after ultrasonication, ^{b}After two days

Table C.2: Average zeta potential values (mV) of untreated and PEI treated ash particle in water.

	Zeta potential (mV)		
0.3 w/w % of the ash particles	-0.047	0.103	-0.539
0.25 w/w % of the ash particles treated with 0.48 w/w % PEI	20.3	18	16.3

tests after two days show further increase in the sizes showing the instability of the suspension. The Malvern Zeta sizer [70] did not measure the particle sizes in some cases due to apparent instability of the suspensions. After two days, we observed a slight decrease in the zeta potential value of most dispersions. Table C.2 shows the effect of PEI treatment on the zeta potential of ash particles in doubly distilled water of pH 6.5. The zeta-potential of untreated ash particles is almost zero at pH 6.5, i.e. at the isoelectric point (IEP) [56]. The observed value of IEP for untreated ash particles is different than the IEP of metal oxide (3.5-4.0 [174]), which is the main component of ash. The high zeta potential values of the treated particles show their improved colloidal stability in a dispersion.

We studied the effect of addition of treated ash particles on the foam stability as described below. A single tube containing 0.5 w/w % PEI treated ash dispersion in 0.03 w/w % AOS was taken. From this dispersion, a portion from the sedimented region (bottom part of the tube) and a portion from the non sedimented region (top part of the tube) were taken. The test tubes were shaken to generate the foam in the test tubes by using a common protocol from biological labs. Figure C.1 shows two plastic tubes of 10 ml foam with a sedimented portion (30 mm) and with a portion obtained from the top region (7 mm). Table C.3 summarizes the foam height measurements for various combinations AOS and ash particles, immediately after shaking, after one day and after two days. It shows that foam with a high percentage of ash particles was more stable than foam from a dispersion with a low percentage of particles or a solution without particles. For example, a 10 ml test tube containing 0.15 w/w% of AOS surfactant solution with 0.25 w/w % ash particle formed a foam column of 40 mm. The foam height reduced to 30 mm after one day and 10 mm after two days. In comparison, a similar solution without particles showed a foam column of 40 mm, though it reduced to 2.5 mm after two days. This result

Table C.3: Effect of treated ash particles on the stability of bulk foam

Dispersion (ml)		Water (ml)	Foam Height (mm)		
			0^a	1^b	2^c
0.03 w/w % AOS	10	0	40	25	2.5
0.015 w/w % AOS and 0.25 w/w % ash	10	0	40	30	10
Portion from sedimented region	1	9.0	5	0	0
	0.1	9.9	0	0	0
0.015 w/w % AOS and 0.25 w/w % ash particles	10	0	40	7	0
Portion above the sediment region	1	9.0	5	0	0
	0.1	9.9	0	0	0

^{a}Immediately after shaking, ^{b}After one day, ^{c}After two days

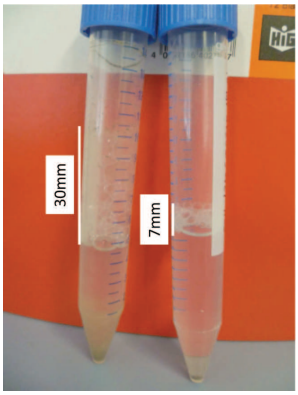

Figure C.1: Figure shows two dispersions obtained from 0.5 w/w % PEI treated ash dispersion in 0.03 w/w % AOS. From this dispersion, a portion from the sedimented region (bottom part of the tube) and a portion from the non sedimented region (top part of the tube) were taken. The test tubes were shaken by using a common protocol to generate the foam in the test tubes from biological labs. The figure shows foam from the tube with the dispersion containing a sedimented portion (30 mm) and the dispersion containing a portion obtained from the top region (7 mm).

suggests that even if ash particles do not affect the generation of foam (foam column); they surely enhance its stability for given testing conditions. It was also observed that smaller amounts of ash particles are less effective in foam stability than that of larger amounts for the same concentration of surfactant in the solution.

C.4. TEST TUBE EXPERIMENTS WITH BULK FOAM

Test tube experiments were carried out to understand the role of adding particles in foam flow through porous media. We prepared 3 ml solution containing 0, 0.075, 0.15, 0.3 and 0.5 w/w% surfactant in 0.3 w/w% NaCl. These solutions were mixed with 3 ml ash particle dispersions (0.125, 0.25 & 0.5 w/w%). The test tubes were of 9.5 mm internal diameter. The height of the air column above the liquid in the test tube was 39.5 mm. The tubes were sealed at the top. The shaking experiments were conducted with six test tubes at a time on the shaking machine as shown in Figure C.2. A routine experiment consisted

Figure C.2: Test tube shaking machine

	Particles w/w%	0	0.125	0.5
		Foam height (mm)		
Surfactant w/w%	0	0	0	0
	0.0375	17	25	74
	0.075	74	21	74
	0.15	25	53	17

Table C.4: Effect of combination of surfactant/particle on foam height (mm) immediately after shaking.

of 10 minutes of shaking at 900 rpm, where the test tubes were deflected 5 mm in up and down swing direction. Table C.4 shows the variation in the foam heights of each sample observed immediately after shaking. The experiments yield no reproducable data about the height of the foam without any possible pattern. Indeed, the foam height variation shows that the tests are unreliable to deduce any useful information about bulk foam. However, it can be observed in these tests that aggregates of particles accumulate at the Plateau borders of the lamellae.

ACKNOWLEDGMENTS

Everybody seems normal until you get to know them.

Anonymous

"...blessed are those who have not seen and yet have believed."[2]. I express my most sincere acknowledgment to my promoter and supervisor, Prof. Hans Bruining with whom I had numerous discussions on all aspects of the thesis. I feel deeply grateful for his guidance throughout the work. Working with Hans is not easy, but certainly fruitful. He listened to my worries, supported me during tough times, removed my doubts and made me a better researcher. I thank his wife, Maria to excuse my presence in their house for many evenings.

The quality of the work would not have been the same without the critical remarks by Prof. Bill Rossen. He has been kind enough to show me the pitfalls I easily overlooked, the possibilities I could not have imagined. In addition I thank him and Prof.dr.ir. Jan-Dirk Jansen to allow me to present my work during petroleum engineering meetings. I appreciate Dr. Rouhi Farajzadeh for initiating the work and for his advice during difficult times. I thank Prof. Pacelli Zitha for his useful suggestions. I thank Prof. Rumen Krastev for letting me work at NMI Germany. I am also very thankful to the rest of the examination committee members, Prof.dr. Timo Heimovaara, Prof.Ruud Schotting, Dr. A Andrianov and dr. S.Y.F.Vincent-Bonnieu for carefully reviewing my work. Financial support from Shell and Erasmus Mundus India Program made it possible for me to complete my study.

"To the untrained eye, we may appear colorful and picturesque; to the critical eye, we are but shoddy imitations of our various masters."[3]. Speaking of masters, I must mention Prof. Sybrand van der Zwaag from the faculty of Aerospace Engineering who strongly influenced my scientific career and helped me to grow up. I acknowledge him for the propositions 7 and 8.

What Newton said about standing on the shoulders of giants, I paraphrase as a student at the Dietz laboratory. I acknowledge the help from Henny van der Meulen, Henk van Asten, Gerard Matthieu, Jan Etienne, Mark Friebel and Karel Heller for constructing experimental set ups. I thank Rob Penners and Tonny Schuit from Civil Engineering to help me with the bulk foam tests and the adsorption tests respectively. I thank Joost van Meel and Guus Lohlefink for helping with laser scattering experiments. I deeply appreciate walks around the campus with Lab Head Dr. Karl-Heinz Wolf. I thank Duco Bosma, Dr. Roman Latsuzbaia, Dr. Krishna Kowlgi and Sumit Sachdeva from the faculty of Chemical Engineering to allow me use the zeta sizer and the ultra-violet visible light Spectrophotometer. Help from Paul Vermeulen and Kees van Beek was very critical for managing

[2] The Holy Bible, John 20:29, New International version

[3] Wings of Fire An autobiography APJ Abdul Kalam with Arun Tiwari 1999 Universities press

data acquisition system. I appreciate Ioannis's help with the initial experimental work with foam. I thank Jolanda Haagen-Donker for pH and electrical conductivity measurements. My sincere thanks to the senior technician Wim Verwaal for approving lab work with great scrutiny for safety consideration. Ellen did the paper work for ordering samples and maintained Lab auxiliary full for the experiments.
Bureaucratic work can be hectic and painfully slow. Margot Bosselaar-Perk, Marja Roep-Van der Klis, Marijke Schillemans-Van Tuijl and Lydia Broekhuijsen-Bentvelzen supported cumbersome visa applications. Ralf Haak has been very patient to provide extra long stay in CiTG buildling. Marlijn Ammerlaan updated about various courses. Their help to practice dutch language can never be appreciated enough. In addition I would like to thank them to laugh at my jokes. I thank Anke Dählmann to introduce me to Delft Global Initiative. I thank Hannie Zwiers for the moral support during last phase of this work. I acknowledge help from Theda Olsder from the valorisation center for visa and insurance and providing helpful advise about funding opportunities.
For me, the essence of life is not competition but cooperation. I sat in section Geotechnology (2010-2012), section Petroleum Engineering (2012-2014) and section Applied Geophysics and Petrophysics (2014-2016). I thank RahulMark Fonseca for interesting lunch discussions, Chris Boeije for occasional swimming and running, Eduardo Barros and Daniel for taking initiatives for group events and Jakolien van der Meer for practicing Dutch. I thank Narjes Shojai Kaveh, Mojtaba Hosseini Nasab, S.A. Fatemi, Saskia Roels, Durgesh Kawale, Nikita Lenchenkov, Leon Kapitas, Elisa Battistuta, Jiakun Gong, Siân Jones and Anna Peksa for the good times together. I thank Siavash Kahrobaei for the advice on publishing the research. I thank fellow students (Ali Akbar Eftekhari, Roozbeh Khosrokhavar, Negar Khoshnevis Gargar, Amin Ameri, Ajay Bhatt and Anas Hassan) to share joys (and pains) of working with Hans. Mohammad Chahardowli has been very supportive in the last years managing time schedule with Hans. I thank Ali Akbar for discussions about nanoparticle foam flow and introducing me to Eureqa, a symbolic regression software. I am inspired by the positive attitude of my officemate, Asiya Kudarova. Ralph Feld and Alex Kirichek from the fourth floor are delightful to discuss any topic with. I thank Niels Grobbe for occasional lunches together.
"But all the while I sit and think, of times there were before, I listen for returning feet and voices at the door."[4] It has been enjoyable times to share housing over the years with Marco (Marcushof), Fernao Beenkens and Stephan (Cesar Franckstraat), Prabu D., Maruxa, Taja Bencina, Francesca Guttierri , David Ojea and Mohammad Karimian (Prof. Evertslaan). I value company of Henk de Haan and Shirishkumar Baviskar for all the pleasant talks. I thank Deborah de Jong, Suvi, and Sidonie Riha for their patience to teach me Violin. Delftse methode people, Piet Meijer, Sonja van Boxtel and Astrid van Laar helped me communicate in Dutch over many years. Heel erg bedankt![5]
As Aristotle says, man is by nature a social animal. My sincere thanks to the Indian student association Delft, the Student Hockey club Scoop and the Student society SoSalsa! for wonderful social experience in Delft. I thank Jan Sonneville and Vivian Gerards for being extremely kind to teach me salsa. I am fortunate to dance with some of the most beautiful girls. Jan and Elleke Koornneef from AV de Koplopers trained me for running

[4] The Lord of the Rings, JRR Tolkien
[5] Thank you very much!

during the last years of my PhD. I adore my fellow runners for "gezelligheid"[6]. Thank you very much! Joost van de Korput, Tomas Giele, Emma Sirks, Rob Coorens and Thomas Breebart trained me to survive and to enjoy tough world of Field Hockey. At difficult times I remember what Bob Speth once told: "You must go on with your life". My special thanks to Rogier Vermeulen, Roland Walta, Boaz Pat-El, Laurens Wester, Stef Maree and Bastijn Bruins for their encouragement on and off ground. I thank other hockey members to help me to overcome social/lingual/age barriers. They were irreplaceable for the life outside the work. I remember drama/heroic, complete exhaustion, bruised/broken body parts and humiliating defeats. But I also remember solidarity, perseverance and that so-rare wins. I acknowledge the suggestions from fellow players on hockey, on beer drinking and on the dutch language. They even advised me on dating, and when it did not work, they were there to cheer me up with words "Grow some balls, Wuss!".
"It is not our abilities that show what we truly are. It is our choices."[7] I have questioned my choices very much. "The whole problem with the world is that fools and fanatics are always so certain of themselves, but wiser people so full of doubts."[8]. However, the drawback of too much doubting is that it blinds oneself. In this case, a life can become a very long monologue with oneself without reflections from others. Words fall short to appreciate Monique Draijer and Paula Meesters from career and counseling office for their support during difficult times. My thoughts from various sessions with them can be best summarized by a sentence from Dany Kaye's essay "The Happiest Man": "Happiness is not a thing you can achieve and keep, but something that must be won over and over again." I thank Studium Generale to fulfill my (philosophical and gastronomical) longings with "Broodje filosofie".
The PhD at TU Delft is enriching but demanding work. Similarly, staying in the Netherlands is wonderful, however, I do miss my family. For the international students and researchers like me, the Delft Project from Immanuel church provides the home away from home experience. Predikant Hans-Jan Roosenbrand and Predikant Simon van der Lugt have been kind to introduce me to the church. Their preaches during service have a lasting influence on me. I feel happy to work about International cultural evenings with Maria de Jong, Marieke van Bergen, Marieke Sneep and Judith Leijenhorst. I have been lucky to have warm company of Tineke Scheepstra for many evenings. John Spruijt has been very kind to accommodate me in the Sunday morning team. I thank the rest of The Delft Project team (Jaap Meijer, Hugo Reijm, Karel Reijm and Frank de Boer) for their compassion and support during last stages of my PhD research. I thank Anita van der Drift and Joke Tummers to introduce me to volunteer for elderly people. I acknowledge the wonderful companionship of Hans and Mariot Kamerling.
"And then, there's another kind of love: the cruelest kind. The one that almost kills its victims. Its called unrequited love. Of that I am an expert."[9]. Characters like Don Tillman[10], Ted Mosby[11] and Rajesh Koothrappali[12] come to my mind. Although we defer by

[6] pleasure, cosyness
[7] Harry Potter
[8] Bertrand Russell
[9] Iris, Introductory monologue, "The Holiday"(2006)
[10] Protagonist in the Novel "The Rosie Project" by Graeme Simsion
[11] Fictional character on the U.S. television sitcom "How I met your mother"
[12] Fictional character on the CBS television series "The Big Bang Theory"

centuries, talent and wisdom, I empathize with Stokes[13]: "You are quite right in saying that it is well not to go brooding over one's own thoughts and feelings, and in a family that is easy, but you don't know what it is to live utterly alone." Anyway, I acknowledge the girls I loved and lusted over the years. They are my inspiration for the proposition 10. They will remain part of my inner world. Sigh!
What is friendship ? It is difficult to define. A lot like love, you just know. "The truth is, everyone is going to hurt you. You just got to find the ones worth suffering for."[14] I thank my friends Ina, Remko Kamminga and Jurjen Vos to suffer my constant nagging: Alstublieft![15] I dedicate my thesis to you because, without you guys, I would not have made it. I thank Ina for Sunday dinners, for practicing dutch language. I thank Remko for occasional walks, for weekend outings and for accompanying to various parties. I thank Jurjen for running together, for Saturday dinners and providing counter views on various things. Above all I thank you guys to listen to my worries and yet, still be my friends.
Alas! I hid Krishna's advice to Arjuna[16] and follow Achilles's footpath[17]. Therefore, I thank my big family in India for their unconditional love and life-long support to pursue my interests, even at the cost of their own happiness. I thank my parents in whose mirror images I have been created. My mind constantly wonders about them. I thank my sister Smita to support me during my stay in the Netherlands. Vicky, Harsha, Priyanka and Prajakta, I love you guys. I hope you might take some inspiration from my journey. Vishu, Jitu and Yash, I am sorry that I was not around while you were growing up. But if anything, this thesis is a small compensation for that. Remember, family makes a house a home, an existence a life.

[13] George Stokes: after Stokes's law
[14] Bob Marley
[15] Here we go!
[16] Get up and Fight!
[17] Achilles preferred to die in Trojan war for an eternal glory rather than to stay with his family for a happy-uneventful-long life.

SHORT SUMMARY

This thesis was performed in the framework of Erasmus Mundus EU-INDIA scholarship programme. The main goal is to elucidate particle enhanced foam flow (surfactant water and nitrogen gas) in porous media near the critical micelle concentration. The thesis is divided in four parts: in the first part the modeling of foam flow is investigated, in the second part variables affecting the steady state pressure drop during foam flow are discussed, in the third part the stability of ash particles in the bulk dispersion is tested and in the final part, the effect of the particles on foam flow stability in porous media is experimentally studied. During the period of the study, the set ups for fluid flow and laser scattering of liquids are built and calibrated. We measured pressure drop histories before and after injection of ash particle dispersions with nitrogen gas (N_2) across the measurement points in unconsolidated sand packs (1860 and 130 Darcy) and a Bentheimer sand stone core (3 Darcy). This was carried out for various surfactant concentrations (0.0375, 0.075 and 0.15 w/w %), for various gas and surfactant solution velocities (0.27-3.97 m/day), for two salinities (0, 0.5M NaCl) and for two pH values (6.5, 3.0). We used a mathematical formulation with a bubble population function by history matching the experiments. The two-phase flow model that leads to four equations, viz., a pressure equation, a water saturation equation, a bubble density equation and a surfactant transport-adsorption equation can describe the pressure drop during the foam flow experiments. Within the model, the rate of change of bubble density during the transient state can be equated to the bubble density generation function plus the terms accounting for the bubble transport, i.e., by convection and diffusion divided by the porosity saturation product. The effect of the variables (e.g. permeability) on the foam flow is studied by using symbolic regression. We applied a Monte Carlo method (Bootstrap) to calculate the parametric uncertainties. The data driven model obtained without prior knowledge of an underlying physical process can elucidate the general behavior and hierarchy of the variables affecting the steady state pressure drop. The statistical model gives the variable spaces for which more experiments are needed. The trends obtained from the subset of data cannot be derived from the complete data set purely on statistical grounds. To use ash particles in foam flow through porous media we measured their colloidal stability when surfactant is present or absent in the dispersion. We measured properties of dispersions, viz., zeta potential, sedimentation-coagulation behavior, light absorption and particle size for pH values ranging from 3 to 11. For the optimal stability of an ash dispersion, we recommend an alkaline medium when surfactant is absent and an acidic medium, when surfactant is present. An ash particle dispersion alone with nitrogen gas cannot generate foam in porous media. The flow of ash particles with foam in porous media (Bentheimer and sandpack) is related to the colloidal stability of the ash dispersion. We observed tiny change in the permeability of the porous media after foam flow experiments with ash particles.

SAMENVATTING

Dit proefschrift is uitgevoerd in het kader van het Erasmus Mundus EU-INDIA scholarship programma. Het belangrijkste doel van het proefschrift is het verhelderen van stroming met deeltjes verstrekt schuim (water met oppervlakte-actievestof en stikstof gas) in poreuze media om en nabij de kritische micel-concentratie. Het proefschrift bestaat uit vier delen: in het eerste deel wordt de modellering van schuimstroming onderzocht; in het tweede deel worden de variabelen die tijdens schuimstroming het tijdonafhankelijk stationaire drukverschil beïnvloeden besproken; in het derde deel wordt de stabiliteit van asdeeltjes in een bulk dispersie getest; het laatste deel omvat een experimentele studie naar het effect van de stabiliteit van deeltjes op schuimstroming in poreuze media. Gedurende de periode van het onderzoek, werden de opstellingen gebouwd en gekalibreerd ten behoeve van de vloeistofstroming en laser verstrooiing aan deze vloeistoffen. We hebben het drukverschil tussen twee meetpunten gemeten vóór en na injectie van dispersies van as deeltjes en stikstofgas zowel in niet-geconsolideerde zand monsters (1860 en 130 Darcy) als in een Bentheimer zandsteen kern (3 Darcy). Hierbij gebruikten wij verschillende surfactant concentraties (0.0375, 0.075 en 0.15 w / w %), verschillende gas-snelheden en verschillende snelheden van de oplossing (0,27-3,97 m / dag) bij twee zoutgehaltes (0, 0.5 m NaCl) en twee pH-waarden (6.5, 3.0). We gebruikten een wiskundige formulering met een gasbel populatie balansmodel en vergeleken de tijdafhankelijke resultaten met experimenten. Het twee-fasestromings-model dat leidt tot vier vergelijkingen, namelijk een drukverschil vergelijking, een waterverzadiging vergelijking, een gasbel-dichtheids vergelijking en een surfactant transport/adsorptievergelijking kan het drukverschil tijdens de schuimstroom experimenten beschrijven. Vóór het bereiken van de stationaire toestand kan de gasbeldichtheids-veranderings-snelheid worden gelijkgesteld aan de bronfunctie van de gasbeldichtheid plus de convectie- en diffusietermen gedeeld door de porositeit-waterverzadigings-product. Het effect van de variabelen (bijvoorbeeld permeabiliteit) op de schuimstroming wordt bestudeerd met behulp van symbolische regressie. Wij gebruiken een Monte Carlo methode (Bootstrap) om de parametrische onzekerheden te berekenen. Het gegevens-gedreven model dat geen gebruikt maakt van een onderliggend fysisch proces kan het algemene gedrag en hiërarchie van de variabelen die het stationaire drukverschil bepalen, enigszins toelichten. Het statistisch model geeft aan voor welke variabele ruimten meer experimenten nodig zijn. De tendens verkregen uit een deelverzameling van gegevens kunnen zuiver op statistische gronden niet wordt afgeleid uit de volledige dataset. We hebben de eigenschappen van dispersies, namelijk de zeta potentiaal, het sedimentatie-coagulatie gedrag, lichtabsorptie en deeltjesgrootte voor een pH tussen 3 en 11, gemeten. Deze studie laat zien dat een optimale stabiliteit van een as-dispersie een alkalisch milieu vereist in afwezigheid van een oppervlakte-actieve stof en een zuur medium in aanwezigheid van een oppervlakte-actieve stof. De stroom van asdeeltjes in schuim in poreuze media (Bentheimer en zandpak) houdt verband met de colloïdale stabiliteit van de as-dispersie. Een

asdeeltjes-dispersie alleen met stikstofgas kan geen schuim genereren in poreuze media. Wij hebben klein verandering gevonden in de permeabiliteit van de poreuze media na schuimstroming met as deeltjes.

CURRICULUM VITÆ

10-04-1980	Born in Varud, India.

EDUCATION

1992–1997	Marathi School, Kadegaon (1985–1990) Mahatma Gandhi Vidyalaya, Kadegaon (1990–1995) Srirang Namdev Kadam Junior College (1995–1997)
1997–2001	Bachelor of Engineering (Mechanical Engineering) Mumbai University
2002–2004	Master of Technology (Manufacturing Engineering) Dr. Babasaheb Ambedkar Technological University

PROFESSIONAL

2004–2005	Research Assistant, Particulate Materials Lab Indian Institute of Technology Bombay India
2005–2006	Research and Development manager Midwest Granite Pvt. Ltd. Hyderabad, India
2006–2008	Researcher Aerospace Engineering, Delft University of Technology, The Netherlands
2008–2009	Development Engineer Fontijne Grotnes BV Vlaardingen, The Netherlands
2009–2010	Materials Scientist Netherlands Organization for Applied Scientific Research (TNO) Safety and Security, Rijswijk, The Netherlands
2010–2015	PhD Researcher Petroleum Engineering, Delft University of Technology, The Netherlands

LIST OF PUBLICATIONS

5. **R. Thorat and H. Bruining**, *Foam flow experiments. I. Estimation of the Bubble generation function*, Transport in Porous Media **112**, 53-76 (2016).

4. **R. Thorat and H. Bruining**, *Determination of the most significant variables affecting the steady state pressure drop in selected foam flow experiments*, Journal of Petroleum Science and Engineering **141**, 144-156 (2016).

3. **R. Thorat and D. Risanti and D. San Martin and P. Rivera Diaz and S. Zwaag**, *On the transformation behaviour of NiTi particulate reinforced AA2124 composites*, Journal of Alloys and Compounds **477**,1-2, 307-315 (2009).

2. **R. Thorat and D. Risanti and D. San Martin and P. Rivera Diaz and S. Zwaag**, *Self-Healing in a NiTi Shape Memory Alloy Particulate Reinforced Aluminum Composite*, First International Conference on Self Healing Materials **XXX**, XXX-XXX (2007).

1. **R. Thorat and P. Brahmankar and T. Rama Mohan**, *Cu-Co-Fe Pre-alloyed Powders as a Matrix Material for Diamond Tools*, Transactions of Powder Metallurgy Association of India **31**, 17-21 (2005).